



12-1989

## **An Investigation of the Combined Heat and Mass Transfer Processes in the Drying of Hygroscopic Porous Media with Two Disparate Length Scales**

Thomas Joseph Phillips  
*University of Tennessee - Knoxville*

Follow this and additional works at: [https://trace.tennessee.edu/utk\\_graddiss](https://trace.tennessee.edu/utk_graddiss)



Part of the [Mechanical Engineering Commons](#)

---

### **Recommended Citation**

Phillips, Thomas Joseph, "An Investigation of the Combined Heat and Mass Transfer Processes in the Drying of Hygroscopic Porous Media with Two Disparate Length Scales. " PhD diss., University of Tennessee, 1989.

[https://trace.tennessee.edu/utk\\_graddiss/2653](https://trace.tennessee.edu/utk_graddiss/2653)

This Dissertation is brought to you for free and open access by the Graduate School at TRACE: Tennessee Research and Creative Exchange. It has been accepted for inclusion in Doctoral Dissertations by an authorized administrator of TRACE: Tennessee Research and Creative Exchange. For more information, please contact [trace@utk.edu](mailto:trace@utk.edu).

To the Graduate Council:

I am submitting herewith a dissertation written by Thomas Joseph Phillips entitled "An Investigation of the Combined Heat and Mass Transfer Processes in the Drying of Hygroscopic Porous Media with Two Disparate Length Scales." I have examined the final electronic copy of this dissertation for form and content and recommend that it be accepted in partial fulfillment of the requirements for the degree of Doctor of Philosophy, with a major in Mechanical Engineering.

Robert J. Krane, J. Roger Parsons, Major Professor

We have read this dissertation and recommend its acceptance:

B. L. Bledsoe, V. Alexiades

Accepted for the Council:

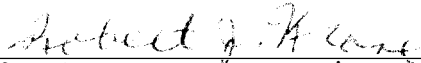
Carolyn R. Hodges


Vice Provost and Dean of the Graduate School

(Original signatures are on file with official student records.)

To The Graduate Council:

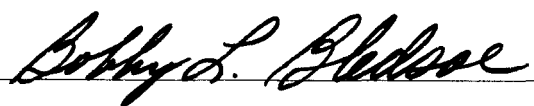
I am submitting herewith a dissertation written by Thomas Joseph Phillips entitled "An Investigation Of The Combined Heat And Mass Transfer Processes In The Drying Of Hygroscopic Porous Media With Two Disparate Length Scales." I have examined the final copy of this dissertation for form and content and recommend that it be accepted in partial fulfillment of the requirements for the degree of Doctor of Philosophy, with a major in Mechanical Engineering.

  
\_\_\_\_\_  
Robert J. Krahe, Major Professor

  
\_\_\_\_\_  
J. Roger Parsons, Major Professor

We have read this dissertation  
and recommend its acceptance:

  
\_\_\_\_\_

  
\_\_\_\_\_

Accepted for the Council:

  
\_\_\_\_\_  
Vice Provost  
and Dean of The Graduate School

AN INVESTIGATION OF THE COMBINED HEAT AND MASS  
TRANSFER PROCESSES IN THE DRYING OF HYGROSCOPIC  
POROUS MEDIA WITH TWO DISPARATE LENGTH SCALES

A Dissertation  
Presented for the  
Doctor of Philosophy  
Degree  
The University Of Tennessee, Knoxville

Thomas Joseph Phillips

December 1989

## ACKNOWLEDGMENTS

The author would like to thank his two advisors, Dr. R.J. Krane and Dr. J.R. Parsons, for their support and encouragement throughout the completion of this project. Their willingness to listen and enthusiasm for research have helped to make this project a very enjoyable one.

The author would also like to express his appreciation to Dr. B.L. Bledsoe for initiating this research effort, as well as providing invaluable advice during the performance of this research. Acknowledgment should also be made of the author's fourth committee member, Dr. V. Alexiades, who also provided a great deal of help and encouragement.

In addition, the author would like to thank his family and friends for their support throughout his (long) college career. Finally, the author would like to thank his lovely wife, Martha, for her patience, help, and understanding throughout all the phases of this project.

## ABSTRACT

A mathematical model describing the drying process in a hygroscopic porous medium with two disparate length scales is formulated. The mathematical model is used to identify the important dimensionless parameters appearing in the problem; and, a parametric study is performed to determine the effects of varying these parameters on the drying process. Of particular interest in this study is to apply the model to the drying of large, round hay bales. Therefore a discussion of how the results of the parametric study impact on the efficient use of a hay drier is also presented.

The results from the parametric study indicate that the drying times of a porous medium may be decreased by increasing the Reynold's number, increasing the inlet air radius of the drier, decreasing the overall aspect ratio of the porous structure, and decreasing the Kossovich number. In addition, it is shown that the velocity distribution through the porous medium plays a significant role on the drying behavior. It was concluded the the greatest potential for improving the drying time for hay bales was to decrease the aspect ratio of the bale.

## TABLE OF CONTENTS

| SECTION  | PAGE |
|--|------|
| 1. INTRODUCTION .....  | 1    |
| 1.1. The Importance Of Drying .....  | 1    |
| 1.2. Analytical Models Of Drying .....   | 1    |
| 1.3. A Review Of Postulated Mechanisms For A<br>Drying Process .....   | 3    |
| 1.4. Description Of A Typical Drying Process ...   | 6    |
| 1.5. Motivation For The Present Research .....   | 9    |
| 2. LITERATURE REVIEW .....   | 12   |
| 2.1. General Analytical Models Of Drying<br>Processes .....  | 12   |
| 2.2. Studies Of Hay Drying .....   | 20   |
| 2.3. Numerical Methods .....   | 24   |
| 2.4. Selection Of The Techniques To Be Employed<br>In The Present Work .....   | 27   |
| 3. THE ANALYTICAL MODEL .....  | 30   |
| 3.1. Physical Description Of The Problem .....   | 30   |
| 3.2. Derivation Of The Governing Equations For<br>The Inner Domain .....   | 33   |
| 3.2.1. Conservation Of Mass .....  | 33   |
| 3.2.2. Conservation Of Energy .....  | 37   |
| 3.2.3. Equation Of State .....   | 42   |
| 3.2.4. Nondimensionalization Of The Governing<br>Equations, Boundary Conditions, And<br>Initial Conditions For The Inner<br>Domain ..... | 44   |
| 3.3. Derivation Of The Governing Equations For<br>The Outer Domain .....   | 47   |
| 3.4. Summary Of The Analytical Model .....   | 57   |

| SECTION  | PAGE |
|--|------|
| 3.5. Discussion Of The Assumptions On Which The Analytical Model Is Based .....                        | 64   |
| 4. THE NUMERICAL INVESTIGATION .....   | 70   |
| 4.1. The Need For A Numerical Solution .....   | 70   |
| 4.2. Determination Of The Velocity And Pressure Fields .....   | 70   |
| 4.3. The Drying Problem .....  | 81   |
| 4.3.1. Governing Equations For The Outer Domain Domain .....   | 81   |
| 4.3.2. Governing Equations For The Inner Domain Domain .....   | 87   |
| 4.3.3. Solution Algorithm For The Inner And Outer Domains .....  | 93   |
| 5. PARAMETRIC STUDY .....  | 100  |
| 5.1. Identification And Discussion Of Important Dimensionless Parameters In The Analytical Model ..... | 100  |
| 5.2. Determination Of Physical Quantities Appearing In The Mathematical Model .....                    | 104  |
| 5.3. Discussion Of The "Base Case" For The Parametric Study .....                                      | 111  |
| 5.4. The Effects Of Varying The Reynolds Number On The Drying Process .....                            | 119  |
| 5.5. The Effects Of Varying The Overall Aspect Ratio Of The Bale On The Drying Process .....           | 127  |
| 5.6. The Effects Of Varying The Inlet Radius Width On The Drying Process .....                         | 135  |
| 5.7. The Effects Of Varying The Kossovich Number On The Drying Process .....                           | 145  |
| 5.8. The Effect Of A Nonuniform Porosity Distribution In The Outer Domain On The Drying Process .....  | 151  |



| SECTION  | PAGE |
|--|------|
| 5.9. The Effects Of Varying The Characteristic Aspect Ratio Of An Inner Domain Element On The Drying Process .....           | 156  |
| 5.10. Summary Of Conclusions .....   | 157  |
| 5.11. Implications Of The Results For The Practical Operation Of Driers .....  | 158  |
| BIBLIOGRAPHY .....   | 162  |
| APPENDIXES .....   | 168  |
| APPENDIX A. DETERMINATION OF THE FUNCTIONAL DEPENDENCIES OF THE BIOT NUMBERS ON THE OTHER DIMENSIONLESS PARAMETERS .....     | 169  |
| APPENDIX B. COMMENTS ON THE NUMERICAL TREATMENT OF THE LATENT HEAT TERM IN THE ENERGY EQUATION FOR THE INNER DOMAIN .....    | 175  |
| APPENDIX C. RATIONALE FOR SELECTING A CHARACTERISTIC VALUE AND RANGE OF VARIATION OF THE INNER DOMAIN ASPECT RATIO .....     | 177  |
| APPENDIX D. NUMERICAL TREATMENT OF THE SORPTION ISOTHERM RELATION .....  | 182  |
| APPENDIX E. DETERMINATION OF THE PERMEABILITY OF A HAY BALE AND THE COEFFICIENT OF THE FORSCHEIMER TERM IN DARCY'S LAW ..... | 185  |
| VITA .....   | 186  |

## LIST OF FIGURES

| FIGURE  | PAGE |
|---|------|
| 1.1. Movement Of Moisture During Drying .....   | 7    |
| 3.1. Schematic Of The Drying Problem To Be Modelled .....   | 31   |
| 3.2. Mass Balance And Nomenclature For A Differential Element Of The Inner Domain .....   | 37   |
| 3.3. Energy Balance On A Differential Element Of The Inner Domain .....   | 40   |
| 4.1. Control Volume Faces Located Half-Way Between Grid Points (Practice A) .....   | 49   |
| 4.2. Grid Points Located At The Center Of The Control Volume (Practice B) .....   | 72   |
| 4.3. Outer Domain Solution Algorithm .....  | 95   |
| 4.4. Inner Domain Solution Algorithm .....  | 96   |
| 5.1. Sorption Isotherm For Alfalfa Hay (Reproduced From Hill, Ross, and Barfield, 1977) .....                                       | 106  |
| 5.2. Variation Of Total Moisture Content In A Bale With Time For The Base Case .....  | 113  |
| 5.3. Air Flow Distribution In The Bale For The Base Case .....  | 114  |
| 5.4. Drying Front Location Shown With Lines Of Constant Moisture Content For The Base Case At Different Times .....                 | 115  |
| 5.5. Isotherms Shown Within The Bale For The Base Case At Different Times .....   | 116  |
| 5.6. Variation Of The Moisture Content At Three Different Axial Locations And A Radial Location Of $r=0.74$ For The Base Case ..... | 118  |
| 5.7. Variation Of The Total Moisture Content Of A Bale With Time For Different Reynolds Numbers .....                               | 120  |

| FIGURE  | PAGE |
|---|------|
| 5.8. Drying Front Location Shown With Lines Of Constant Moisture Content For A Reynolds Number Of 4.7 At Different Dimensionless Times .....  | 122  |
| 5.9. Drying Front Location Shown With Lines Of Constant Moisture Content For A Reynolds Number Of 18.8 At Different Dimensionless Times ..... | 123  |
| 5.10. Isotherm Distribution For A Reynolds Number Of 4.7 At Different Dimensionless Times .....   | 125  |
| 5.11. Isotherm Distribution For A Reynolds Number Of 18.8 At Different Dimensionless Times .....  | 126  |
| 5.12. Streamlines And The Velocity Distribution On The Outer Surface For The Air Flow Through A Bale With An Aspect Ratio Of 2.0 .....        | 128  |
| 5.13. Streamlines And The Velocity Distribution On The Outer Surface For The Air Flow Through A Bale With An Aspect Ratio Of 0.75 .....       | 128  |
| 5.14. Variation Of Total Moisture Content Of A Bale With Time For Different Bale Aspect Ratios ....   | 129  |
| 5.15. Drying Front Locations Shown With Lines Of Constant Moisture Content For An Aspect Ratio Of 2.0 At Different Dimensionless Times .....  | 131  |
| 5.16. Drying Front Locations Shown With Lines Of Constant Moisture Content For An Aspect Ratio Of 0.75 At Different Dimensionless Times ..... | 132  |
| 5.17. Isotherm Distributions In A Bale For An Aspect Ratio Of 2.0 At Different Dimensionless Times .....                                      | 133  |
| 5.18. Isotherm Distributions In A Bale For An Aspect Ratio Of 0.75 At Different Dimensionless Times .....                                     | 134  |
| 5.19. Variation Of Total Moisture Content Of A Bale With Time For Different Air Inlet Radii .....   | 136  |
| 5.20. Streamlines And The Velocity Distribution On The Outer Surface For The Air Flow Through A Bale With An Air Inlet Radius Of 0.8 .....    | 137  |

| FIGURE  | PAGE |
|---|------|
| 5.21. Streamlines And The Velocity Distribution On The Outer Surface For The Air Flow Through A Bale With An Air Inlet Radius Of 0.2 .....          | 137  |
| 5.22. Drying Front Locations Shown With Lines Of Constant Moisture Content For An Air Inlet Radius Of 0.8 At Different Dimensionless Times .....    | 139  |
| 5.23. Drying Front Locations Shown With Lines Of Constant Moisture Content For An Air Inlet Radius Of 0.2 At Different Dimensionless Times .....    | 140  |
| 5.24. Isotherm Distributions In A Bale For A Dimensionless Air Inlet Radius Of 0.8 At Different Times .....   | 142  |
| 5.25. Isotherm Distributions In A Bale For A Dimensionless Air Inlet Radius Of 0.2 At Different Times .....   | 143  |
| 5.26. Axial Temperature Distribution For A Dimensionless Air Inlet Radius Of 0.2 .....  | 144  |
| 5.27. Variation Of The Total Moisture Content Of A Bale With Time For Different Kossovich Numbers .....   | 146  |
| 5.28. Drying Front Locations Shown With Lines Of Constant Moisture Content For A Kossovich Number Of 10 At Different Dimensionless Times .....      | 147  |
| 5.29. Isotherm Distributions In A Bale For A Kossovich Number Of 10 At Different Dimensionless Times .....  | 148  |
| 5.30. Drying Front Locations Shown With Lines Of Constant Moisture Content For A Kossovich Number Of 10 At Different Dimensionless Times .....      | 149  |
| 5.31. Isotherm Distributions In A Bale For A Kossovich Number Of 400 At Different Dimensionless Times .....   | 150  |
| 5.32. Streamlines And The Velocity Distribution On The Outer Surface For The Air Flow Through A Bale With A Typical Dry Matter Density Distribution | 152  |

| FIGURE  | PAGE |
|---|------|
| 5.33. Drying Front Locations Shown With Lines Of<br>Constant Moisture Content For A Nonuniform<br>Porosity Distribution At Different<br>Dimensionless Times ..... | 154  |
| 5.34. Isotherm Distributions In A Bale With A<br>Nonuniform Porosity Distribution .....   | 155  |
| 5.35. Variation Of The Total Moisture Content Of A<br>Bale With Time For A Nonuniform Porosity<br>Distribution .....  | 157  |
| C.1. Comparison Of The Experimental Drying Curve To<br>The Numerical Solution For A One Dimensional<br>Case (Hay Dried In A Tube) .....                           | 178  |
| D.1. Comparison Of Fit For The Sorption Isotherm Of<br>Alfalfa Hay With The Experimental Data Of Hill,<br>Ross, And Barfield (1977) .....                         | 184  |

## LIST OF TABLES

| TABLE |  | PAGE |
|-------|--|------|
| 3.1.  | Summary Of The Dimensionless Parameters And Their Physical Interpretation .....            | 63   |
| 5.1.  | Values Of The Dimensionless Parameters Held Constant For The Entire Parametric Study ..... | 105  |
| 5.2.  | Ranges Of Values For The Dimensionless Parameters In The Parametric Study .....            | 106  |
| D.1.  | Least Squares Fit Coefficients For The Sorption Isotherm Of Alfalfa Hay .....              | 183  |

## NOMENCLATURE

|                                  |   |
|----------------------------------|---|
| <i>a</i>                         | - Numerical coefficient (dimensionless)                     |
| <i>A</i>                         | - Cross sectional area of inner domain element ( $m^2$ )    |
| <i>A<sub>s</sub></i>             | - Surface area of inner domain element ( $m^2$ )            |
| <i>b</i>                         | - Forscheimer term coefficient ( $kg/m^4$ or dimensionless) |
| <i>Bi</i>                        | - Biot number (dimensionless)                               |
| <i>Bi<sub>m</sub></i>            | - Mass transfer Biot number (dimensionless)                 |
| <i>C<sub>p</sub></i>             | - Specific heat (J/kg C)                                    |
| <i>D</i>                         | - Diameter of inner domain element (m)                      |
| <i>D<sub>b</sub><sup>*</sup></i> | - Bound liquid conductivity ( $m^2/s$ )                     |
| <i>D<sub>c</sub><sup>*</sup></i> | - Capillary liquid conductivity ( $m^2/s$ )                 |
| <i>D<sub>L</sub></i>             | - Liquid Conductivity ( $m^2/s$ or dimensionless)           |
| <i>D<sub>Lr</sub></i>            | - Reference liquid conductivity ( $m^2/s$ )                 |
| <i>D<sub>v</sub></i>             | - Vapor diffusion coefficient (m/s)                         |
| <i>D<sub>vr</sub></i>            | - Reference vapor diffusion coefficient (m/s)               |
| <i>h<sub>c</sub></i>             | - Convection heat transfer coefficient ( $W/m^2$ s C)       |
| <i>h<sub>m</sub></i>             | - Convection mass transfer coefficient (m/s)                |
| <i>H</i>                         | - Overall height of outer domain (m)                        |
| <i>J</i>                         | - Mass flux ( $kg/m^2$ s)                                   |
| <i>K</i>                         | - Thermal conductivity (W/m C)                              |
| <i>Ko</i>                        | - Kossovich number (dimensionless)                          |
| <i>L</i>                         | - Half length of inner domain element (m)                   |
| <i>L<sub>v</sub></i>             | - Latent heat of vaporization (J/kg)                        |
| <i>Lu</i>                        | - Luikov number (dimensionless)                             |
| <i>m<sub>ev</sub></i>            | - Evaporative mass flow rate ( $kg/m^3$ s)                  |
| <i>N<sub>ID</sub></i>            | - Number of inner domain elements                           |
| <i>P</i>                         | - Pressure ( $N/m^2$ )                                      |
| <i>P'</i>                        | - Length of distance around inner domain element (m)        |
| <i>Pr</i>                        | - Prandtl number  |
| <i>q''''</i>                     | - Energy source ( $W/m^3$ )                                 |
| <i>r</i>                         | - Radial position (m or dimensionless)                      |
| <i>R</i>                         | - Overall radius of outer domain (m)                        |

|            |  |
|------------|--|
| $Re_x$     | - Reynolds number (dimensionless)  |
| $S_c$      | - Constant component of source term in numerical algorithm (dimensionless)   |
| $S_{mass}$ | - Mass source ( $\text{kg}/\text{m}^3 \text{ s}$ )                           |
| $S_p$      | - Coefficient of variable source term in numerical algorithm (dimensionless) |
| $t$        | - Time (s or dimensionless)  |
| $T$        | - Temperature (C or dimensionless)   |
| $u$        | - Moisture content (kg/kg)   |
| $V$        | - Velocity (m/s)   |
| $V_{cv}$   | - Volume of outer domain control volume ( $\text{m}^3$ )                     |
| $V_{od}$   | - Volume of outer domain ( $\text{m}^3$ )                                    |
| $V_{rs}$   | - Radial "psuedo" velocity (dimensionless)                                   |
| $V_{zs}$   | - Axial "psuedo" velocity (dimensionless)                                    |
| $z$        | - Axial position (m or dimensionless)  |

#### Greek Symbols

|              |  |
|--------------|--|
| $\alpha$     | - Thermal diffusivity ( $\text{m}^2/\text{s}$ )      |
| $\Delta\rho$ | - $\rho_o - \rho_e$ ( $\text{kg}/\text{m}^3$ )       |
| $\Delta T$   | - $T_e - T_o$ ( $^\circ\text{C}$ )                   |
| $\Delta u$   | - $u_o - u_e$ (kg/kg)                                |
| $\epsilon$   | - porosity ( $\text{m}^3/\text{m}^3$ )               |
| $\kappa$     | - Permeability ( $\text{m}^2$ or dimensionless)      |
| $\rho$       | - Density ( $\text{kg}/\text{m}^3$ or dimensionless) |
| $\mu$        | - Dynamic viscosity (kg/m s)                         |
| $\nu$        | - Kinematic viscosity ( $\text{m}^2/\text{s}$ )      |

#### Subscripts and Superscripts

|      |                      |
|------|----------------------|
| $a$  | - Ambient            |
| $e$  | - Equilibrium        |
| $i$  | - Inner domain       |
| IN   | - Inlet              |
| L    | - Liquid phase       |
| $ms$ | - Maximum sorptional |



- 0 - Initial state
- r - Radial direction
- s - Solid phase
- v - Vapor phase
- z - Axial direction
- \* - Dimensional quantity

## 1. INTRODUCTION

### 1.1. The Importance Of Drying

The drying of porous media is a problem with a diverse range of applications. From simple tasks in the home to complex industrial processes, drying is involved in both the production and use of a large number of products. Drying laundry in the home, freeze drying foodstuffs, and drying paper and agricultural products are but a few examples of these applications.

The consumption of energy required for drying tasks is enormous. An estimated 10% of the total fuel consumed in the U.S.S.R. (Lebedev and Ginzburg, 1971) and 7% of the industrial energy demand in the United Kingdom (Keey, 1980) can be attributed to drying. This large energy consumption together with an ever-increasing variety of applications has resulted in a need for fundamental research in this area.

### 1.2. Analytical Models Of Drying

Many analytical models of drying have been proposed. As will be seen in the following chapter, however, each of these models is typically applicable over only a narrow range of drying conditions. To efficiently design and operate any

drier, an analytical model must be formulated that is general enough to be applicable throughout the drying regimes of interest, while being simple enough to be readily solved.

In formulating such a theory, the physical makeup of the medium to be dried becomes important as it affects the mechanisms by which drying occurs. In many drying problems, disparate physical scales may be identified in which the modes of heat and mass transfer differ. Examples in which such situations arise may be found in the drying of agricultural products. One such example is the drying of large round hay bales.

A hay bale is a porous structure, which is composed of individual hay stalks, each of which is also a porous structure, but on a much smaller scale. Normally, it is the hay stalks themselves that actually contain the moisture to be removed. That is, no liquid exists in between the closely packed hay stalks throughout the bale. Thus, two disparate length scales, one characterizing the overall bale structure and the other the individual hay stalks, emerge in this problem with different physical processes occurring on each scale. In this work, the analytical method of Krischer (1963) describing the drying of a hygroscopic porous solid has been modified and expanded to model the drying processes that occur in a porous medium with two distinct length scales.

The present method takes into account the two length scales discussed above. In addition, a more general form of the

equations governing the phase change processes than that formulated by Krischer (and modified by Berger and Pei, 1973) is presented here. This more general form allows the diffusional coefficients to vary with both moisture content and temperature, as has been observed to be true. In the formulation of the model presented in this work, an attempt was made to preserve the generalities of the model. That is, the model should be valid for any hygroscopic porous media. The model may be applied to the limiting case of a single element, or "stalk", which corresponds to one physical length scale. Or, the model may be applied to a structure composed of many elements where there are two disparate length scales with coupled heat and mass transfer.

### 1.3. A Review Of Postulated Mechanisms For A Drying Process

A brief description of the physical processes involved during the drying of a porous medium is presented here to provide the reader with a basic understanding of these phenomena and to introduce the common terminology used in the field of drying.

Several mechanisms have been proposed for the transport of moisture in a porous body. Fortes and Okos(1980) have identified seven such mechanisms that are discussed in the literature as: (1) liquid diffusion, (2) vapor diffusion, (3) capillary movement, (4) liquid and/or vapor flow due to

pressure differences, (5) effusion (Knudsen) flow, (6) liquid movement due to gravitational effects, and (7) surface diffusion.

Liquid diffusion was the basis of the first theories proposed for drying (Lewis, 1921 and Sherwood, 1929a, 1929b, 1930, and 1931). Several authors (see Caelgske and Hougen, 1937 and Chen, 1987) have noted, however, that the term liquid diffusion is "constrained and sometimes misleading." A diffusional process occurs on the molecular level (for example, the mixing of gases), but the flow of liquid through a porous medium is not such a mixing process. Liquid movement does not result from the mixing of liquid in the porous solid with the vapor in the porous solid, but rather is the result of complicated phenomena involving the surface tension of the liquid, as well as the properties of the solid structure and vapor. (It should be noted that concentration gradients of a liquid mixture may indeed exist in a porous solid. This would cause "true" liquid diffusion to occur.)

The second mechanism identified is vapor diffusion. Vapor diffusion may occur as a result of a vapor pressure gradient within the porous solid. This mechanism has been used in the formulation of several theories limited to describing the latter stages of drying (King, 1968 and Harmathy, 1969).

Capillary movement of a liquid is driven by surface tension forces. Thus, capillary movement of liquid can play an

important role in the overall transfer of moisture in regions of the porous solid where continuous paths of liquid exist. This mode of moisture transfer has also been used either alone or in combination with other mechanisms to provide the basis for several drying theories (Van Arsdel, 1947, Philip and DeVries, 1957).

The fourth mechanism identified is the movement of liquid and/or vapor via a pressure gradient. This mechanism is important in situations in which a large pressure gradient induced across a porous solid "forces" the liquid and vapor to flow. This mechanism, as well as the fifth and sixth, are allowed for in some of the more "sophisticated" theories (Whitaker, 1966, 1967, 1969, 1971, 1973, 1977a, 1977b, 1986a, 1986b, 1986c and Chen and Pei, 1989).

The fifth mechanism proposed, effusion, or Knudsen, flow is important only under rarefied conditions and will not be considered further in this dissertation.

Liquid movement due to gravitational effects is the sixth mechanism identified for moisture transfer. This mechanism is usually not important in porous bodies, however, due to the large surface tension effects that overcome the tendency of the liquid to move due to gravitational forces. The relative importance of gravitational forces to surface tension forces is indicated by the value of the Bond number. The Bond number is a dimensionless parameter defined as,

$$Bo = \frac{\rho L^2 g}{\sigma g_c}$$

Thus, if the Bond number is much less than one, surface tension forces dominate over gravitational forces. Most studies performed have implicitly assumed low Bond numbers and have ignored gravitational effects (see Fortes and Okos, 1980).

The seventh mechanism identified as a source of moisture transfer by Fortes and Okos is surface diffusion. They noted that at the time their paper was written (1980) no existing theories had accounted for this mechanism. This author has also not found any mention of this mechanism in other sources; and, it will not be considered in this work.

#### 1.4. Description Of A Typical Drying Process

A drying process often involves placing a moist porous body into a "controlled" environment. To illustrate the physical processes involved during drying, the case of a moist, porous semi-infinite slab with air of controlled humidity, temperature, and pressure on either side is discussed. The drying process for this case is graphically presented in Figure 1.1.

Provided the initial moisture content of the slab is high enough to saturate the surface, a so-called "constant rate phase" of drying is initially observed. In this phase, the liquid evaporation is essentially constant and equal to that from a free liquid surface. As drying continues, a critical point is reached where the water cannot be conducted to the

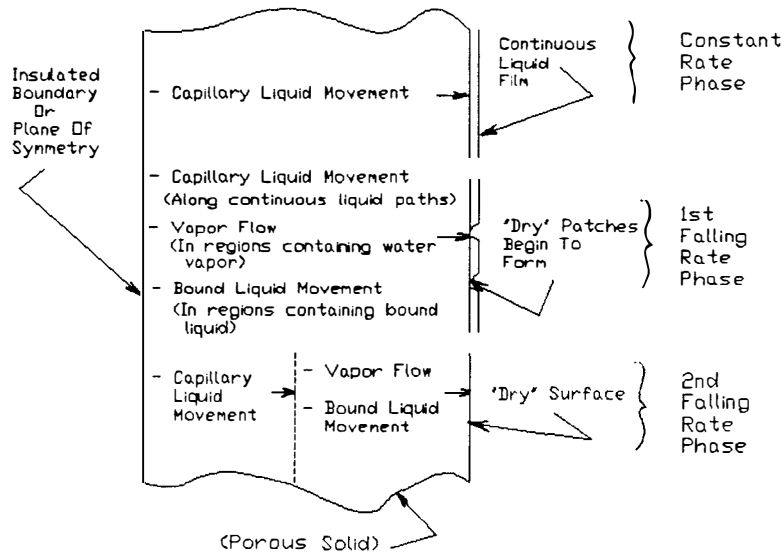


Figure 1.1. Movement Of Moisture During Drying.

surface fast enough to keep the surface moist. At this point, dry patches begin to emerge on the surface of the slab. The drying rate then decreases marking the so-called "first falling rate" period of drying. This period continues until the wet patches disappear from the surface. The time at which all the wet patches disappear marks the start of the "second falling rate" phase of drying. A drying front forms, and begins to retreat into the solid structure. Thus, two regions may be identified within the solid structure: (1) the wet region and (2) the "sorption" region.

In the wet region, there are still continuous paths of liquid present. The principal mechanism of moisture movement in this region is the capillary forces acting on the liquid.



In the sorption region, however, these continuous paths of free liquid do not exist. Moisture transfer in this region occurs primarily as a result of vapor diffusion (water vapor diffuses from regions of "high" to "low" vapor pressures) and the movement of "bound" liquid, controlled by the processes described below. Water contained in the solid is termed free water if the vapor pressure exerted is equal to that of saturated liquid at the same temperature. Any water contained in the solid where the vapor pressure is less than that at saturated conditions is termed bound water. This bound water may be thought of, for example, as water contained in very fine capillaries or water contained in plant cells. Free water, on the other hand, may exist as water contained between the cells or held in the larger voids of the solid.

The characteristics of the solid to be dried have an important effect on the drying behavior. Materials may generally be classified as either hygroscopic, or non-hygroscopic, depending on their ability to "bind" water. As drying begins (with a high initial moisture content), the vapor pressure in the air over the solid is equal to the pressure of saturated liquid at the same temperature. As drying progresses, a point is reached where the vapor pressure begins to decrease due to the presence of the porous solid. Materials containing a significant moisture content at this point are termed hygroscopic.

A relationship between the relative humidity of the air and the moisture content of the solid at a specified temperature is provided by the sorption isotherm. This curve is determined experimentally for any given material. The moisture content corresponding to a relative humidity of 100% on this curve is thus the dividing point where the solid contains free water or only bound water. This moisture content is referred to as the maximum sorptional moisture content. At any moisture content above the maximum sorptional moisture content, the solid contains free water. If the moisture content is below this value, however, only bound water exists in the solid structure.

As can be seen, modeling a specific drying process requires a knowledge of the different drying regimes encountered, the principal modes of mass transport that occur as well as the type of porous structure to be dried. Once these have been identified, a mathematical model of the drying process may be formulated.

#### 1.5. Motivation For The Present Research

The specific application chosen for the present investigation involves the drying of large round hay bales. Hay is used primarily as feed for animals. It is therefore desirable to obtain the highest quality hay possible; that is, to obtain the hay with the highest possible nutritional value. As will be discussed, one way to maintain the feed quality is to use a drier to dry the hay. One factor that

affects the drying of hay is the method in which it is handled. For economic reasons, it has been found beneficial to bundle hay in as large a package as possible. Unfortunately, this practice has several disadvantages.

One disadvantage is the dilemma faced as to the best time to bale the hay to preserve quality. If the hay is baled at too high a moisture content, the larger package results in increased drying time which may allow mold growth to begin before drying is completed (Bledsoe, 1988). It is currently common practice to allow hay to dry to a moisture content safe for storage in the swath prior to baling. This practice, however, causes excessive losses. When hay is allowed to dry to a moisture content below 18% wet basis (Wet basis refers to the ratio of mass of water to the mass of water plus the mass of dry matter and will be abbreviated as w.b.) in the swath, the nutrient rich leaves of the hay become brittle and fall off the stem during subsequent handling, a condition referred to as "leaf shatter." Prolonged exposure to sunlight also bleaches nutrients from leaves and stems. Thus, the hay should not be baled at too low a moisture content either. It has been found that it is best to bale the hay at a moisture content of approximately 35% (w.b.).

This relatively high initial moisture content presents another problem associated with increased microbial heat generation. This heat generation takes place as microorganisms, which feed on the hay, convert starch to sugar

in an exothermic reaction (Miller, 1947). As a result, excessive temperatures may be reached within the bale. These high temperatures can actually cause spontaneous combustion in the hay and so represent a safety hazard to farmers. Even when temperatures do not reach the combustion point, they may cause a "binding" of the proteins in the hay. Since proteins in the bound form are largely indigestible by feed animals, the feed quality of the hay is reduced. In any case, excessive temperatures must be avoided.

One method employed to counter these problems is to use a drier which both speeds up the drying process and helps to minimize microbial heating. To efficiently implement this approach, an analytical model of the drying process must be developed. Solutions of this model will provide the understanding necessary to improve upon current design criteria for the drying process.

The motivation for the proposed work, then, is based on the need for an accurate analytical model of the drying of large round hay bales. This model should provide the information necessary to minimize hay loss by providing a rational basis for hay drier design.

## 2. LITERATURE REVIEW

### 2.1. General Analytical Models Of Drying Processes

Many studies of drying of porous media have been performed. These studies vary considerably in their generality and practicality. An assessment of these studies is presented below.

A number of literature surveys, Lebedev and Ginzburg (1971), Keey (1980), Fortes and Okos (1980), Bruin and Luyben (1980), Mujumdar (1984), Fulford (1969), Filkova (1984), Sharp (1982), Bakker-Arkema (1984), and Parry (1985), summarize advances in the drying field. A particularly good review paper is the one presented by Fortes and Okos (1980). In this paper, the theoretical bases of several drying theories are examined and compared. The limitations of these theories as they apply to the drying of foodstuffs are also discussed. The review by Bruin and Luyben (1980) is also worthy of note. It contains over 300 citations to the literature on the drying of food materials.

Historically, the development of an analytical approach to the drying problem began with Lewis (1921). Lewis hypothesized that drying of a porous solid consisted of two distinct processes: the first was movement of the moisture from the interior of the solid to the surface by liquid diffusion, and the second was evaporation of the moisture from the surface to the surrounding environment. Sherwood

(1929a,1929b,1930,1931) developed these hypotheses in a series of papers utilizing the one-dimensional diffusion equation.

McCready and McCabe (1933) improved on the diffusion approach by assuming that moisture movement was the result of the diffusion of free water (i.e. bound water movement was not considered) and also a result of vapor diffusion through the solid structure. They assumed that the vapor was in equilibrium with the solid and used the sorption isotherm as a constitutive relation.

At about this time, it was noted by several authors that capillary effects could be important in drying processes. One such author was Richards(1931), who described the flow through unsaturated porous media in terms of capillary movement of the liquid, and experimentally determined values of capillary potential, conductivity, and capacity for various solids. The capillary potential (introduced by Buckingham(1907) is the pressure difference across the air-water interface. It thus represents a driving force for the unsaturated capillary flow of the liquid through a porous medium which may be expressed as

$$J_l = -K_H \nabla \psi, \quad (2.1)$$

where:

$J_l$  = the liquid mass flux due to capillary flow,

$K_H$  = the capillary conductivity,

and,

$\psi$  = the capillary potential.

The capillary capacity is the rate of change of the moisture content with respect to the capillary potential.

Caeglske and Hougen(1937) claimed that capillary action was not only important, but in fact was the dominant mechanism in drying. They conducted experiments with sand and obtained good agreement with an analytical approach based on the capillary movement of water. This approach utilized experimentally determined values for capillary pressure (or potential) as a function of saturation.

Hougen, McCauley, and Marshal(1940) made an extensive study of the applicability of the diffusion equations to drying of porous solids. Experimental results for several materials were compared to results obtained from both diffusion and capillary models. For most materials examined (the exception being wood), the diffusion model did not follow the observed trends of the experimental data. The results of this study indicate that the assumption that moisture transfer occurs only by liquid diffusion in all stages of drying is not physically realistic. Thus, the theories of Lewis, Sherwood, etc. which assume that moisture transfer occurs solely by liquid diffusion are not accurate and are incomplete. The same argument may be made for any theory based on a single mechanism since there is no doubt that mass transfer may occur in a given application by more than one mechanism. It has

been pointed out by Hougén et. al. that for many materials, during the latter stages of drying, the diffusion equation may be applicable provided one uses a variable diffusivity.

Van Arsdell (1947), in an attempt to numerically model the drying process in the falling rate phase for vegetables, made use of the diffusion equation, and allowed for variable diffusivity. The predicted drying rate curves showed similar trends to experimental studies of previous investigators. Some physical justification for this approach lies in the fact that for isothermal conditions, the mass flux for capillary liquid flow may be expressed as

$$J_l = -\rho_s K_H \nabla u^* \quad (2.2)$$

where:

$K_H$  = capillary conductivity,

$\rho_s$  = solid density,

and,

$u^*$  = moisture content (mass water/mass solid).

Philip and DeVries (1957) formulated a model which considered moisture movement as a combination of movement of vapor by diffusion and movement of liquid by capillary action. Both terms were expressed as functions of the temperature and moisture content gradients, so that a diffusion equation resulted. DeVries (1958) then generalized this approach somewhat by considering separately the changes in moisture content of the liquid and vapor phases. In developing this



theory, Philip and DeVries have made use of relations which assume liquid continuity within the pores and capillaries. As drying proceeds to the latter stages, this would obviously not be valid and so represents a major limitation to their theory.

Whitaker (1966, 1967, 1969, 1970, 1971, 1977a, 1977b, 1986a, 1986b, 1986c, 1986d) has extensively developed a volume-averaged approach to simultaneous mass, momentum, and energy transfer in porous media. This approach is fundamental in that Whitaker starts with the basic conservation equations and proceeds to average these equations over a representative finite volume (containing solid, liquid, and vapor). These equations are then used (along with constitutive relations) to solve the drying problem. One drawback to this method is that some of the terms obtained in the analysis are difficult to determine experimentally. Whitaker himself states that "what does appear overwhelmingly difficult at this point is the comparison between theory and experiment." He has suggested that some of these terms might be simplified for specific cases to enable independent verification. This author knows of no studies in which this has been done, although some numerical solutions have been performed in which simplifying assumptions (in addition to those made by Whitaker) have been employed (see Nasrallah and Perre, 1988).

Dyer and Sunderland(1968) obtained a closed form analytical solution to a drying problem in which a material is dried from one side. The solution essentially uses a quasi-stationary approximation which is common to solutions of melting-freezing problems. Both drying and melting-freezing problems may involve a front with different phases of a material on either side (in drying there is a liquid-vapor interface; in melting-freezing problems there is a liquid-solid interface). Basically, the method includes the assumption that the sensible heat is small compared to the latent heat. In their analysis, all heat and mass transfer were assumed to be one-dimensional, internal convection was neglected, and the porous region being dried was assumed to consist of a bundle of straight parrallel capillary tubes. This approach is obviously highly idealized and of limited applicability.

King(1968) and Harmathy(1969) developed models of the drying process using the concept of sorption isotherms. As mentioned previously, a sorption isotherm is a curve showing the equilibrium moisture content versus the relative humidity at constant temperature. Both authors assume that moisture movement takes place as a result of vapor diffusion only, and so they neglect movement of bound liquid. Their model is thus limited to the second falling rate stage of drying for cases where bound liquid movement is not significant.

Chen and Johnson(1969), Hussain, Chen, and Clayton(1970) and Hussain et al.(1970, 1972) presented analyses based on the method of Luikov(1964, 1965, 1966) to model the drying process in various agricultural products. Luikov uses relations from irreversible thermodynamics to express vapor and liquid fluxes in terms of temperature and concentration gradients. This approach is similar to that of Philip and DeVries (1957), although both works were performed independently. In his theory, Luikov introduces the moisture transfer potential,  $\Theta$  which is defined to be a function of moisture content and temperature such that

$$d\theta = \frac{\partial \theta}{\partial M} dM + \frac{\partial \theta}{\partial T} dT. \quad (2.3)$$

This term was intended to account for the mass transfer from one body to another in the presence of an adverse concentration gradient; that is, for mass transfer from a region of lower to a region higher concentration. This method has been criticized (Chen and Pei, 1988) because it lumps together a number of effects and thus tends to mask the actual physical processes involved.

Krischer (1963) proposed a model that allows for the movement of liquid via capillary flow and the movement of vapor by diffusion. Krischer assumed that all the diffusion coefficients are constant and that the sorption isotherm is a linear function of temperature. He also assumed that the

void volume,  $V_d$ , is independent of moisture content. This approach allowed Krischer to obtain a general solution to a drying problem for a case with simplified boundary conditions.

Berger and Pei (1973) extended Krischer's work by proposing that the Clausius-Clapyron equation replace the sorption isotherm relation when the moisture content is greater than the maximum sorptional value. They also employed boundary conditions deduced from mass and energy flux balances rather than the simplified conditions assumed by Krischer. Berger (1973) solved the resulting equations numerically and correctly predicted the start of the first falling rate phase for beds of glass beads. As drying proceeded, however, the model failed to correctly predict the drying rate, although the overall trends in behavior seem to be correct. Berger and Pei, as well as Krischer, used the assumption of constant diffusion coefficients. A more physically realistic approach might be to allow the diffusion coefficients to vary with both moisture content and temperature. The movement of bound moisture may also be important and should therefore be included in any model.

Chen (1987) and Chen and Pei (1988) have presented a method in which the movement of liquid by capillary effects, vapor movement by diffusion, and bound liquid movement are all included. The diffusional coefficients are allowed to vary

with both moisture content and temperature and the concept of bound liquid conductivity is introduced. The bound liquid flux is given by

$$J_b = -\rho_s D_b \nabla u^*, \quad (2.4)$$

where:

$D_b$  = the bound liquid conductivity.

The method is analogous to the use of two zone models in melting-freezing problems and utilizes a front tracking numerical scheme to solve the governing equations. Capillary movement is considered to be the dominant mechanism in the "wet" region of the porous medium (the region where free water exists) and a combination of vapor diffusion and bound liquid movement are assumed to predominate in the "sorption" region (the region where only vapor and bound liquid exist). This method was applied to the drying of wool, brick, and corn. The drying curve, the temperature and the moisture distributions were accurately predicted for all three of these materials. The drawback to this procedure is the front tracking scheme itself. Such schemes are generally complicated to implement and also are expensive in terms of computer time.

## 2.2. Studies Of Hay Drying

Since the application chosen for the present investigation involves the drying of hay, some studies specifically aimed at this problem will be discussed.

Bagnall, Miller, and Scott (1970) performed a combined numerical and experimental study of the drying of alfalfa stems. Their mathematical model consists of the simple diffusion equation with constant diffusion coefficients. They noted, however, that the diffusivity in the radial direction varies due to the different diffusivity of the cuticular layer (A thin, waxy layer surrounding the stem) and the diffusivity of the "other tissue." Bagnall et al. combined the cuticular diffusivity with the convection coefficient to obtain an "effective convection coefficient" for use in the boundary condition. This procedure does not take into account the transient nature of the problem and appears to be physically incorrect. The results obtained in their study, however, show that the axial diffusivity was on the order of  $10^{-5}$  ( $m^2/hr$ ), the radial diffusivity of the plant tissue was  $10^{-6}$  ( $m^2/hr$ ), and the radial diffusivity of the cuticular layer was  $10^{-9}$  ( $m^2/hr$ ). Since the cuticular diffusivity is four orders of magnitude smaller than the axial diffusivity, the moisture flow in the radial direction should be very small compared to that in the axial direction. Thus, the effect of incorrectly combining terms in the radial direction may also be small, and the results presented may be acceptable.

Ohm et al. (1971) studied heat and mass transfer in a ventilated hay stack. In this drying system, referred to as "barn-drying", a central vertical duct blows air radially through a hay stack. The bulk density, the porosity, and

other properties of the stack are assumed to vary with height. A method of predicting these variables as a function of height was proposed and a simplified procedure for obtaining a mass and energy balance was used to model the problem. The results show that the drying rate decreases significantly from the top to the bottom of the hay stack. It was therefore proposed to improve the drying rate by employing a conical duct to regulate the air flow through the stack.

Hill, Ross, and Barfield (1977) performed experiments to determine sorption isotherms for alfalfa hay and used these results to obtain a correlation for the time required to dry hay in the field. The sorption isotherm was obtained from experiments in which samples of alfalfa hay were exposed to air of controlled humidity and temperature. The temperature range studied was between 20 and 35°C.

Rotz and Chen (1985) studied the field drying of alfalfa hay and formulated an empirical correlation of the drying rate as a function of the environmental variables. A total of 13,000 sets of data over an eight year period were obtained during this study. The empirical model based on these data incorporates such factors as solar insolation, swath density, soil moisture content, humidity and air temperature. The drying rate for hay in the swath was determined to be most sensitive to solar insolation.

Bledsoe et al. (1985) studied a forced air drying system for large round hay bales. The drier studied consists of a barn equipped with an air duct system built into the floor. The bales are positioned over the duct outlets and solar heated air is then forced through the bales using fans. Caps were placed on the bales to prevent air flow out the tops of the bales. This procedure has been observed to improve the air flow characteristics of a bale and results in faster drying time. A "least drying streamtube" (a region where the moisture content has not reached an acceptable level) was seen to form along the centerline of the bale as well as radially outward in the upper portion of the bale (for capped bales). These authors emphasize the need for improved air flow distribution throughout the bale to help eliminate this problem. As currently operated the drier requires 2-4 days to dry bales with an initial moisture content of 35-45% (w.b.) and dry matter densities in the range of 64-128 kg/m<sup>3</sup> (4-8 lbm/ft<sup>3</sup>). Bales with densities greater than 64 kg/m<sup>3</sup> could not be dried quickly enough to prevent mold growth. The bales must have a moisture content less than 18% w.b. to be considered "dry". Thus, the study of Bledsoe et al. (1985) indicates that a more accurate model of the hay drying process is needed to improve the drying capability and efficiency of such systems.



### 2.3. Numerical Methods

Many different numerical techniques exist for solving sets of partial differential equations. The most commonly used methods fall into two broad categories: (1) finite difference methods and (2) finite element methods.

The finite difference methods are generally considered the easiest to apply (at least in cases where the geometry is "regular"; that is, in cases where physical surfaces of interest coincide with constant coordinate planes). Although many different solution schemes exist, the basic idea behind the various finite difference schemes is the same. The differential equation(s) to be solved is discretized. This discretization process results in a set of algebraic equations which are then solved simultaneously to obtain an approximate solution. The popularity of these methods results from the ease of the discretization process and from the widely available and easy to use solution algorithms for algebraic systems of equations.

Jaluria and Torrance (1986) have identified and described three basic methods for discretizing differential equations: (1) Direct Approximation, (2) Taylor Series, and (3) Finite Volume approaches.

In the Direct Approximation approach, the derivatives are simply replaced by difference ratios. For example,

$$\frac{\partial \phi}{\partial x} \approx \frac{\phi_{i+1} - \phi_i}{\Delta x}$$

These ratios are then substituted into the equations to obtain the algebraic system of equations to be solved.

In the Taylor Series method, derivatives are expressed in terms of a Taylor Series expansion. The truncation error resulting from the discretization process may thus be easily estimated.

The Finite Volume (or Control Volume) approach is particularly well-suited for the discretization of conservation laws (conservation of mass, for example). In this approach, which has been described in detail by Patankar (1980), one starts with the integral conservation statement. The domain is divided into many nonoverlapping control volumes and the integration is performed over each control volume. The solution variable is approximated in piece-wise form between grid points, thus allowing the integrals to be evaluated. The resulting equations have the advantage that the physical quantities are conserved over each control volume (and, therefore, globally over the entire domain). Thus, a coarse grid solution may be used in debugging a code. Once the code is working properly, a more refined grid may be used to obtain a more accurate solution.

The finite element method has been used for a number of years in structural mechanics and has been more recently applied to heat transfer and fluid mechanics problems as well. Baker (1983) has described the method as it applies to fluid mechanics and heat transfer in some detail. The main advantage

of the finite element method is that it may be applied to irregularly shaped geometries quite readily. The main disadvantage is that it is generally much harder to implement (see Jaluria and Torrance). The finite element method consists of subdividing a region in space into many smaller regions (which can be triangular, quadrilateral, etc. in shape). The differential equation is assumed to apply over each element and an interpolation function is then chosen. This function represents the assumed functional form the solution will have throughout each element. Using the interpolation function, the finite element equations governing each element are obtained. These are then "assembled" into a global matrix for all the elements. The system of equations is then solved to obtain an approximate solution.

The specific application being investigated in this dissertation concerns the drying of cylindrically shaped hay bales. These bales may in turn be assumed to consist of cylindrically shaped hay stalks. The geometry involved is thus "regular" if a cylindrical coordinate system is employed. Therefore, a finite difference method may be used, and the additional complexity involved in the finite element formulation may be avoided. Since the finite volume approach allows the conservation relations to hold for each element and is also quite easy to formulate, this method has been chosen to formulate the numerical model in this dissertation.

#### 2.4. Selection Of The Techniques To Be Employed In The Present Work

The papers reviewed concerning hay drying have indicated a need for an accurate model of the hay drying problem. Many authors have employed empirical correlations in an attempt to predict the drying times; however, these methods are extremely limited in applicability. Thus, the need exists for a method capable of accurately modeling the drying process. The model should be straightforward to implement and should be readily verified by experiment.

Several approaches to modeling the drying process have been tried; however, all are limited either in accuracy, range of applicability, or ease of implementation.

The diffusion theories of drying have been shown to be physically unrealistic and are very limited in scope. Similarly, any of the methods which assume that mass transfer occurs as a result of a single mechanism are limited due to the fact that other mechanisms of moisture movement exist and can make significant contributions to the overall drying.

Some of the theories proposed (such as those of McCready and McCabe (1933), Philip and DeVries (1957), and Krischer (1963)) involve some combination of mechanisms. However, these theories also have several shortcomings. Some assume that the coefficients involved in the governing equations are constant although these coefficients have been found to be functions of both moisture content and temperature. Others,

while allowing for variable coefficients, make assumptions which limit the applicability of their theories (such as Philip and DeVries (1957) whose assumptions imply continuous liquid paths, which is valid only in the constant and first falling rate phases of drying). At the same time, most of these theories ignore the possibility of bound liquid movement. Chen and Pei (1989) have formulated a theory which answers most of the objections raised previously. However, this method requires a front tracking numerical scheme which is both difficult to implement and costly in terms of computer time. Whitaker has rather extensively developed a quite general approach in which the governing conservation equations are volume averaged over a representative control volume. The major drawback to this method is that many of the terms appearing in the equations are difficult to determine experimentally. Thus, the theory is difficult to apply to practical situations.

One approach to the problems cited above is to modify an existing theory to address some of these objections. This was done by Berger and Pei (1973) in an attempt to generalize Krischer's (1963) theory. They succeeded in modeling the constant rate phase and in predicting the onset of the first falling rate phase of drying. Berger and Pei did not, however, allow for variable diffusion coefficients or for bound liquid movement. In addition, the numerical method used would not converge for realistic values of the convection coefficients.

Thus, their model does not correctly predict the drying rate during the falling rate phases. This method is very attractive, however, due to its simplicity and ease of (numerical) solution. Furthermore, as will be seen, it may be easily modified to incorporate the variable diffusion coefficients and to allow for movement of bound liquid. Once these modifications are made, this theory is applicable to a wide range of drying problems. Therefore, the approach adopted for the present work was to modify the model of Berger and Pei to include the effects of variable diffusion coefficients and to allow for the movement of bound liquid. The present method also allows for the solution of problems in which the drying medium has at least two characteristic length scales appear.

### 3. THE ANALYTICAL MODEL

#### 3.1. Physical Description Of The Problem

The problem under investigation involves the drying of a large round hay bale, which may be idealized as a porous medium that is comprised of porous elements containing the liquid to be removed. Thus, an essential feature of the present work is that it is concerned with a medium that has two disparate length scales. Specifically, it is desired to examine the case where drying is accomplished by forcing a heated stream of air through the global porous structure as shown schematically in Figure 3.1. The drying performed in this manner involves a simultaneous heat and mass transfer process coupled between the "inner" and "outer" porous structures. As stated previously, this type of configuration occurs in the drying of certain agricultural products; among them, the drying of hay. To fix ideas, the model will be developed with this application in mind.

Since there are two disparate length scales involved, it is convenient to define two regions, or domains, in the problem. The "inner domain" is defined to consist of the individual (cylindrical) solid elements making up the global porous structure and everything contained in these elements. The inner domain, then, is a porous structure containing a solid matrix, liquid water, water vapor, and air. Hay stalks have a "waxy" coating around the circumference which is very resistant to mass transfer. Thus, it is here assumed that

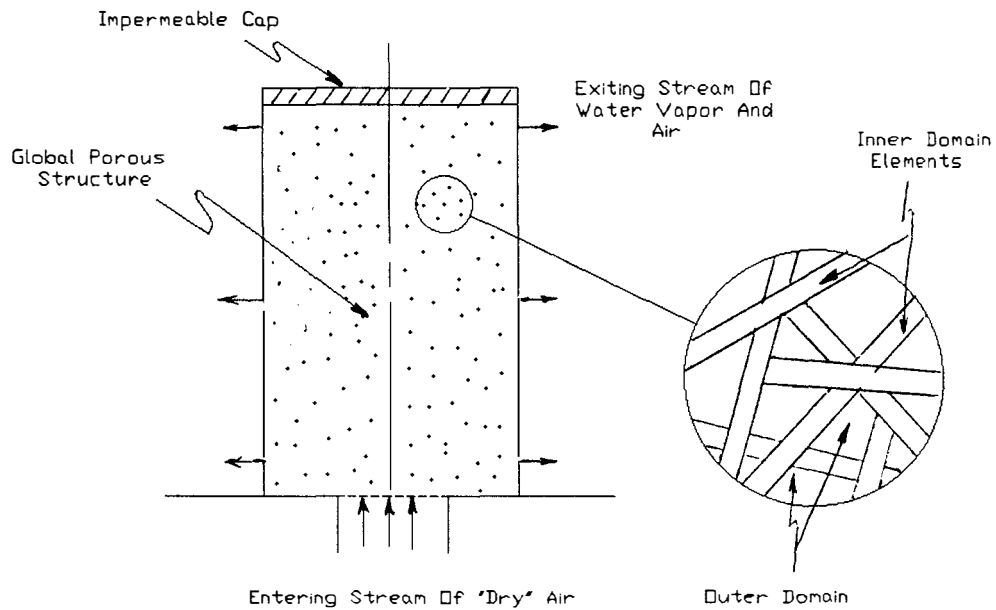


Figure 3.1. Schematic Of The Drying Problem To Be Modelled.

the inner domain processes may be treated as one-dimensional. The "outer domain" is considered to be everything external to the inner domain and internal to the global porous structure. The outer domain is thus comprised of only water vapor and air. The global porous structure thus includes the outer domain along with many (typically  $1.7 \times 10^6$ ) inner domain elements which are assumed to be randomly oriented throughout the global structure. The global porous structure and the inner domain elements are assumed to be right circular cylinders. In addition, there is assumed to be no angular variation of properties (or processes) within the global structure (i.e. the problem may be considered axisymmetric).



The drying process to be modelled proceeds as follows. A (heated) stream of relatively dry air is forced into the outer domain from an inlet located at the bottom of the global structure. As this stream of air flows through the outer domain, it convects heat to the inner domain elements. Some of this energy is used to vaporize the liquid water. The water vapor then diffuses through the inner domain and is then convected away at the boundary between the inner and outer domains by the air flowing through the outer domain.

The drying rate may be either convection limited (by the outer domain) or diffusion limited (by the inner domain) depending on the geometry and boundary conditions of the specific porous medium that is being dried. It should be noted, however, that the limiting mechanism may be different in different regions of the porous structure. Near the air inlet, the drying rate may be diffusion limited due to the relatively dry high-velocity air passing through this section of the structure. However, in the upper portion of the porous structure where the air velocity is quite low, the limiting process may be convection. Thus, a scheme that takes into account only one rate-limiting mechanism would probably not accurately portray the drying process, at least over a wide range of conditions.

Based on this physical description of the problem, a mathematical model of the drying process will be developed in the following sections. An attempt was made to keep the

mathematical formulation as general as possible, however, some assumptions were made for the specific application of interest here; namely, the drying of hay bales. All assumptions will be stated during the model development and then summarized and discussed in greater detail at the end of the chapter. Since the physical processes occurring are different in the two domains, each domain will be considered separately.

### 3.2. Derivation Of The Governing Equations For The Inner Domain

#### 3.2.1. Conservation Of Mass

As was stated previously, Krischer's model will be modified to compute the heat and mass transfer occurring in the inner domain. The previous modifications of Berger and Pei will also be incorporated into the present model. Thus, the current formulation is actually a modification of the method presented by Berger and Pei.

It is assumed that the dominant modes of mass transfer (for the inner domain) include capillary conduction of liquid, diffusion of water vapor, and movement of bound liquid. Additionally, it is assumed that the different phases (solid, liquid, and vapor) of the inner domain are in thermodynamic equilibrium and that the inner domain is an isotropic, homogeneous, porous medium.

Under these assumptions, Miller and Miller (1955) have shown that the capillary liquid flux may be written as

$$J_c = -\rho_s D_c^* \nabla u^* \quad (3.1)$$

The capillary conductivity,  $D_c^*$ , is (in general) a function of moisture content and temperature and will, therefore, not be regarded as constant.

Chen and Pei (1989) have shown that the bound liquid movement may also be expressed in terms of a moisture content gradient. The bound liquid flux takes the form,

$$J_b = -\rho_s D_b^* \nabla u^* \quad (3.2)$$

The bound liquid conductivity,  $D_b^*$ , is also a function of moisture content and temperature. Implicit in their development is the assumption that temperature gradients are negligible. Thus, it is here assumed that no significant temperature gradients exist within the inner domain. This assumption does not rule out the possibility of heat transfer by convection from the outer domain to the inner domain or by conduction through the inner domain.

Note that the application of equations 3.1 and 3.2 is limited to specific drying regimes. Capillary conduction will occur only in regions where continuous streams of free liquid are present. Similarly, bound water movement will be significant only in regions where no free water exists (see Chen and Pei, 1989). Since it is desirable to avoid a front tracking scheme, a method of incorporating these two modes

of moisture transfer into the model must be devised. The dependance of both terms on the moisture content gradient suggests formulating a liquid movement term of the form

$$J_L = -\rho_s D_L^* \nabla u^* \quad (3.3)$$

where the liquid conductivity,  $D_L^*$  is assumed to be a function of moisture content and temperature and must be determined from experimental data. This is somewhat of a moot point in the present application since the initial moisture content of the hay is such that all the liquid is bound from the start. However, in problems involving higher initial moisture contents, it should be possible to obtain a relation for  $D_L^*(u, T)$  over the entire ranges of moisture content of interest.

The vapor diffusive flux may be written as

$$J_v = -\frac{D_v^* \epsilon_v^*}{RT_i^*} \nabla P_v^* \quad (3.4)$$

Noting that

$$\epsilon_v^* = \left( \epsilon^* - \frac{\rho_s}{\rho_L} u^* \right) \quad (3.5)$$

and again assuming that temperature gradients are negligible results in

$$J_v = -D_v^* \left( \epsilon^* - \frac{\rho_s}{\rho_L} u^* \right) \nabla \left( \frac{P_v^*}{RT_i^*} \right) = -D_v^* \left( \epsilon^* - \frac{\rho_s}{\rho_L} u^* \right) \nabla \rho_{iv}^* \quad (3.6)$$

With the mass flux terms identified, a mass balance over a differential element (Note: The term "differential element" in this work does not refer to an arbitrarily small volume.

The volume must be large enough so that quantities such as porosity retain their meaning. See Bear, 1972) shown in Figure 3.2 gives:

$$\left[ \begin{array}{c} \text{Mass Flow} \\ \text{Rate In} \end{array} \right] = \left[ \begin{array}{c} \text{Mass Flow} \\ \text{Rate Out} \end{array} \right] + \left[ \begin{array}{c} \text{Rate Of Change} \\ \text{Of Mass Stored} \end{array} \right] \quad (3.7)$$

$$\begin{aligned} J_L + J_v &= \left( J_L + \frac{\partial J_L}{\partial z_i^*} dz_i^* \right) + \left( J_v + \frac{\partial J_v}{\partial z_i^*} dz_i^* \right) + \frac{\partial(\rho_s u^*)}{\partial t^*} dz_i^* \\ &+ \frac{\partial}{\partial t^*} \left[ \left( \epsilon^* - \frac{\rho_s}{\rho_L} u^* \right) \rho_{iv}^* \right] dz_i^* \end{aligned} \quad (3.8)$$

or,

$$- \frac{\partial J_L}{\partial z_i^*} - \frac{\partial J_v}{\partial z_i^*} = \rho_s \frac{\partial u^*}{\partial t^*} + \frac{\partial}{\partial t^*} \left[ \left( \epsilon^* - \frac{\rho_s}{\rho_L} u^* \right) \rho_{iv}^* \right]. \quad (3.9)$$

Substitution of equations 3.3 and 3.6 into equation 3.9 and assuming that the porosity is not a function of time (rigid solid) yields

$$\begin{aligned} - \frac{\partial}{\partial z_i^*} \left[ -\rho_s D_L^* \frac{\partial u^*}{\partial z_i^*} \right] - \frac{\partial}{\partial z_i^*} \left[ -D_v^* \left( \epsilon^* - \frac{\rho_s}{\rho_L} u^* \right) \frac{\partial \rho_{iv}^*}{\partial z_i^*} \right] &= \rho_s \frac{\partial u^*}{\partial t^*} + \\ &\frac{\partial}{\partial t^*} \left[ \left( \epsilon^* - \frac{\rho_s}{\rho_L} u^* \right) \rho_{iv}^* \right], \end{aligned} \quad (3.10)$$

or,

$$\begin{aligned} \frac{\partial}{\partial z_i^*} \left[ \rho_s D_L^* \frac{\partial u^*}{\partial z_i^*} + D_v^* \left( \epsilon^* - \frac{\rho_s}{\rho_L} u^* \right) \frac{\partial \rho_{iv}^*}{\partial z_i^*} \right] &= \rho_s \left( 1 - \frac{\rho_{iv}^*}{\rho_L} \right) \frac{\partial u^*}{\partial t^*} + \\ &\left( \epsilon^* - \frac{\rho_s}{\rho_L} u^* \right) \frac{\partial \rho_{iv}^*}{\partial t^*}. \end{aligned} \quad (3.11)$$

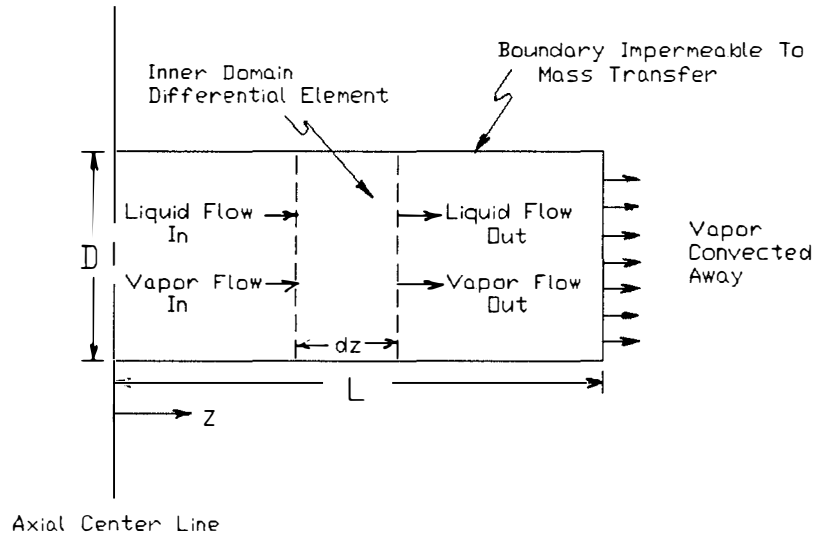


Figure 3.2. Mass Balance And Nomenclature For A Differential Element Of The Inner Domain.

### 3.2.2. Conservation Of Energy

To develop an expression for energy conservation, a differential element is again considered. Energy transfer may take place as a result of convection heat transfer, evaporation of liquid, and heat conduction (radiation heat transfer is assumed to be negligible).

The conductive term may be thought of as being composed of contributions from two sources. The first arises from the conduction of heat through an inner domain element (hereafter referred to as "local" conduction heat transfer) and, the second from the conduction through the global porous structure (hereafter referred to as "global" conduction heat transfer). The global conduction term results from the physical contact of many inner domain elements. The problem of how to handle this global contribution is greatly complicated by the fact

that the points of contact with other elements are not known. Even if this geometry could be specified for every element, the mathematical treatment of such a problem would be so complex that it would not be feasible.

A simplified treatment of this phenomenon is formulated here by considering a succession of porous media. In one limit, the global porous structure may be thought of as containing only a single inner domain element. In this case, there is no global, or element-to-element, conduction. If a second element is added so that there are two elements in contact (at least at one point), then global conduction occurs due to any temperature difference between the two elements. For a control volume surrounding only the first element, global conduction appears to be an energy source (sink) at the point(s) of contact. As more elements are added, these energy sources (sinks) become distributed more closely along the length of the first element. In the limiting case, the energy sources (sinks) are distributed along the entire length of the element. Provided that the amount of heat conducted to an element from the neighboring elements is approximately constant, the global conduction term may be treated as an evenly distributed energy source along the entire length of the element.

For many porous media, there are indeed a large number of elements in a small volume and thus there will be many contact points. It is assumed, then, that the global

conduction term may be adequately modelled as an energy source (sink) of constant strength distributed along the entire length of the element. This approximation is admittedly simplistic and is employed only to include one possible treatment of the conductive load. In the present application, it is anticipated that the convective contribution to total heat transfer to an element will dominate. In other applications in which conduction dominates, a more detailed assessment of this term may be required.

An energy balance on a differential element (Figure 3.3) in the inner domain gives:

$$\left[ \begin{array}{c} \text{Rate At Which} \\ \text{Energy Enters} \\ \text{The Element} \end{array} \right] = \left[ \begin{array}{c} \text{Rate At Which} \\ \text{Energy Leaves} \\ \text{The Element} \end{array} \right] + \left[ \begin{array}{c} \text{Rate Of Change} \\ \text{Of Energy Stored} \\ \text{In The Element} \end{array} \right]. \quad (3.12)$$

The energy balance may also be written as

$$\left[ \begin{array}{c} \text{Rate At Which} \\ \text{Energy Enters The Element} \\ \text{From The "Source" Term} \end{array} \right] + \left[ \begin{array}{c} \text{Rate At Which} \\ \text{Energy Is Conducted} \\ \text{Into The Element} \end{array} \right] + \left[ \begin{array}{c} \text{Rate At Which} \\ \text{Energy Is Convected} \\ \text{To (From) The Element} \end{array} \right] + \left[ \begin{array}{c} \text{Rate At Which} \\ \text{Latent Heat Is} \\ \text{Used In The Element} \end{array} \right] = \left[ \begin{array}{c} \text{Rate At Which} \\ \text{Energy Is Conducted} \\ \text{Out Of The Element} \end{array} \right] + \left[ \begin{array}{c} \text{Rate Of Change} \\ \text{Of Energy Stored} \\ \text{In The Element} \end{array} \right] \quad (3.13)$$



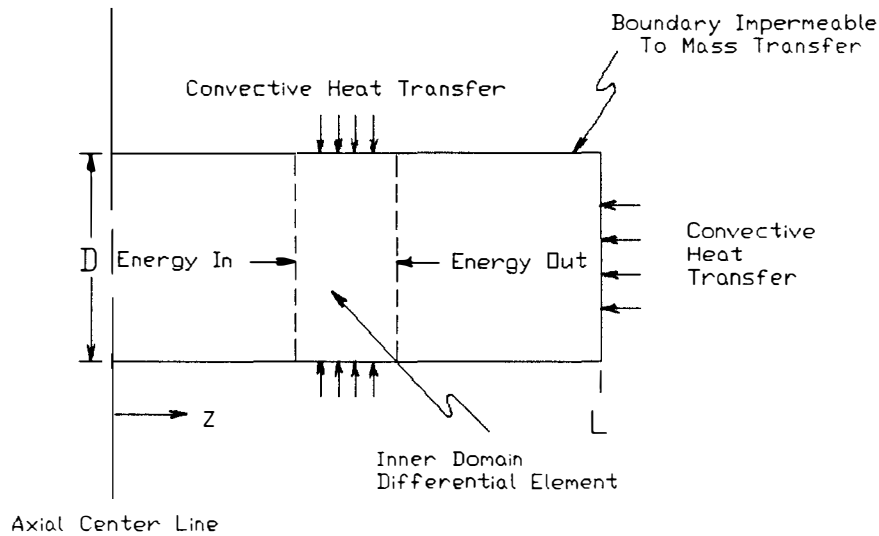


Figure 3.3. Energy Balance On A Differential Element Of The Inner Domain.

or,

$$q_s''' Adz_i^* - K_s A \frac{\partial T_s^*}{\partial z_i^*} + h_c (T_A^* - T_i^*) P' dz_i^* - \dot{m}_{ev} L_v Adz_i^* =$$

$$\left[ -K_s A \frac{\partial T_i^*}{\partial z_i^*} - \frac{\partial}{\partial z_i^*} \left( K_s A \frac{\partial T_i^*}{\partial z_i^*} \right) dz_i^* \right] + \rho_s C_s \frac{\partial T_i^*}{\partial t} dz_i^*. \quad (3.14)$$

To obtain an expression for  $\dot{m}_{ev}$  a mass balance on the vapor phase in the element is performed. This yields

$$\left[ \begin{array}{c} \text{Rate At Which Liquid} \\ \text{Is Evaporated In} \\ \text{The Element} \end{array} \right] + \left[ \begin{array}{c} \text{Mass Flow Rate Of} \\ \text{Vapor Into The} \\ \text{Element} \end{array} \right] =$$

$$\left[ \begin{array}{c} \text{Mass Flow Rate Of} \\ \text{Vapor Out Of} \\ \text{The Element} \end{array} \right] + \left[ \begin{array}{c} \text{Rate Of Change Of The} \\ \text{Mass Of Vapor Stored} \\ \text{In The Element} \end{array} \right], \quad (3.15)$$

$$\begin{aligned} \dot{m}_{ev} A dz_i^* - D_v^* A \left( \epsilon^* - \frac{\rho_s}{\rho_L} u^* \right) \frac{\partial \rho_{iv}^*}{\partial z_i^*} &= \left\{ -D_v^* A \left( \epsilon^* - \frac{\rho_s}{\rho_L} u^* \right) \frac{\partial \rho_{iv}^*}{\partial z_i^*} - \right. \\ &\left. \frac{\partial}{\partial z_i^*} \left[ D_v^* A \left( \epsilon^* - \frac{\rho_s}{\rho_L} u^* \right) \frac{\partial \rho_{iv}^*}{\partial z_i^*} \right] dz_i^* \right\} + \frac{\partial}{\partial t^*} \left[ \left( \epsilon^* - \frac{\rho_s}{\rho_L} u^* \right) \rho_{iv}^* \right] A dz_i^*, \end{aligned} \quad (3.16)$$

or,

$$\dot{m}_{ev} = -\frac{\partial}{\partial z_i^*} \left[ D_v^* \left( \epsilon^* - \frac{\rho_s}{\rho_L} u^* \right) \frac{\partial \rho_{iv}^*}{\partial z_i^*} \right] + \frac{\partial}{\partial t^*} \left[ \left( \epsilon^* - \frac{\rho_s}{\rho_L} u^* \right) \rho_{iv}^* \right]. \quad (3.17)$$

Substituting equation 3.17 into 3.14 yields

$$\begin{aligned} q_s''' + h_c (T_a - T_i) \frac{P'}{A} + L_v \left\{ \frac{\partial}{\partial z_i^*} \left[ D_v^* \left( \epsilon^* - \frac{\rho_s}{\rho_L} u^* \right) \frac{\partial \rho_{iv}^*}{\partial z_i^*} \right] - \frac{\partial}{\partial t^*} \left[ \left( \epsilon^* - \frac{\rho_s}{\rho_L} u^* \right) \rho_{iv}^* \right] \right\} \\ + \frac{\partial}{\partial z_i^*} \left( K_s \frac{\partial T_i^*}{\partial z_i^*} \right) = \rho_s C_s \frac{\partial T_i^*}{\partial t^*}. \end{aligned} \quad (3.18)$$

Assuming  $K_s$  is constant, and rewriting equation 3.18 gives

$$\begin{aligned} \frac{\partial T_i^*}{\partial t^*} &= \alpha_s \frac{\partial^2 T_i^*}{\partial z_i^{*2}} + \frac{L_v}{\rho_s C_s} \left\{ \frac{\partial}{\partial z_i^*} \left[ D_v^* \left( \epsilon^* - \frac{\rho_s}{\rho_L} u^* \right) \frac{\partial \rho_{iv}^*}{\partial z_i^*} \right] - \frac{\partial}{\partial t^*} \left[ \left( \epsilon^* - \frac{\rho_s}{\rho_L} u^* \right) \rho_{iv}^* \right] \right\} \\ &+ \frac{h_c}{\rho_s C_s} \frac{P'}{A} (T_a - T_i) + \frac{q_s'''}{\rho_s C_s}. \end{aligned} \quad (3.19)$$

The boundary conditions for equations 3.11 and 3.19 are obtained by performing flux balances on the boundaries of the inner domain. Assuming that  $z=0$  is a plane of symmetry, allows one to write

$$\rho_s D_L^* \frac{\partial u^*}{\partial z_i^*} = 0, \quad (3.20)$$

$$D_v^* \left( \epsilon^* - \frac{\rho_s}{\rho_L} u^* \right) \frac{\partial \rho_{iv}^*}{\partial z_i^*} = 0, \quad (3.21)$$

and,

$$K_s \frac{\partial T^*}{\partial z_i^*} = 0. \quad (3.22)$$

A mass balance at  $z=L$  gives

$$\rho_s D_L^* \frac{\partial u^*}{\partial z_i^*} + D_v^* \left( \epsilon^* - \frac{\rho_s}{\rho_L} u^* \right) \frac{\partial \rho_{iv}^*}{\partial z_i^*} = h_m (\rho_{va} - \rho_{iv}^*). \quad (3.23)$$

An energy balance at  $z=L$  results in

$$K_s \frac{\partial T_i^*}{\partial z_i^*} - L_v \rho_s D_L^* \frac{\partial u^*}{\partial z_i^*} = h_c (T_a - T_i^*). \quad (3.24)$$

The initial conditions are

$$u^* = u_0^* \quad 0 \leq z_i \leq L, \quad (3.25)$$

$$\rho_{iv}^* = \rho_{iv0}^* \quad 0 \leq z_i \leq L, \quad (3.26)$$

and,

$$T^* = T_{i0}^* \quad 0 \leq z_i \leq L. \quad (3.27)$$

### 3.2.3. Equation Of State

Equations 3.11 and 3.19 form a system of two equations in the three unknowns,  $u^*, \rho_{iv}^*, T_i^*$ . Therefore, another relation is needed to mathematically complete the model. Berger and Pei have noted that the liquid content and partial vapor pressure (and, hence, vapor density) are independent for moisture contents greater than the maximum sorptional moisture content ( $u_{ms}^*$ ). For this reason, two different equations of state will be needed depending on the moisture content of the inner domain.

For moisture contents above  $u_{ms}$ , Berger and Pei (1973) proposed using the Clausius-Clapyron equation, which is given by

$$\rho_{iv}^* = \frac{1}{RT_i^*} e^{\left(\alpha + \frac{b}{T_i^*} + c \ln T_i^*\right)}. \quad (3.28)$$

For moisture contents below  $u_{ms}$ , the sorptional isotherm provides the necessary relation. This curve must be determined experimentally and may be written as

$$\frac{P_v^*}{P_{vs}^*} = \frac{\rho_{iv}^*}{\rho_{vs}^*} = f(u^*, T_i^*). \quad (3.29)$$

The coupling relation may thus be written as

$$\rho_{iv}^* = \rho_{vs}^* f(u^*, T_i^*) \quad u^* \leq u_{ms}, \quad (3.30a)$$

or,

$$\rho_{iv}^* = \frac{1}{RT_i^*} e^{\left[\alpha + \frac{b}{T_i^*} + c \ln T_i^*\right]} \quad u^* > u_{ms}. \quad (3.30b)$$

Thus, the two governing equations (3.11 and 3.19), the equation of state (equation 3.30), the boundary conditions (equations 3.20 - 3.24), and the initial conditions (equations 3.25 - 3.27) provide the complete mathematical statement of the coupled heat and mass transfer problem for the inner domain. Examination of these equations reveals that the heat and mass transfer processes in the inner domain are coupled to those in the outer domain as they must be. Thus, the solution of the governing equations for the inner domain requires the simultaneous solution of the governing equations

for the outer domain. It should also be emphasized that the diffusion coefficients,  $D_i^*$  and  $D_v^*$ , are not assumed constants, but are allowed to vary with both the moisture content and temperature. These functions are dependent upon the specific porous media being considered and should be determined from experimental data.

#### 3.2.4. Nondimensionalization Of The Governing Equations, Boundary Conditions, and Initial Conditions For The Inner Domain

Identification of the nondimensional parameters that affect the solution field in the inner domain may be achieved by non-dimensionalizing the governing equations, the boundary conditions, and the initial conditions. Thus, the following nondimensional variables are defined for the inner domain:

$$z_i = \frac{z_i^*}{L} = \begin{array}{l} \text{Nondimensional Spatial} \\ \text{Coordinate} \end{array}, \quad (3.31)$$

$$\rho_{iv} = \frac{\rho_{iv}^* - \rho_{ve}^*}{\rho_{ve}^* - \rho_{vo}^*} = \frac{\rho_{iv}^* - \rho_{ve}^*}{\Delta \rho_v} = \begin{array}{l} \text{Nondimensional Vapor} \\ \text{Density} \end{array}, \quad (3.32)$$

$$u = \frac{u^* - u_e^*}{u_e^* - u_o^*} = \frac{u^* - u_e^*}{\Delta u} = \begin{array}{l} \text{Nondimensional Moisture} \\ \text{Content} \end{array}, \quad (3.33)$$

$$t = \frac{\alpha_s t^*}{L^2} = \begin{array}{l} \text{Nondimensional} \\ \text{Time} \end{array}, \quad (3.34)$$

$$T_i = \frac{T_e^* - T_i^*}{T_e^* - T_o^*} = \frac{T_e^* - T_i^*}{\Delta T} = \begin{array}{l} \text{Nondimensional} \\ \text{Temperature} \end{array}, \quad (3.35)$$

$$q_s = \frac{q_s^* L^2}{K_s \Delta T} = \begin{array}{l} \text{Nondimensional Source} \\ \text{Term} \end{array}, \quad (3.36)$$

$$D_L = \frac{D_L^*}{D_{Lr}^*} = \begin{array}{l} \text{Nondimensional Liquid} \\ \text{Conductivity} \end{array}, \quad (3.37)$$

$$D_v = \frac{D_v^*}{D_{vr}^*} = \begin{array}{l} \text{Nondimensional Vapor} \\ \text{Conductivity} \end{array}, \quad (3.38)$$

$$\epsilon = \frac{\epsilon^* - \frac{\rho_s}{\rho_L} u_e^*}{\Delta u} = \begin{array}{l} \text{"Nondimensional"} \\ \text{Porosity} \end{array}. \quad (3.39)$$

Rewriting equation 3.11 for conservation of mass in terms of these nondimensional variables gives

$$\begin{aligned} \frac{\partial}{\partial z_i} \left[ Lu_L \left( \frac{\rho_s}{\Delta \rho_v} \right) D_L \frac{\partial u}{\partial z_i} + Lu_v \left( \epsilon - \frac{\rho_s}{\rho_L} u \right) D_v \frac{\partial \rho_{iv}}{\partial z_i} \right] &= \left( \frac{\rho_s}{\Delta \rho_v} \right) \left( 1 - \frac{\rho_{ve} + \Delta \rho_v \rho_{iv}}{\rho_L} \right) \frac{\partial u}{\partial t} \\ + \left( \epsilon - \frac{\rho_s}{\rho_L} u \right) \frac{\partial \rho_{iv}}{\partial t}. \end{aligned} \quad (3.40)$$

Similarly, rewriting the equations for conservation of energy (3.19) and the equation of state in nondimensional form gives

$$\begin{aligned} \frac{\partial T_i}{\partial t} &= \frac{\partial^2 T_i}{\partial z_i^2} - Ko \left( \frac{\Delta \rho_v}{\rho_s} \right) \left\{ Lu_v \frac{\partial}{\partial z_i} \left[ D_v \left( \epsilon - \frac{\rho_s}{\rho_L} u \right) \frac{\partial \rho_{iv}}{\partial z_i} \right] + \frac{(\rho_{ve} + \Delta \rho_v \rho_{iv}) \left( \frac{\rho_s}{\rho_L} \right) \frac{\partial u}{\partial t}}{\Delta \rho_v} \right. \\ &- \left. \left( \epsilon - \frac{\rho_s}{\rho_L} u \right) \frac{\partial \rho_{iv}}{\partial t} \right\} + Bi \left( \frac{P'L}{A} \right) (T_a - T_i) - q_s, \end{aligned} \quad (3.41)$$

and,

$$\rho_{iv} = f'(u, T) \text{ for } u \leq u_{ms}, \quad (3.42a)$$

or,

$$\rho_{iv} = \frac{1}{\Delta \rho_v R (T_e - \Delta T T_i)} e^{\left[ a + \frac{b}{(T_e - \Delta T T_i)^*} + c \ln(T_e - \Delta T T_i) \right]} \text{ for } u > u_{ms}, \quad (3.42b)$$

where:

$$f'(u, T) = \frac{\rho_{vs} f(u^*, T_i^*) - \rho_{ve}}{\Delta \rho_v}. \quad (3.43)$$

Rewriting the boundary conditions in terms of the nondimensional variables gives

$$\frac{\partial u}{\partial z_i} = 0 \quad \text{at } z_i = 0, \quad (3.44)$$

$$\frac{\partial \rho_{iv}}{\partial z_i} = 0 \quad \text{at } z_i = 0, \quad (3.45)$$

$$\frac{\partial T_i}{\partial z_i} = 0 \quad \text{at } z_i = 0 \quad (3.46)$$

$$\Delta u \left[ \left( \frac{\rho_s}{\Delta \rho_v} \right) (Lu_v) D_L \frac{\partial u}{\partial z_i} + (Lu_v) D_v \left( \epsilon - \frac{\rho_s}{\rho_L} u \right) \frac{\partial \rho_{iv}}{\partial z_i} \right] = \text{Bi}_m (\rho_{va} - \rho_{iv}) \quad \text{at } z_i = 1, \quad (3.47)$$

and,

$$\frac{\partial T_i}{\partial z_i} + \text{Ko} (Lu_L) D_L \frac{\partial u}{\partial z_i} = \text{Bi}_m (T_a - T_i) \quad \text{at } (z_i = 1). \quad (3.48)$$

Finally, rewriting the initial conditions in terms of the nondimensional variables yields

$$\rho_{iv} = 1 \quad \text{for } 0 \leq z_i \leq 1, \quad (3.49)$$

$$u = 1 \quad \text{for } 0 \leq z_i \leq 1, \quad (3.50)$$

and,

$$T_i = 1 \quad \text{for } 0 \leq z_i \leq 1. \quad (3.51)$$

The dimensionless parameters appearing above are defined as follows:

$$Lu_L = \frac{D_{Lr}}{\alpha_s} = \text{Luikov Number For Liquid}, \quad (3.52)$$

$$Lu_v = \frac{D_{vr}}{\alpha_s} = \text{Luikov Number for Vapor}, \quad (3.53)$$

$$Ko = \frac{L_v \Delta u}{C_s \Delta T} = \text{Kossovich Number,} \quad (3.54)$$

$$Bi = \frac{h_c L}{K_s} = \text{Biot Number,} \quad (3.55)$$

$$Bi_m = \frac{h_m L}{\alpha_s} = \text{Modified Mass Transfer Biot Number.} \quad (3.56)$$

These parameters, as well as those appearing in the outer domain, will be summarized and the physical significance of each discussed in the section below entitled "Summary of Analytical Model." Note that some of the parameters identified above depend on quantities (such as  $Re_\kappa, Pr$ ) which appear in the outer domain equations. Therefore, some of these parameters are not independent parameters in this problem. Once the dimensionless form of the outer domain equations has been obtained, this facet of the analysis will be discussed in more detail.

### 3.3. Derivation Of The Governing Equations For The Outer Domain

A homogeneous porous medium is one in which the properties of the medium do not vary with position (Bear 1972). An isotropic porous medium, however, is a medium in which the properties do not exhibit directional dependence. As stated previously, the global porous structure is assumed to be composed of randomly oriented inner domain elements. The distribution of these elements (and, hence, of the porosity and permeability) may vary with position. Thus, the global



porous structure is (in general) nonhomogeneous. Since the inner domain elements are randomly distributed, there is no directional dependence and the global structure may be considered isotropic. In addition, the solid structure is assumed to be rigid so that the porosity will not vary with time.

Water is removed from the inner domain in the vapor phase which is then convected to the outer domain. Thus, the outer domain is composed of dry air and water vapor. For a typical case considered in the present work, the liquid removal occurs over a period of days so that the rate of change of the mass of water vapor in the outer domain is extremely small. Since the volumetric flow rate of water vapor is small compared to the flow rate of air ("typically" this ratio is approximately  $1.5 \times 10^{-3}$  ), it is assumed that the forced air flow through the outer domain will not be significantly affected. It is also assumed that natural convection effects and mass diffusion effects are negligible. With these assumptions the mathematical model may be formulated as described below.

In obtaining an expression for the conservation of mass within the outer domain, the flows of dry air and water vapor will be considered separately. Equations for the conservation of air and water vapor are obtained by considering a mass balance through a differential element as shown in Figure 3.4. For dry air, conservation of mass may be written as

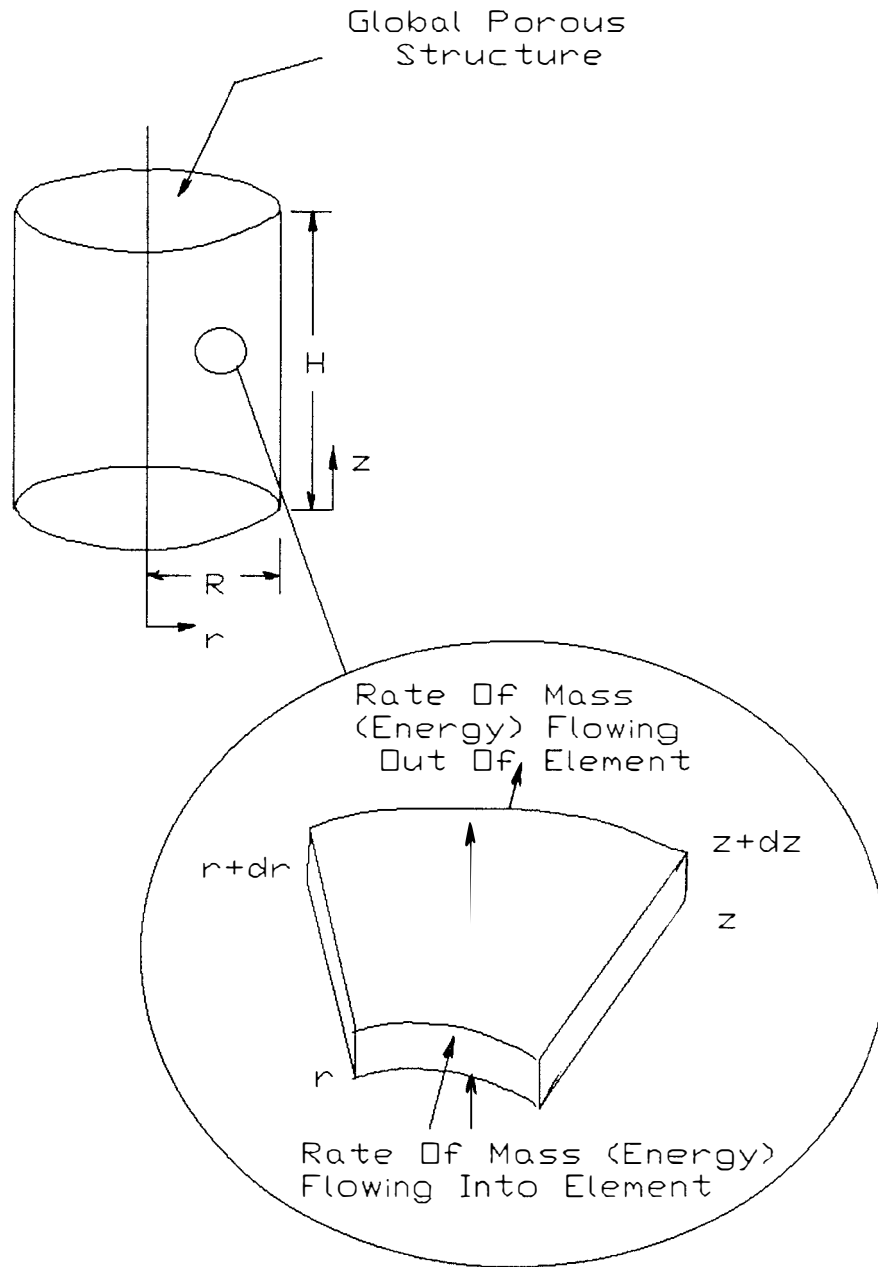


Figure 3.4. Mass And Energy Balances On A Differential Element Of The Outer Domain.

$$\frac{1}{r^*} \frac{\partial}{\partial r^*} (r^* \epsilon^* V_r^*) + \frac{\partial}{\partial z^*} (\epsilon^* V_z^*) = 0. \quad (3.57)$$

Note that since the mass transfer and natural convection effects have been assumed negligible, the velocity field may be considered steady in time.

Since the density of water vapor directly influences the mass transfer from the inner domain, conservation of mass must be applied to the water vapor separately to determine its density distribution. Again, considering a differential element, the equation of conservation of mass may be written as

$$\epsilon^* \frac{\partial \rho_v^*}{\partial t^*} + \frac{1}{r^*} \frac{\partial}{\partial r^*} (r^* \epsilon^* \rho_v^* V_r^*) + \frac{\partial}{\partial z^*} (\rho_v^* \epsilon^* V_z^*) = S_{\text{mass}} \quad (3.58)$$

where  $S_{\text{mass}}$  is the volumetric mass source that represents the transfer of water vapor from the inner domain to the outer domain. This mass source may be expressed as

$$S_{\text{mass}} = \frac{h_m (\rho_{iv}^* - \rho_v^*) N_{ID} A_s^*}{V_{CV}}. \quad (3.59)$$

Substitution of the above relation into equation 3.57 gives

$$\epsilon^* \frac{\partial \rho_v^*}{\partial t^*} + \frac{1}{r^*} \frac{\partial}{\partial r^*} (r^* \epsilon^* \rho_v^* V_r^*) + \frac{\partial}{\partial z^*} (\epsilon^* \rho_v^* V_z^*) = \frac{h_m (\rho_{iv}^* - \rho_v^*) N_{ID} A_s^*}{V_{CV}}. \quad (3.60)$$

Implicit in this equation is the assumption that the water vapor and dry air are "well mixed"; that is, both the water vapor and dry air have the same velocity at any point in the outer domain.

For a porous medium, Newton's Second Law may be replaced by Darcy's Law (Bear, 1972, Scheidegger, 1960). Darcy's Law is based on the experimental observation that the pressure drop across a porous medium is proportional to the velocity (at low  $Re_v$ ). At higher  $Re_v$ , inertial effects become important and the pressure drop becomes proportional to the velocity squared. The so-called Forchheimer term is then added to Darcy's Law to describe this flow regime. Several authors have presented experimental and theoretical discussions of Darcy's Law when inertial effects are taken into account (Niield and Joseph, 1985, Joseph, Niields, and Papanicolaou, 1982, Beavers and Sparrow, 1969, Bachmat, 1967, and Irmay, 1958). Based on the discussion of Niields and Joseph (1985), Darcy's Law with inertial effects included may be written as

$$-\frac{\partial P^*}{\partial r^*} = \frac{\mu}{\kappa^*} V_r^* + b^* |\overline{V^*}| V_r^*, \quad (3.61)$$

and,

$$-\frac{\partial P^*}{\partial z^*} = \frac{\mu}{\kappa^*} V_z^* + b^* |\overline{V^*}| V_z^*. \quad (3.62)$$

Equations 3.57, 3.61, and 3.62 form a system of three equations in the three unknowns  $V_r^*$ ,  $V_z^*$ , and  $P^*$ . Thus, the velocity and pressure fields may be determined separately from the solution of the vapor density and temperature fields.

The energy equation is found by considering an energy balance on a differential element as shown in Figure 3.4. The energy equation may be written as

$$\begin{aligned}
& \left[ \begin{array}{l} \text{Rate At Which} \\ \text{Energy Enters Element} \\ \text{From "Source" Terms} \end{array} \right] + \left[ \begin{array}{l} \text{Rate At Which} \\ \text{Energy Is Convected} \\ \text{Into The Element} \end{array} \right] + \\
& \left[ \begin{array}{l} \text{Rate At Which} \\ \text{Energy Is Conducted} \\ \text{Into The Element} \end{array} \right] + \left[ \begin{array}{l} \text{Rate At Which} \\ \text{Energy Is Convected} \\ \text{Out Of The Element} \end{array} \right] + \\
& \left[ \begin{array}{l} \text{Rate At Which} \\ \text{Energy Is Conducted} \\ \text{Out Of The Element} \end{array} \right] + \left[ \begin{array}{l} \text{Rate Of Change} \\ \text{Of Energy Stored} \\ \text{In The Element} \end{array} \right] . \quad (3.63)
\end{aligned}$$

or,

$$\begin{aligned}
& q_a''' [(r+dr)^2 - r^2] \frac{d\theta}{2} dz + \left[ (\rho_a \epsilon^* V_r T) - K_a \epsilon^* \frac{\partial T}{\partial r} \right] r d\theta dz \\
& + \left[ (\rho_a \epsilon^* V_z T) - K_a \epsilon^* \frac{\partial T}{\partial z} \right] [(r+dr)^2 - r^2] \frac{d\theta}{2} = \left[ (\rho_a \epsilon^* V_z T) \right. \\
& + \left. \frac{\partial}{\partial r} (\rho_a \epsilon^* V_r T) dr - K_a \epsilon^* \frac{\partial T}{\partial r} - \frac{\partial}{\partial r} \left( K_a \epsilon^* \frac{\partial T}{\partial r} dr \right) \right] (r+dr) d\theta dz \\
& + \left[ (\rho_a \epsilon^* V_z T) + \frac{\partial}{\partial z} (\rho_a \epsilon^* V_z T) dz - K_a \epsilon^* \frac{\partial T}{\partial z} - \frac{\partial}{\partial z} \left( K_a \epsilon^* \frac{\partial T}{\partial z} \right) dz \right] [(r+dr)^2 \\
& - r^2] \frac{d\theta}{2} + \frac{\partial}{\partial t} (\rho_a C_{pa} \epsilon^* T) [(r+dr)^2 - r^2] \frac{d\theta}{2} dz. \quad (3.64)
\end{aligned}$$

Equation 3.64 may be rewritten as

$$\begin{aligned}
& \frac{\partial}{\partial t} (\rho_a C_{pa} \epsilon^* T^*) + \frac{1}{r^*} \frac{\partial}{\partial r^*} (\epsilon^* \rho_a C_{pa} r^* V_r^* T^*) + \frac{\partial}{\partial z^*} (\epsilon^* \rho_a C_{pa} V_z^* T^*) \\
& = \frac{1}{r^*} \frac{\partial}{\partial r^*} \left( \epsilon^* r^* K_a \frac{\partial T^*}{\partial r^*} \right) + \frac{\partial}{\partial z^*} \left( \epsilon^* K_a \frac{\partial T^*}{\partial z^*} \right) + q_a''' \quad (3.65)
\end{aligned}$$

The volumetric source term,  $q_a'''$ , includes the energy transferred by convection to the inner domain as well as any heat sources that may be present.

Assuming that no significant energy sources are present in the outer domain and that the fluid properties may be considered constant allows one to rewrite the energy equation in the form

$$\begin{aligned} \epsilon^* \frac{\partial T^*}{\partial t^*} + \frac{1}{r^*} \frac{\partial}{\partial r^*} (\epsilon^* r^* V_r^* T^*) + \frac{\partial}{\partial z^*} (\epsilon^* V_z^* T^*) &= \frac{\alpha_a}{r^*} \frac{\partial}{\partial r^*} \left( \epsilon^* r^* \frac{\partial T^*}{\partial r^*} \right) \\ &+ \alpha_a \frac{\partial}{\partial z^*} \left( \epsilon^* \frac{\partial T^*}{\partial z^*} \right) + \frac{h_c A_s^* (T_i^* - T^*) N_{ID}}{\rho_a C_{p_a} V_{CV}} \end{aligned} \quad (3.66)$$

The appearance of the convective source terms in equations 3.60 and 3.66 couples the equations of conservation of mass and energy for the inner and outer domains.

In order to identify the important dimensionless parameters in the outer domain, the governing equations may be nondimensionalized. Define the following nondimensional variables for the outer domain

$$t = \frac{\alpha_s t^*}{L^2} = \begin{array}{l} \text{Dimensionless} \\ \text{Time} \end{array}, \quad (3.67)$$

$$r = \frac{r^*}{R} = \begin{array}{l} \text{Dimensionless Radial} \\ \text{Spatial Coordinate} \end{array}, \quad (3.68)$$

$$z = \frac{z^*}{H} = \begin{array}{l} \text{Dimensionless Axial} \\ \text{Spatial Coordinate} \end{array}, \quad (3.69)$$

$$P = \frac{P^* \sqrt{\kappa_r}}{R \rho_a V_{IN}^2} = \begin{array}{l} \text{Dimensionless} \\ \text{Pressure} \end{array}, \quad (3.70)$$

$$T = \frac{T_e - T^*}{T_e - T_o} = \frac{T_e - T^*}{\Delta T} = \begin{array}{l} \text{Dimensionless} \\ \text{Temperature} \end{array}, \quad (3.71)$$

$$V_r = \frac{V_r^*}{V_{IN}} = \begin{array}{l} \text{Dimensionless Radial} \\ \text{Velocity} \end{array}, \quad (3.72)$$

$$V_z = \frac{V_z^*}{V_{IN}} = \begin{array}{l} \text{Dimensionless Axial} \\ \text{Velocity} \end{array}, \quad (3.73)$$

$$\rho_v = \frac{\rho_v^* - \rho_{ve}}{\rho_{v0} - \rho_{ve}} = \begin{array}{l} \text{Dimensionless Vapor} \\ \text{Density} \end{array}, \quad (3.74)$$

$$b = \frac{b^* \sqrt{\kappa_r}}{\rho_a} = \begin{array}{l} \text{Dimensionless Coefficient} \\ \text{In The Forcheimer} \\ \text{Term} \end{array}, \quad (3.75)$$

$$\kappa = \frac{\kappa^*}{\kappa_r} = \begin{array}{l} \text{Dimensionless} \\ \text{Permeability} \end{array}. \quad (3.76)$$

Rewriting the governing equations (3.57, 3.58, 3.61, 3.62, and 3.66) in terms of these nondimensional variables yields

$$\left(\frac{H}{R}\right) \frac{1}{r} \frac{\partial}{\partial r} (\epsilon^* r V_r) + \frac{\partial}{\partial z} (\epsilon^* V_z) = 0, \quad (3.77)$$

$$-\frac{\partial P}{\partial r} = \frac{1}{Re_x \kappa} \frac{V_r}{r} + b |\vec{V}| V_r, \quad (3.78)$$

$$-\frac{\partial P}{\partial z} = \frac{1}{Re_x \kappa} V_z + b |\vec{V}| V_z \quad (3.79)$$

$$\begin{aligned} \epsilon^* \frac{\partial \rho_v}{\partial t} + Re_x Pr \frac{\alpha_a}{\alpha_s} \frac{L}{\sqrt{\kappa_r}} \frac{L}{H} \left[ \left(\frac{H}{R}\right) \frac{1}{r} \frac{\partial}{\partial r} (\epsilon^* \rho_v r V_r) + \frac{\partial}{\partial z} (\epsilon^* \rho_v V_z) \right] = \\ Bi_m \left( \frac{\kappa_r A_s N_{ID}}{L V_{CV}} \right) \frac{L^2}{\kappa_r} (\rho_{iw} - \rho_v), \end{aligned} \quad (3.80)$$

and,

$$\begin{aligned} \epsilon^* \frac{\partial T}{\partial t} + Re_x Pr \frac{\alpha_a}{\alpha_s} \frac{L}{\sqrt{\kappa_r}} \frac{L}{H} \left[ \left(\frac{H}{R}\right) \frac{1}{r} \frac{\partial}{\partial r} (\epsilon^* r V_r T) + \frac{\partial}{\partial z} (\epsilon^* V_z T) \right] = \\ \left(\frac{\alpha_a}{\alpha_s}\right) \left(\frac{L}{H}\right)^2 \left[ \left(\frac{H}{R}\right)^2 \frac{1}{r} \frac{\partial}{\partial r} (\epsilon^* r \frac{\partial T}{\partial r}) + \frac{\partial}{\partial z} (\epsilon^* \frac{\partial T}{\partial z}) \right] + \\ Bi \left(\frac{\alpha_a}{\alpha_s}\right) \left(\frac{K_s}{K_a}\right) \left(\frac{\kappa_r A_s N_{ID}}{L V_{CV}}\right) \frac{L^2}{\kappa_r} (T_i - T). \end{aligned} \quad (3.81)$$

Equations 3.80 and 3.81 may be simplified by noting that

$$N_{1D} = \frac{V_{CV}}{2AL}(1-\epsilon^*) \quad (3.82)$$

Substitution of this relation into 3.80 and 3.81 gives

$$\begin{aligned} \epsilon^* \frac{\partial \rho_v}{\partial t} + Re_x Pr \frac{\alpha_a}{\alpha_s} \frac{L}{\sqrt{\kappa_r}} \frac{L}{H} \left[ \left( \frac{H}{R} \right) \frac{1}{r} \frac{\partial}{\partial r} (\epsilon^* \rho_v r V_r) + \frac{\partial}{\partial z} (\epsilon^* \rho_v V_z) \right] = \\ Bi_m \left( \frac{A_s}{A} \right) \frac{(1-\epsilon)}{2} (\rho_{iv} - \rho_v), \end{aligned} \quad (3.83)$$

and,

$$\begin{aligned} \epsilon^* \frac{\partial T}{\partial t} + Re_x Pr \frac{\alpha_a}{\alpha_s} \frac{L}{\sqrt{\kappa_r}} \frac{L}{H} \left[ \left( \frac{H}{R} \right) \frac{1}{r} \frac{\partial}{\partial r} (\epsilon^* r V_r T) + \frac{\partial}{\partial z} (\epsilon^* V_z T) \right] = \\ \left( \frac{\alpha_a}{\alpha_s} \right) \left( \frac{L}{H} \right)^2 \left[ \left( \frac{H}{R} \right)^2 \frac{1}{r} \frac{\partial}{\partial r} \left( \epsilon^* r \frac{\partial T}{\partial r} \right) + \frac{\partial}{\partial z} \left( \epsilon^* \frac{\partial T}{\partial z} \right) \right] + \\ Bi \left( \frac{\alpha_a}{\alpha_s} \right) \left( \frac{K_s}{K_a} \right) \left( \frac{A_s}{A} \right) \frac{(1-\epsilon)}{2} (T_i - T). \end{aligned} \quad (3.84)$$

Rewriting the boundary conditions in terms of the nondimensional variables gives

$$\frac{\partial V_r}{\partial r} = 0 \quad \text{at } r=0, \quad (3.85)$$

$$\frac{\partial T}{\partial r} = 0 \quad \text{at } r=0, \quad (3.86)$$

$$\frac{\partial \rho_v}{\partial r} = 0 \quad \text{at } r=0, \quad (3.87)$$

$$\frac{\partial (r V_r)}{\partial r} = 0 \quad \text{at } r=1, \quad (3.88)$$

$$\frac{\partial T}{\partial r} = 0 \quad \text{at } r=1, \quad (3.89)$$



$$\frac{\partial \rho_v}{\partial r} = 0 \quad \text{at } r=1, \quad (3.90)$$

$$T = 0 \quad \text{at } z=0 \quad \text{and } 0 \leq r \leq R_{IN}, \quad (3.91a)$$

$$\frac{\partial T}{\partial z} = 0 \quad \text{at } z=0 \quad \text{and } R_{IN} < r \leq 1, \quad (3.91b)$$

$$\rho_v = 0 \quad \text{at } z=0 \quad \text{and } 0 \leq r \leq R_{IN}, \quad (3.92a)$$

$$\frac{\partial \rho_v}{\partial z} = 0 \quad \text{at } z=0 \quad \text{and } R_{IN} < r \leq 1, \quad (3.92b)$$

$$V_z = 1 \quad \text{at } z=0 \quad \text{and } 0 \leq r \leq R_{IN}, \quad (3.93a)$$

$$V_z = 0 \quad \text{at } z=0 \quad \text{and } R_{IN} < r \leq 1, \quad (3.93b)$$

$$V_z = 0 \quad \text{at } z=1, \quad (3.94)$$

$$\frac{\partial T}{\partial z} = 0 \quad \text{at } z=1, \quad (3.95)$$

and,

$$\frac{\partial \rho_v}{\partial z} = 0 \quad \text{at } z=1. \quad (3.96)$$

Similarly, when the initial conditions are rewritten in terms of the nondimensional variables, there results

$$\rho_v = 1 \quad \text{at } t=0 \quad \text{for } 0 \leq r \leq 1 \quad \text{and } 0 \leq z \leq 1, \quad (3.97)$$

and,

$$T = 1 \quad \text{at } t=0 \quad \text{for } 0 \leq r \leq 1 \quad \text{and } 0 \leq z \leq 1, \quad (3.98)$$

### 3.4. Summary Of The Analytical Model

The development presented in the previous sections resulted in a set of eight governing equations (3.40,3.41,3.42,3.77,3.78,3.79,3.83, and 3.84) in the eight unknowns

$$V_r, V_z, P, \rho_v, T, u, \rho_{iv}, T_i,$$

along with an appropriate set of initial conditions (equations 3.49,3.50,3.51,3.97, and 3.98) and boundary conditions (equations 3.44-3.48, and 3.85-3.96).

It has been mentioned that equations 3.77, 3.78, and 3.79 in the three unknowns  $V_r, V_z$  and  $P$  are uncoupled from the rest of the problem. The problem, then, may be subdivided into two smaller problems: one for the determination of the velocity field, and another for the solution of the "drying problem."

Solving for the velocity field requires the solution of three equations: 1) the continuity equation, 2) Darcy's law in the radial direction, and 3) Darcy's law in the axial direction. These equations may be written

$$\left(\frac{H}{R}\right) \frac{1}{r} \frac{\partial}{\partial r} (\epsilon^* r V_r) + \frac{\partial}{\partial z} (\epsilon^* V_z) = 0, \quad (3.77)$$

$$-\frac{\partial P}{\partial r} = \frac{1}{\text{Re}_\kappa} \frac{V_r}{\kappa} + b |\vec{V}| V_r, \quad (3.78)$$

and,

$$-\frac{\partial P}{\partial z} = \frac{1}{\text{Re}_\kappa} \frac{V_z}{\kappa} + b |\vec{V}| V_z, \quad (3.79)$$

respectively, in the three unknowns

$V_r$ ,  $V_z$ , and  $P$ .

The boundary conditions for the velocity equations are

$$\frac{\partial V_r}{\partial r} = 0 \quad \text{at } r=0, \quad (3.85)$$

$$\frac{\partial(rV_r)}{\partial r} = 0 \quad \text{at } r=1, \quad (3.88)$$

$$V_z = 1 \quad \text{at } z=0 \quad \text{and } 0 \leq r \leq R_{IN}, \quad (3.93a)$$

$$V_z = 0 \quad \text{at } z=0 \quad \text{and } R_{IN} < r \leq 1, \quad (3.93b)$$

and,

$$V_z = 0 \quad \text{at } z=1. \quad (3.94)$$

The solution of the "drying problem" requires the solution of equations 3.40, 3.41, 3.42, 3.83, and 3.84. As noted earlier, however, not all the parameters appearing in these equations are independent parameters.  $Bi$  and  $Bi_m$  depend on other parameters appearing in the problem as well as on the local velocity. It may be shown (see Appendix A) that

$$Bi = f_1\left(\frac{A}{A_s}, \frac{\sqrt{\kappa_r}}{L}, \frac{K_a}{K_s}, \epsilon^*, Re_x, Pr, |\vec{V}|\right), \quad (A.9)$$

and,

$$Bi_m = f_2\left(\frac{\alpha_a}{\alpha_s}, \frac{A}{A_s}, \frac{K_a}{K_s}, \frac{\sqrt{\kappa_r}}{L}, \epsilon^*, Lu_v, Re_x, Pr, |\vec{V}|\right). \quad (A.16)$$

Also, the groups  $P^*L/A$  and  $A_s/A$  may be expressed as

$$\frac{P^*L}{A} = \frac{4\pi DL}{\pi D^2} = \frac{4L}{D} \quad (3.99)$$

and,

$$\frac{A_s}{A} = \frac{2[4\pi DL + \pi D^2]}{\pi D^2} = \frac{8L}{D} + 2, \quad (3.100)$$

respectively. Substitution of these relations into equations 3.41, 3.83, and 3.84 yields,

$$\begin{aligned} \frac{\partial T_i}{\partial t} = & \frac{\partial^2 T_i}{\partial z_i^2} - Ko \left( \frac{\Delta \rho_v}{\rho_s} \right) \left\{ Lu_v \frac{\partial}{\partial z_i} \left[ K_v \left( \epsilon - \frac{\rho_s}{\rho_L} u \right) \frac{\partial \rho_{iv}}{\partial z_i} \right] + \right. \\ & \left. \frac{(\rho_{ve} + \Delta \rho_v \rho_{iv})}{\Delta \rho_v} \left( \frac{\rho_s}{\rho_L} \right) \frac{\partial u}{\partial t} - \left( \epsilon - \frac{\rho_s}{\rho_L} u \right) \frac{\partial \rho_{iv}}{\partial t} \right\} + \\ & f_1 \left( \frac{L}{D}, \frac{\sqrt{\kappa_r}}{L}, \frac{K_a}{K_s}, \epsilon^*, Re_x, Pr, |\vec{V}| \right) \left( \frac{4L}{D} \right) (T_a - T_i) - q_s, \end{aligned} \quad (3.101)$$

$$\begin{aligned} \epsilon^* \frac{\partial \rho_v}{\partial t} + Re_x Pr \frac{\alpha_a}{\alpha_s} \frac{L}{\sqrt{\kappa_r}} \frac{L}{H} \left[ \left( \frac{H}{R} \right) \frac{1}{r} \frac{\partial}{\partial r} (\epsilon^* \rho_v r V_r) + \frac{\partial}{\partial z} (\epsilon^* \rho_v V_z) \right] = \\ f_2 \left( \frac{\alpha_a}{\alpha_s}, \frac{L}{D}, \frac{\sqrt{\kappa_r}}{L}, \frac{K_a}{K_s}, \epsilon^*, Lu_v, Re_x, Pr, |\vec{V}| \right) \left( \frac{8L}{D} + 2 \right) \frac{(1-\epsilon)}{2} (\rho_{iv} - \rho_v), \end{aligned} \quad (3.102)$$

and,

$$\begin{aligned} \epsilon^* \frac{\partial T}{\partial t} + Re_x Pr \left( \frac{\alpha_a}{\alpha_s} \right) \left( \frac{L}{\sqrt{\kappa_r}} \right) \left( \frac{L}{H} \right) \left[ \left( \frac{H}{R} \right) \frac{1}{r} \frac{\partial}{\partial r} (\epsilon^* r V_r T) + \frac{\partial}{\partial z} (\epsilon^* V_z T) \right] = \\ \left( \frac{\alpha_a}{\alpha_s} \right) \left( \frac{L}{H^2} \right) \left[ \left( \frac{H}{R} \right)^2 \frac{1}{r} \frac{\partial}{\partial r} \left( \epsilon^* r \frac{\partial T}{\partial r} \right) + \frac{\partial}{\partial z} \left( \epsilon^* \frac{\partial T}{\partial z} \right) \right] + \\ f_1 \left( \frac{L}{D}, \frac{\sqrt{\kappa_r}}{L}, \frac{K_a}{K_s}, \epsilon^*, Re_x, Pr, |\vec{V}| \right) \left( \frac{8L}{D} + 2 \right) \frac{(1-\epsilon^*)}{2} (T_i - T). \end{aligned} \quad (3.103)$$

Thus, the mathematical model for the "drying problem" consists of five equations: 1) conservation of mass in the inner domain, 2) conservation of energy in the inner domain, 3) the inner domain equation of state, 4) conservation of mass in the outer domain, and 5) conservation of energy in the outer domain. These equations are given by

$$\begin{aligned} \frac{\partial}{\partial z_i} \left[ Lu_L \left( \frac{\rho_s}{\Delta \rho_v} \right) D_L \frac{\partial u}{\partial z_i} + Lu_v \left( \epsilon - \frac{\rho_s}{\rho_L} u \right) D_v \frac{\partial \rho_{iv}}{\partial z_i} \right] = \\ \left( \frac{\rho_s}{\Delta \rho_v} \right) \left( 1 - \frac{\rho_{ve} + \Delta \rho_v \rho_{iv}}{\rho_L} \right) \frac{\partial u}{\partial t} + \left( \epsilon - \frac{\rho_s}{\rho_L} u \right) \frac{\partial \rho_{iv}}{\partial t}, \end{aligned} \quad (3.40)$$

$$\begin{aligned} \frac{\partial T_i}{\partial t} = \frac{\partial^2 T_i}{\partial z_i^2} - Ko \left( \frac{\Delta \rho_v}{\rho_s} \right) \left\{ Lu_v \frac{\partial}{\partial z_i} \left[ K_v \left( \epsilon - \frac{\rho_s}{\rho_L} u \right) \frac{\partial \rho_{iv}}{\partial z_i} \right] + \right. \\ \left. \frac{(\rho_{ve} + \Delta \rho_v \rho_{iv})}{\Delta \rho_v} \left( \frac{\rho_s}{\rho_L} \right) \frac{\partial u}{\partial t} - \left( \epsilon - \frac{\rho_s}{\rho_L} u \right) \frac{\partial \rho_{iv}}{\partial t} \right\} + \\ f_1 \left( \frac{L}{D}, \frac{\sqrt{\kappa_r}}{L}, \frac{K_a}{K_s}, \epsilon^*, Re_x, Pr, |\vec{V}| \right) \left( \frac{4L}{D} \right) (T_a - T_i) - q_s, \end{aligned} \quad (3.101)$$

$$\rho_{iv} = f'(u, T) \quad u \leq u_{ms}, \quad (3.42a)$$

$$\rho_{iv} = \frac{1}{\Delta \rho_v R (T_e - \Delta T T_i)} e^{\left[ \alpha + \frac{b}{(T_e - \Delta T T_i)} + c \ln(T_e - \Delta T T_i) \right]} \quad u > u_{ms}, \quad (3.42b)$$

$$\begin{aligned} \epsilon^* \frac{\partial \rho_v}{\partial t} + Re_x Pr \frac{\alpha_a}{\alpha_s} \frac{L}{\sqrt{\kappa_r}} \frac{L}{H} \left[ \left( \frac{H}{R} \right) \frac{1}{r} \frac{\partial}{\partial r} (\epsilon^* \rho_v r V_r) + \frac{\partial}{\partial z} (\epsilon^* \rho_v V_z) \right] = \\ f_2 \left( \frac{\alpha_a}{\alpha_s}, \frac{L}{D}, \frac{\sqrt{\kappa_r}}{L}, \frac{K_a}{K_s}, Lu_v, \epsilon^*, Re_x, Pr, |\vec{V}| \right) \left( \frac{8L}{D} + 2 \right) \frac{(1 - \epsilon^*)}{2} (\rho_{iv} - \rho_v), \end{aligned} \quad (3.102)$$

and,

$$\begin{aligned} \epsilon^* \frac{\partial T}{\partial t} + Re_x Pr \left( \frac{\alpha_a}{\alpha_s} \right) \left( \frac{L}{\sqrt{\kappa_r}} \right) \left( \frac{L}{H} \right) \left[ \left( \frac{H}{R} \right) \frac{1}{r} \frac{\partial}{\partial r} (\epsilon^* r V_r T) + \frac{\partial}{\partial z} (\epsilon^* V_z T) \right] = \\ \left( \frac{\alpha_a}{\alpha_s} \right) \left( \frac{L}{H^2} \right) \left[ \left( \frac{H}{R} \right)^2 \frac{1}{r} \frac{\partial}{\partial r} \left( \epsilon^* r \frac{\partial T}{\partial r} \right) + \frac{\partial}{\partial z} \left( \epsilon^* \frac{\partial T}{\partial z} \right) \right] + \\ f_1 \left( \frac{L}{D}, \frac{\sqrt{\kappa_r}}{L}, \frac{K_a}{K_s}, \epsilon^*, Re_x, Pr, |\vec{V}| \right) \left( \frac{8L}{D} + 2 \right) \frac{(1 - \epsilon^*)}{2} (T_i - T) \end{aligned} \quad (3.103)$$

respectively, in the five unknowns

$$u, \rho_{iv}, \rho_v, T, \text{ and } T_i.$$

The boundary and initial conditions are given by:

$$\frac{\partial u}{\partial z_i} = 0 \quad \text{at } z_i = 0, \quad (3.44)$$

$$\frac{\partial \rho_{iv}}{\partial z_i} = 0 \quad \text{at } z_i = 0, \quad (3.45)$$

$$\frac{\partial T_i}{\partial z_i} = 0 \quad \text{at } z_i = 0, \quad (3.46)$$

$$\Delta u \left[ \left( \frac{\rho_s}{\Delta \rho_v} \right) (Lu_v) D_L \frac{\partial u}{\partial z_i} + (Lu_v) D_v \left( \epsilon - \frac{\rho_s}{\rho_L} u \right) \frac{\partial \rho_{iv}}{\partial z_i} \right] = \text{Bi}_m (\rho_{va} - \rho_{iv}) \quad \text{at } z_i = 1, \quad (3.47)$$

$$\frac{\partial T_i}{\partial z_i} + \text{Ko} (Lu_L) D_L \frac{\partial u}{\partial z_i} = \text{Bi}_m (T_a - T_i) \quad \text{at } (z_i = 1), \quad (3.29)$$

$$\frac{\partial T}{\partial r} = 0 \quad \text{at } r = 0, \quad (3.86)$$

$$\frac{\partial \rho_v}{\partial r} = 0 \quad \text{at } r = 0, \quad (3.87)$$

$$\frac{\partial T}{\partial r} = 0 \quad \text{at } r = 1, \quad (3.89)$$

$$\frac{\partial \rho_v}{\partial r} = 0 \quad \text{at } r = 1, \quad (3.90)$$

$$T = 0 \quad \text{at } z = 0 \quad \text{and} \quad 0 \leq r \leq R_{IN}, \quad (3.91a)$$

$$\frac{\partial T}{\partial z} = 0 \quad \text{at } z = 0 \quad \text{and} \quad R_{IN} < r \leq 1, \quad (3.91b)$$

$$\rho_v = 0 \quad \text{at } z = 0 \quad \text{and} \quad 0 \leq r \leq R_{IN}, \quad (3.92a)$$

$$\frac{\partial \rho_v}{\partial z} = 0 \quad \text{at } z = 0 \quad \text{and} \quad R_{IN} < r \leq 1, \quad (3.92b)$$

$$\frac{\partial T}{\partial z} = 0 \quad \text{at } z = 1, \quad (3.95)$$

$$\frac{\partial \rho_v}{\partial z} = 0 \quad \text{at } z=1, \quad (3.96)$$

$$\rho_{iv} = 1 \quad \text{for } 0 \leq z_i \leq 1, \quad (3.49)$$

$$u = 1 \quad \text{for } 0 \leq z_i \leq 1, \quad (3.50)$$

$$T_i = 1 \quad \text{for } 0 \leq z_i \leq 1, \quad (3.51)$$

$$\rho_v = 1 \quad \text{at } t=0 \quad \text{for } 0 \leq r \leq 1 \quad \text{and } 0 \leq z \leq 1, \quad (3.97)$$

and,

$$T = 1 \quad \text{at } t=0 \quad \text{for } 0 \leq r \leq 1 \quad \text{and } 0 \leq z \leq 1. \quad (3.98)$$

Examination of the nondimensional equations shows that there are 15 dimensionless parameters appearing in the problem,

$$\frac{K_\alpha}{K_s}, \quad \frac{\alpha_\alpha}{\alpha_s}, \quad \frac{H}{L}, \quad \frac{\sqrt{\kappa_r}}{L}, \quad \frac{\rho_{ve}}{\Delta \rho_v}, \quad \frac{\rho_s}{\rho_L}, \quad \frac{\rho_s}{\Delta \rho_v}, \quad \frac{L}{D},$$

$$R_{IN}, \quad Ko, \quad Lu_L, \quad Lu_v, \quad \frac{H}{R}, \quad Re_\kappa, \quad Pr.$$

Each dimensionless parameter holds some physical significance in the mathematical model. The dimensionless terms and their physical interpretations are presented in Table 3.1.

Table 3.1. Summary Of The Dimensionless Parameters And Their Physical Interpretations

|                                  |                                     |  |
|----------------------------------|-------------------------------------|--|
| $\frac{K_a}{K_s}$                | ---                                 | Ratio of the thermal conductivity of air to that of the solid                                    |
| $\frac{\alpha_a}{\alpha_s}$      | ---                                 | Ratio of the thermal diffusivity of air to that of the solid                                     |
| $\frac{H}{L}$                    | ---                                 | Ratio of the height of the outer domain to the (half) length of an inner domain element          |
| $\frac{\sqrt{\kappa_r}}{L}$      | ---                                 | Ratio of the length scale in the outer domain to the (half) length of an inner domain element    |
| $\frac{\rho_{ve}}{\Delta\rho_v}$ | ---                                 | Ratio of equilibrium vapor density to a characteristic change in vapor density                   |
| $\frac{\rho_s}{\rho_L}$          | ---                                 | Ratio of the solid density to the density of liquid water  |
| $\frac{\rho_s}{\Delta\rho_v}$    | ---                                 | Ratio of the solid density to a characteristic change in vapor density                           |
| $\frac{L}{D}$                    | ---                                 | Ratio of (half) length to diameter of an inner domain element                                    |
| $\frac{H}{R}$                    | ---                                 | Ratio of the height to the radius of the outer domain structure                                  |
| $Ko$                             | $\frac{L_s\Delta u}{C_s\Delta T}$   | Ratio of thermal energy used for evaporation to sensible energy stored in the solid              |
| $Lu_L$                           | $\frac{D_{lr}}{\alpha_s}$           | Ratio of the rate of capillary transfer of liquid water to diffusion of heat in the inner domain |
| $Lu_v$                           | $\frac{D_{vr}}{\alpha_s}$           | Ratio of the rate of diffusion of water vapor to diffusion of heat in the inner domain           |
| $Re_x$                           | $\frac{V_{IN}\sqrt{\kappa_r}}{\nu}$ | Ratio of inertial forces to viscous forces   |
| $Pr$                             | $\frac{\nu}{\alpha_a}$              | Ratio of the diffusivity of momentum to the diffusivity of thermal energy                        |
| $R_{IN}$                         | $\frac{r_{IN}}{R}$                  | Ratio of air inlet radius to the radius of the outer domain                                      |



### 3.5. Discussion Of The Assumptions On Which The Analytical Model Is Based

In the formulation of the present mathematical model, several assumptions were made. The assumptions for the inner domain include:

1. The porous solid is isotropic and homogeneous and contains liquid water, water vapor, and air.
2. The inner domain elements are assumed to be randomly oriented throughout the overall region comprising the outer domain.
3. Moisture movement may occur as a result of capillary transfer of liquid, diffusion of water vapor, and movement of bound liquid.
4. The inner domain phases (solid, liquid, and vapor) are in thermodynamic equilibrium.
5. Temperature gradients are negligible in the inner domain.
6. The solid structure is rigid so that the porosity does not vary with time as the drying process takes place.

Additional assumptions for the outer domain include:

7. The overall structure of the outer domain is isotropic, but may be nonhomogeneous.
8. The porosity does not vary with time.
9. No liquid is present in the outer domain.

10. The addition of mass (as water vapor) to the outer domain does not significantly affect the velocity distribution in the outer domain.

11. Natural convection is negligible.

Assumption number one concerns the physical structure of the porous medium in the inner domain. For the present application, the inner domain represents a single hay stalk. Examination of the interior of a hay stalk under a magnifying glass reveals that the material is distributed rather uniformly throughout. Thus, the assumption that the medium is homogeneous should be reasonable for the present case. Additionally, it has been assumed that the liquid held within the inner domain may be treated as pure water. The energy required to vaporize the liquid in the hay stalks has reportedly been measured and is within approximately 15% of the heat of vaporization of pure water (Bledsoe, 1989). Thus, treating the liquid as pure water should not result in a large error for the present case.

Assumption two concerns the physical makeup of the global porous structure. Again, examination of a hay bale reveals that the hay stalks are randomly oriented throughout the bale. (Note: There is a tangential pattern that appears in a hay bale as a result of baling. As the hay is picked up from the wind row, it is "wrapped" around the outside of the bale. However, the hay stalks themselves do appear to be randomly

oriented within each layer. Furthermore, no change in the flow has been observed to occur at the interface of these layers. Thus, the assumption that the stalks are randomly oriented throughout the entire outer domain has been made.)

As was discussed in Section 1, several different mechanisms of mass transport have been identified. Of these, vapor diffusion, capillary movement of liquid, and movement of bound liquid have been assumed to predominate. The pressure gradient along the outside (from end to end) of an inner domain element is negligible (a typical pressure drop across the entire bale structure is around 0.1 psi). Thus, the liquid and vapor flow induced by an external pressure gradient is very small. Since the flow is not rarefied, effusion (Knudsen) flow may also be dismissed as negligible for the present case. Surface diffusion has not been included in any studies known to the author. However, this mode of mass transfer will be negligible except in the very last stages of drying where the liquid content is very low. Therefore, this term will also be neglected. Thus, the only modes of moisture movement that have been included in the present model are capillary movement of liquid, diffusion of water vapor, and movement of bound liquid.

Assumption number four involves the presumption that thermodynamic equilibrium exists between the phases of the inner domain. The typical drying process occurs over a period

of days and the temperature changes occur gradually during this time. Thus, it is expected that the inner domain phases are close to being in equilibrium with each other.

The temperature gradients in the inner domain have been assumed negligible. The typical element in the inner domain is approximately one to two inches in length. Thus, the air temperature in the outer domain will not change significantly over such a short length. Since convective heat transfer between the domains is assumed to be the primary mode of heat transfer in the present work, the temperature gradient along a stalk should also be small.

Assumption number six regards the shrinkage of the solid structure. It has been observed that the shrinkage of hay during the drying process is small. The porosity, therefore, will not change significantly due to shrinkage and may be assumed constant over time.

Since the outer domain structure has been assumed to consist of randomly oriented inner domain elements, it will be isotropic. Current baling practice, however, often results in an uneven distribution of hay inside a hay bale. Thus, the dry matter density varies considerably with position in the bale (Bledsoe, Shoulders, and Hitch, 1986). Therefore, the porosity is a function of position so that the bale is actually a nonhomogeneous porous structure.

As has been mentioned, the typical drying process occurs over a period of days. Thus, the addition of mass to the outer domain (as water vapor) occurs very slowly. For the typical case under consideration, the initial moisture content is approximately 35% (w.b.) and the final moisture content is approximately 18% (w.b.). The initial weight of a bale is on the order of 8900 (N) (2000 lbf). Thus, approximately 210 (kg) (470 lbf) of moisture is removed over a three day period. The average mass transfer rate is thus approximately  $8.2 \times 10^{-4}$  (kg/s) which is small compared to the mass of air flowing through the bale structure (the ratio of water vapor to air mass flow rates is approximately  $1.5 \times 10^{-3}$ ). Therefore, it is assumed that this slow addition of mass will not significantly affect the velocity distribution in the outer domain.

A typical Reynolds number (Re) for the flow in the outer domain is approximately 10 and the typical Grashof number (Gr) is approximately 3.5. The relative importance of natural convection to forced convection is given by a function involving  $Gr/Re^n$  (Gebhart et al., 1988). When the value of this parameter is close to zero, forced convection dominates. When the value of this parameter is very large, natural convection is of primary importance. The value of the exponent n depends on such quantities as geometry, boundary conditions, and fluid properties. However, there is a large difference

between the Reynolds number and the Grashof number; and, it is therefore expected that natural convective effects will be small.

## 4. THE NUMERICAL INVESTIGATION

### 4.1. The Need For A Numerical Solution

The mathematical model formulated in Section 3 cannot be solved in closed analytical form; therefore, a numerical solution of the set of coupled partial differential equations subject to the stated initial and boundary conditions is required. It was decided to use the finite volume approach (Patankar, 1980) due to the simplicity of formulation and ease of solution of the resulting equations. This approach also guarantees satisfaction of all conservation relations and can be solved on extremely coarse grids during the development phase of the numerical study.

As mentioned previously, it is possible to obtain the velocity and pressure fields independently of the other solution variables. Thus, two different numerical schemes will be derived below: one for the velocity and pressure field solution and the other for the solution to all other unknown variables appearing in the problem.

### 4.2. Determination Of The Velocity And Pressure Fields

The equations to be solved are:

$$\left(\frac{H}{R}\right) \frac{1}{r} \frac{\partial}{\partial r} (\epsilon^* r V_r) + \frac{\partial}{\partial z} (\epsilon^* V_z) = 0, \quad (3.77)$$

$$-\frac{\partial P}{\partial r} = \frac{1}{\text{Re}_x} V_r + b |\vec{V}| V_r, \quad (3.78)$$

and,

$$-\frac{\partial P}{\partial z} = \frac{1}{\text{Re}_x} V_x + b |\vec{V}| V_x, \quad (3.79)$$

The finite volume approach requires that the calculation domain be divided into nonoverlapping control volumes. The size of these control volumes may be uniform, or nonuniform, as desired. Nonuniform control volume spacing allows more flexibility in the code as a closer spacing may be used in areas where large gradients of the solution variables are expected. The present numerical scheme will thus be derived for the case of variable grid spacing.

Any finite difference scheme (finite volume approach included) involves solving the solution variables at discrete locations, or "grid points." The placement of the grid points within the control volumes for the finite volume approach must therefore be specified. Patankar has discussed two possible approaches which he designates as "practice A" and "practice B." Practice A consists of locating the control volume faces half-way between the grid points, while practice B involves locating the grid points at the center of each control volume. Figures 4.1 and 4.2 illustrate the differences between the two approaches. Patankar has noted that practice B has several advantages and so this practice will be used throughout the present derivation.

The notation used throughout the present derivation (and used by Patankar) is also illustrated in Figures 4.1 and 4.2. The subscript P is used to designate a particular grid point



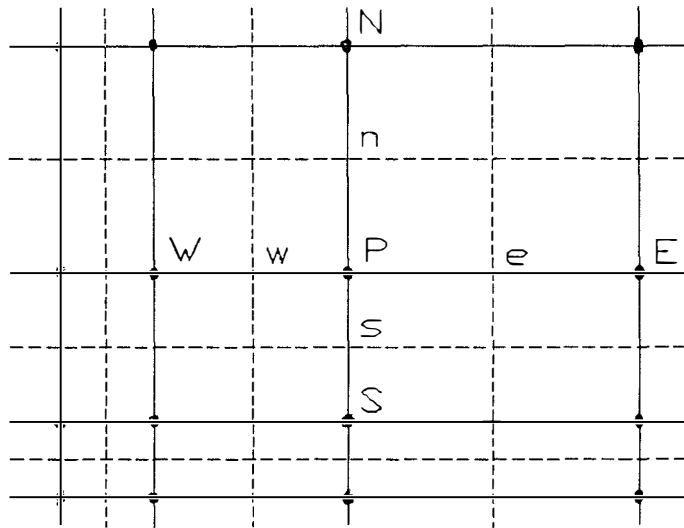


Figure 4.1. Control volume faces located half-way between grid points (Practice A).

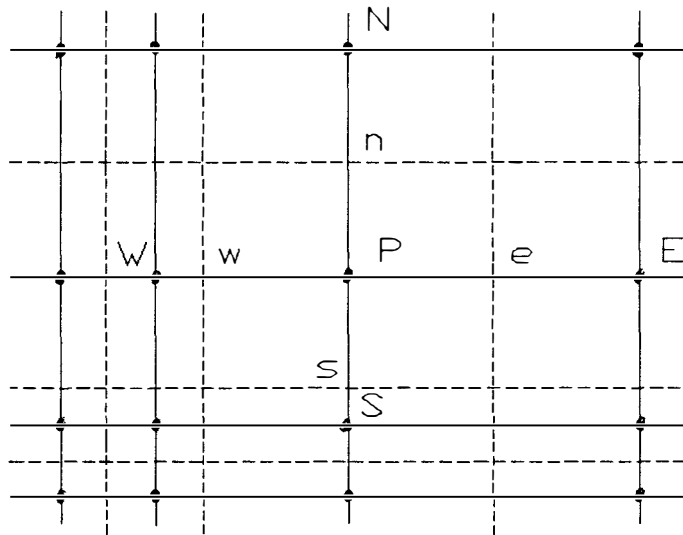


Figure 4.2. Grid points located at the center of the control volumes (Practice B).

while the subscripts E,W,N, and S denote the east, west, north, and south neighboring points, respectively. Quantities evaluated at the east, west, north, and south control volume faces are designated with subscripts e,w,n, and s respectively.

One other aspect concerning the grid should be mentioned. In problems involving convective terms, a staggered grid is employed for the velocity components to avoid the possibility of obtaining an unrealistic pressure field. The velocity grid points are thus located at the control volume faces, while all other grid points are located at the center of each control volume (Patankar, 1980).

Once the grid is specified, the governing equations are integrated over a single time interval and an individual control volume. Integration of equation 3.77 gives

$$\int_t^{t+\Delta t} \int_s^n \int_w^e \left( \frac{H}{R} \right) \frac{1}{r} \frac{\partial}{\partial r} (r \epsilon^* V_r) r dr dz dt + \int_t^{t+\Delta t} \int_s^n \int_w^e \frac{\partial}{\partial z} (\epsilon^* V_z) dz r dr dt = 0, \quad (4.1)$$

or,

$$\frac{H}{R} (r_e \epsilon_e^* V_{re} - r_w \epsilon_w^* V_{rw}) (z_n - z_s) + (\epsilon_n^* V_{zn} - \epsilon_s^* V_{zs}) \left( \frac{r_e^2 - r_w^2}{2} \right) = 0. \quad (4.2)$$

It was desired to have the option of solving for the velocity field by running a transient solution to steady state. Including the temporal terms, equations 3.78 and 3.79 may be written as

$$\left( \frac{1}{Re_x Pr} \right) \frac{\sqrt{\kappa} \partial V_r}{\epsilon^* \partial t} = -\frac{\partial P}{\partial r} - \left[ \frac{1}{Re_x \sqrt{\kappa}} V_r + b |\vec{V}| V_r \right], \quad (4.3)$$

and,

$$\left( \frac{1}{Re_x Pr} \right) \frac{\sqrt{\kappa} \partial V_z}{\epsilon^* \partial t} = -\frac{\partial P}{\partial z} - \left[ \frac{1}{Re_x \sqrt{\kappa}} V_z + b |\vec{V}| V_z \right]. \quad (4.4)$$

The usual form of the conservation expression for a variable  $\phi$  may be written as

$$\frac{\partial}{\partial t}(\rho \phi) + \nabla \cdot (\rho \vec{V} \phi) = \nabla \cdot (\Gamma \nabla \phi) + S. \quad (4.5)$$

Equations 4.3 and 4.4 may be considered to be in this standard form if the terms enclosed in the square brackets are assumed to be part of the source terms. (Note: The pressure term is customarily not included in the source term.) Thus, equations 4.3 and 4.4 may be written as

$$\frac{1}{Re_x Pr} \left( \frac{\sqrt{\kappa}}{\epsilon^*} \right) \frac{\partial V_r}{\partial t} = -\frac{\partial P}{\partial r} + S_r \quad (4.6)$$

and,

$$\frac{1}{Re_x Pr} \left( \frac{\sqrt{\kappa}}{\epsilon^*} \right) \frac{\partial V_z}{\partial t} = -\frac{\partial P}{\partial z} + S_z \quad (4.7)$$

where:

$$S_r = - \left[ \frac{1}{Re_x \sqrt{\kappa}} V_r + b |\vec{V}| V_r \right] \quad (4.8)$$

and,

$$S_z = - \left[ \frac{1}{Re_x \sqrt{\kappa}} V_z + b |\vec{V}| V_z \right]. \quad (4.9)$$

The source term may be linearized as described by Patankar to get

$$S = S' + \frac{\partial S'}{\partial \phi} (\phi - \phi'), \quad (4.10)$$

where the prime indicates the previous iteration values.

Thus,

$$S_r = - \left[ \left( \frac{1}{Re_x} \right) \frac{V_r'}{\sqrt{\kappa}} + b (V_r'^2 + V_z'^2)^{1/2} V_r' \right] - \left[ \left( \frac{1}{Re_x} \right) \left( \frac{1}{\sqrt{\kappa}} \right) + \frac{b(2V_r'^2 + V_z'^2)}{(V_r'^2 + V_z'^2)^{1/2}} \right] (V_r - V_r'). \quad (4.11)$$

This may be rewritten as

$$S_r = b \frac{V_r'^3}{[V_r'^2 + V_z'^2]^{1/2}} - \left[ \left( \frac{1}{Re_x} \right) \left( \frac{1}{\sqrt{\kappa}} \right) + \frac{b(2V_r'^2 + V_z'^2)}{[V_r'^2 + V_z'^2]^{1/2}} \right] V_r. \quad (4.12)$$

It was desired that the code should run for situations in which the Forscheimer term was not applicable (i.e.  $b = 0$ ). Since  $\vec{V}$  is initially zero, the source term as formulated above becomes zero, which results in no numerical change in the velocity field with time. This situation is avoided by slightly modifying the source term as shown above to the form

$$S_r = \left[ \frac{bV_r'^3}{[V_r'^2 + V_z'^2]^{1/2}} + \frac{V_r'}{\sqrt{\kappa} Re_x} \right] - \left[ \frac{2}{\sqrt{\kappa} Re_x} + \frac{b(2V_r'^2 + V_z'^2)}{[V_r'^2 + V_z'^2]^{1/2}} \right] V_r. \quad (4.13)$$

Similarly, the source term  $S_z$  is modified to give

$$S_z = \left[ \frac{bV_z'^3}{[V_r'^2 + V_z'^2]^{1/2}} + \frac{V_z'}{\sqrt{\kappa} Re_x} \right] - \left[ \frac{2}{\sqrt{\kappa} Re_x} + \frac{b(V_r'^2 + 2V_z'^2)}{[V_r'^2 + V_z'^2]^{1/2}} \right] V_z. \quad (4.14)$$

Note that upon convergence,  $V_r' = V_r$  and  $V_z' = V_z$  and the correct source terms are obtained. Equations 4.6 and 4.7 may now be written as

$$\frac{1}{Re_x Pr} \left( \frac{\sqrt{\kappa}}{\epsilon^*} \right) \frac{\partial V_r}{\partial t} = -\frac{\partial P}{\partial r} + (S_{cr} + S_{pr} V_r) \quad (4.15)$$

and,

$$\frac{1}{Re_x Pr} \left( \frac{\sqrt{\kappa}}{\epsilon^*} \right) \frac{\partial V_z}{\partial t} = -\frac{\partial P}{\partial z} + (S_{cz} + S_{pz} V_z) \quad (4.16)$$

where:

$$S_{cr} = \frac{b V_r^{3'}}{[V_r^{2'} + V_z^{2'}]^{1/2}} + \frac{V_r'}{\sqrt{\kappa} Re_x}, \quad (4.17)$$

$$S_{pr} = -\left[ \frac{2}{\sqrt{\kappa} Re_x} + \frac{b(2V_r^{2'} + V_z^{2'})}{[V_r^{2'} + V_z^{2'}]^{1/2}} \right], \quad (4.18)$$

$$S_{cz} = \frac{b V_z^{3'}}{[V_r^{2'} + V_z^{2'}]^{1/2}} + \frac{V_z'}{\sqrt{\kappa} Re_x}, \quad (4.19)$$

and,

$$S_{pz} = -\left[ \frac{2}{\sqrt{\kappa} Re_x} + \frac{b(V_r^{2'} + 2V_z^{2'})}{[V_r^{2'} + V_z^{2'}]^{1/2}} \right]. \quad (4.20)$$

Integration of equation 4.15 over a control volume and a time interval gives

$$\begin{aligned} \left( \frac{1}{Re_x Pr} \right) \left( \frac{\sqrt{\kappa}}{\epsilon^*} \right) \frac{V_{re} - V_{re}^0}{\Delta t} \left( \frac{r_e^2 - r_w^2}{2} \right) (z_n - z_s) &= \frac{P_P - P_E}{r_E - r_W} \left( \frac{r_e^2 - r_w^2}{2} \right) (z_n - z_s) \\ + S_{cre} \left( \frac{r_e^2 - r_w^2}{2} \right) (z_n - z_s) &+ S_{pre} V_{re} \left( \frac{r_e^2 - r_w^2}{2} \right) (z_n - z_s). \end{aligned} \quad (4.21)$$

Solving for the velocity gives

$$V_{re} = \left( \frac{1}{A_{re}} \right) \left[ \frac{P_P - P_E}{\Gamma_E - \Gamma_P} \right] + V_{rs_e} \quad (4.22)$$

where:

$$A_{re} = \frac{\sqrt{\kappa_e}}{\text{Re}_x \text{Pr} \epsilon_e^* \Delta t} - S_{pr_e} \quad (4.23)$$

and,

$$V_{rs_e} = \left( S_{cr_e} + \frac{\sqrt{\kappa_e}}{\text{Re}_x \text{Pr} \epsilon_e^* \Delta t} V_{re}^o \right) \left( \frac{1}{A_{re}} \right). \quad (4.24)$$

Similarly, it is easily shown that

$$V_{rw} = \left( \frac{1}{A_{rw}} \right) \left[ \frac{P_W - P_P}{\Gamma_P - \Gamma_W} \right] + V_{rs_w}, \quad (4.25)$$

$$V_{zr} = \left( \frac{1}{A_{zr}} \right) \left[ \frac{P_P - P_N}{z_N - z_P} \right] + V_{zs_e}, \quad (4.26)$$

and,

$$V_{zs} = \left( \frac{1}{A_{zs}} \right) \left[ \frac{P_S - P_P}{z_P - z_S} \right] + V_{zs_e}, \quad (4.27)$$

where:

$$A_{rw} = \frac{\sqrt{\kappa_w}}{\text{Re}_x \text{Pr} \epsilon_w^* \Delta t} - S_{pr_w}, \quad (4.28)$$

$$V_{rs_w} = \left( S_{cr_w} + \frac{\sqrt{\kappa_w}}{\text{Re}_x \text{Pr} \epsilon_w^* \Delta t} V_{rw}^o \right) \left( \frac{1}{A_{rw}} \right), \quad (4.29)$$

$$A_{zr} = \frac{\sqrt{\kappa_r}}{\text{Re}_x \text{Pr} \epsilon_r^* \Delta t} - S_{pz_r}, \quad (4.30)$$

$$V_{zs_e} = \left( S_{cz_r} + \frac{\sqrt{\kappa_r}}{\text{Re}_x \text{Pr} \epsilon_r^* \Delta t} V_{zr}^o \right) \left( \frac{1}{A_{zr}} \right), \quad (4.31)$$

$$A_{zs} = \frac{\sqrt{\kappa_s}}{\text{Re}_x \text{Pr} \epsilon_s^* \Delta t} - S_{\rho z_s}, \quad (4.32)$$

and,

$$V_{zs_s} = \left( S_{cz_s} + \frac{\sqrt{\kappa_s}}{\text{Re}_x \text{Pr} \epsilon_s^* \Delta t} V_{zs_s}^0 \right) \left( \frac{1}{A_{zs}} \right). \quad (4.33)$$

The expressions for the velocities (equations 4.22, 4.25, 4.26, 4.27) may be substituted into equation 4.2 giving

$$\begin{aligned} & \left\{ \Gamma_e \epsilon_e^* \left[ \frac{1}{A_{re}} \left( \frac{P_P - P_E}{\Gamma_E - \Gamma_P} \right) + V_{rs_e} \right] - \Gamma_w \epsilon_w^* \left[ \frac{1}{A_{rw}} \left( \frac{P_W - P_P}{\Gamma_P - \Gamma_W} \right) + V_{rs_w} \right] \right\} (z_n - z_s) \\ & + \left\{ \epsilon_n^* \left[ \frac{1}{A_{zn}} \left( \frac{P_P - P_N}{z_N - z_P} \right) + V_{zs_n} \right] - \epsilon_s^* \left[ \frac{1}{A_{zs}} \left( \frac{P_S - P_P}{z_P - z_S} \right) + V_{zs_s} \right] \right\} \left( \frac{r_e^2 - r_w^2}{2} \right) \\ & = 0. \end{aligned} \quad (4.34)$$

This equation may be rearranged to give

$$a_P P_P = a_E P_E + a_W P_W + a_N P_N + a_S P_S + b \quad (4.35)$$

where:

$$a_E = \left[ \frac{\Gamma_e \epsilon_e^* (z_n - z_s)}{A_{re} (\Gamma_E - \Gamma_P)} \right], \quad (4.36)$$

$$a_W = \left[ \frac{\Gamma_w \epsilon_w^* (z_n - z_s)}{A_{rw} (\Gamma_P - \Gamma_W)} \right], \quad (4.37)$$

$$a_N = \left[ \frac{\epsilon_n^* (r_e^2 - r_w^2)}{2 A_{zn} (z_N - z_P)} \right], \quad (4.38)$$

$$a_S = \left[ \frac{\epsilon_s^* (r_e^2 - r_w^2)}{2 A_{zs} (z_P - z_S)} \right], \quad (4.39)$$

$$a_P = a_E + a_W + a_N + a_S, \quad (4.40)$$

and,

$$b = [\Gamma_w \epsilon_w^* (z_n - z_s) V_{rs_w} - \Gamma_e \epsilon_e^* (z_n - z_s) V_{rs_e} + \epsilon_s^* \left( \frac{\Gamma_e^2 - \Gamma_w^2}{2} \right) V_{zs_e} - \epsilon_n^* \left( \frac{\Gamma_e^2 - \Gamma_w^2}{2} \right) V_{zs_n}]. \quad (4.41)$$

A means of correcting the velocity field so that the resulting velocities come closer and closer to satisfying the continuity equation (4.2) must be obtained. This procedure is outlined in great detail by Patankar (1980). A pressure correction term ( $P$ ) may be obtained by solving

$$a_p P_{1P} = a_E P_{1E} + a_W P_{1W} + a_N P_{1N} + a_S P_{1S} + b_1 \quad (4.42)$$

where:

$$b_1 = \left[ \Gamma_w \epsilon_w^* (z_n - z_s) V_{rw'} - \Gamma_e \epsilon_e^* (z_n - z_s) V_{re'} + \epsilon_s^* \left( \frac{\Gamma_e^2 - \Gamma_w^2}{2} \right) V_{zs'} - \epsilon_n^* \left( \frac{\Gamma_e^2 - \Gamma_w^2}{2} \right) V_{zn'} \right], \quad (4.43)$$

and, the coefficients  $a_p, a_E, a_W, a_N,$  and  $a_S$  are given by equations 4.36 - 4.40. The resulting solution for the pressure correction term ( $P$ ) is then used to correct velocities by substitution in the following equations.

$$V_{re} = \left( \frac{1}{A_{re}} \right) \left[ \frac{P_{1P} - P_{1E}}{\Gamma_E - \Gamma_P} \right] + V_{re}', \quad (4.44)$$

$$V_{rw} = \left( \frac{1}{A_{rw}} \right) \left[ \frac{P_{1W} - P_{1P}}{\Gamma_P - \Gamma_W} \right] + V_{rw}', \quad (4.45)$$

$$V_{zn} = \left( \frac{1}{A_{zn}} \right) \left[ \frac{P_{1P} - P_{1N}}{z_N - z_P} \right] + V_{zn}', \quad (4.46)$$

and,

$$V_{zs} = \left( \frac{1}{A_{zs}} \right) \left[ \frac{P_{1S} - P_{1P}}{z_P - z_S} \right] + V_{zs}'. \quad (4.47)$$



The equations formulated above provide the means for determining the solution fields. The SIMPLER algorithm (Patankar, 1980) was used and proceeds as follows:

1. An initial velocity field ( $V_r$  and  $V_z$ ) is guessed. ( $V_r$  and  $V_z$  were both initially set equal to zero.)
2. Using equations 4.24, 4.29, 4.31, and 4.33, the pseudo-velocities ( $V_{rs}, V_{rs_w}, V_{zs_a}, V_{zs}$ ) are calculated.
3. The coefficients ( $a_p, a_E, a_W, a_N, a_S$ ) in the pressure equation (4.35) are evaluated and a pressure field is solved for.
4. Using this pressure field, the momentum equations (4.22, 4.25, 4.26, and 4.27) are solved for the velocity components ( $V_r$  and  $V_z$ ).
5. These velocities are substituted into the continuity equation (4.2, page 73). If this velocity field is not correct, equation (4.2) will not be satisfied and an apparent "mass source" will arise. This mass source (from equation 4.43) is then used to obtain a pressure correction term,  $P$ , from equation 4.42.
6. The pressure correction term is then used to correct the velocities according to the relations given in 4.44 - 4.47.
7. If convergence is not obtained, the algorithm returns to step 2.

### 4.3. The Drying Problem

Once the velocity field has been determined, the set of coupled equations describing the drying process may be solved. The drying problem is described by two sets of equations: one set for the outer domain, and a second set for the inner domain. Each set of equations requires a separate solution algorithm, both of which will be discussed individually.

#### 4.3.1. Governing Equations For The Outer Domain

In the outer domain, the problem consists of determining the temperature and vapor density fields. The equations to be solved are the equation governing the conservation of mass given by:

$$\epsilon^* \frac{\partial \rho_v}{\partial t} + Re_x Pr \frac{\alpha_a}{\alpha_s} \frac{L}{\sqrt{\kappa_r}} \frac{L}{H} \left[ \left( \frac{H}{R} \right) \frac{1}{r} \frac{\partial}{\partial r} (\epsilon^* \rho_v r V_r) + \frac{\partial}{\partial z} (\epsilon^* \rho_v V_z) \right] =$$

$$Bi_m \left( \frac{8L}{D} + 2 \right) \frac{(1 - \epsilon^*)}{2} (\rho_{iv} - \rho_v) \quad (3.102)$$

and, the equation governing the conservation of energy given by:

$$\epsilon^* \frac{\partial T}{\partial t} + Re_x Pr \frac{\alpha_a}{\alpha_s} \frac{L}{\sqrt{\kappa_r}} \frac{L}{H} \left[ \left( \frac{H}{R} \right) \frac{1}{r} \frac{\partial}{\partial r} (\epsilon^* r V_r T) + \frac{\partial}{\partial z} (\epsilon^* V_z T) \right] =$$

$$\frac{\alpha_a}{\alpha_s} \left( \frac{L}{H} \right)^2 \left[ \left( \frac{H}{R} \right)^2 \frac{1}{r} \frac{\partial}{\partial r} \left( \epsilon^* r \frac{\partial T}{\partial r} \right) + \frac{\partial}{\partial z} \left( \epsilon^* \frac{\partial T}{\partial z} \right) \right] +$$

$$Bi \frac{\alpha_a}{\alpha_s} \left( \frac{8L}{D} + 2 \right) \frac{(1 - \epsilon^*)}{2} (T_i - T). \quad (3.103)$$

(Note: For clarity,  $Bi$  and  $Bi_m$  will be used throughout the following derivation of the numerical scheme instead of using functional notation. It should be kept in mind that these are not independent parameters for the problem.)

Since the computational grid has already been established during the solution of the velocity and pressure fields, the first step is to integrate the governing equations over a control volume. Integration of equation 3.102 gives

$$\begin{aligned} \epsilon_p^* \frac{(\rho_{vp} - \rho_{vp}^0)}{\Delta t} \left( \frac{r_e^2 - r_w^2}{2} \right) (z_n - z_s) + Re_x Pr \left( \frac{\alpha_a}{\alpha_s} \right) \left( \frac{L}{\sqrt{\kappa_r}} \right) \left( \frac{L}{H} \right) \left[ \frac{H}{R} (\epsilon_e^* r_e \rho_{ve} V_{re} \right. \\ \left. - \epsilon_w^* r_w \rho_{vw} V_{rw}) (z_n - z_s) + (\epsilon_n^* \rho_{vn} V_{zn} - \epsilon_s^* \rho_{vs} V_{zs}) \left( \frac{r_e^2 - r_w^2}{2} \right) \right] = \\ Bi_m \left( \frac{8L}{D} + 2 \right) \frac{(1 - \epsilon_p^*)}{2} (\rho_{iv} - \rho_{vp}^*) \left( \frac{r_e^2 - r_w^2}{2} \right) (z_n - z_s). \end{aligned} \quad (4.48)$$

Next, expressions for the interface vapor densities are needed. Let

$$F_e = Re_x Pr \frac{\alpha_a}{\alpha_s} \frac{L}{\sqrt{\kappa_r}} \frac{L}{R} r_e \epsilon_e^* V_{re} (z_n - z_s), \quad (4.49)$$

$$F_w = Re_x Pr \frac{\alpha_a}{\alpha_s} \frac{L}{\sqrt{\kappa_r}} \frac{L}{R} r_w \epsilon_w^* V_{rw} (z_n - z_s), \quad (4.50)$$

$$F_n = Re_x Pr \frac{\alpha_a}{\alpha_s} \frac{L}{\sqrt{\kappa_r}} \frac{L}{H} \epsilon_n^* V_{zn} \left( \frac{r_e^2 - r_w^2}{2} \right), \quad (4.51)$$

and,

$$F_s = Re_x Pr \frac{\alpha_a}{\alpha_s} \frac{L}{\sqrt{\kappa_r}} \frac{L}{H} \epsilon_s^* V_{zs} \left( \frac{r_e^2 - r_w^2}{2} \right). \quad (4.52)$$

From the integrated continuity equation for dry air (equation 4.2, page 73)

$$F_e - F_w + F_n - F_s = 0. \quad (4.53)$$

Thus,

$$F_e \rho_{vp} - F_w \rho_{vp} + F_n \rho_{vp} - F_s \rho_{vp} = 0. \quad (4.54)$$

Letting

$$\alpha_p^0 = \epsilon_p^* \left( \frac{r_e^2 - r_w^2}{2} \right) \frac{(z_n - z_s)}{\Delta t} \quad (4.55)$$

and,

$$S = \text{Bi}_m \left( \frac{8L}{D} + 2 \right) \frac{(1 - \epsilon_p^*)}{2} (\rho_{iv} - \rho_{vp}^*) \left( \frac{r_e^2 - r_w^2}{2} \right) (z_n - z_s) \quad (4.56)$$

and subtracting equation 4.54 from equation 4.48 gives

$$\begin{aligned} \alpha_p^0 (\rho_{vp} - \rho_{vp}^0) + (J_e - F_e \rho_{vp}) - (J_w - F_w \rho_{vw}) + \\ (J_n - F_n \rho_{vp}) - (J_s - F_s \rho_{vp}) = S \end{aligned} \quad (4.57)$$

where:

$$J_e = F_e \rho_{ve}, \quad (4.58)$$

$$J_w = F_w \rho_{vw}, \quad (4.59)$$

$$J_n = F_n \rho_{vn}, \quad (4.60)$$

and,

$$J_s = F_s \rho_{vs}. \quad (4.61)$$

Following Patankar (1980), let

$$J_e - F_e \rho_{vp} = \alpha_E (\rho_{vE} - \rho_{vE}), \quad (4.62)$$

$$J_w - F_w \rho_{vp} = \alpha_W (\rho_{vW} - \rho_{vE}), \quad (4.63)$$

$$J_n - F_n \rho_{vp} = \alpha_N (\rho_{vE} - \rho_{vN}), \quad (4.64)$$

and,

$$J_s - F_s \rho_{vp} = \alpha_S (\rho_{vS} - \rho_{vE}) \quad (4.65)$$

where:

$$\alpha_E = |-F_e, 0|, \quad (4.66)$$

$$\alpha_W = |F_w, 0|, \quad (4.67)$$

$$\alpha_N = |-F_n, 0|, \quad (4.68)$$

and,

$$\alpha_S = |F_s, 0|. \quad (4.69)$$

(Note:  $a, b$  is a quantity which is equal to either  $a$  or  $b$  depending on which is the larger number.) Substitution of equations 4.62 - 4.65 into 4.57 yields

$$\begin{aligned} \alpha_P^0(\rho_{vP} - \rho_{vP}^0) + \alpha_E(\rho_{vP} - \rho_{vE}) - \alpha_W(\rho_{vW} - \rho_{vP}) + \alpha_N(\rho_{vP} - \rho_{vN}) \\ - \alpha_S(\rho_{vS} - \rho_{vP}) = S. \end{aligned} \quad (4.70)$$

Rearranging equation 4.58 gives

$$\begin{aligned} [\alpha_P^0 + \alpha_E + \alpha_W + \alpha_N + \alpha_S]\rho_{vP} = \alpha_E\rho_{vE} + \\ \alpha_W\rho_{vW} + \alpha_N\rho_{vN} + \alpha_S\rho_{vS} + [\alpha_P^0\rho_{vP}^0 + S]. \end{aligned} \quad (4.71)$$

The discretized form of the energy equation 3.103 is obtained by integrating over a control volume. This yields

$$\begin{aligned} \epsilon_P^* \frac{T_P - T_P^0}{\Delta t} \left( \frac{r_e^2 - r_w^2}{2} \right) (z_n - z_s) + \left( \frac{L}{\sqrt{\kappa_r}} \right) \left( \frac{L}{R} \right) (Re_x Pr) \left( \frac{\alpha_a}{\alpha_s} \right) (r_e \epsilon_e^* V_{re} T_e - \\ r_w \epsilon_w^* V_{rw} T_w) (z_n - z_s) + \left( \frac{L}{\sqrt{\kappa_r}} \right) \left( \frac{L}{H} \right) (Re_x Pr) \left( \frac{\alpha_a}{\alpha_s} \right) (\epsilon_n^* V_{zn} T_n - \\ \epsilon_s^* V_{zs} T_s) \left( \frac{r_e^2 - r_w^2}{2} \right) = \left( \frac{\alpha_a}{\alpha_s} \right) \left( \frac{L}{H} \right)^2 \left[ \left( \frac{H}{R} \right)^2 \left( r_e \epsilon_e^* \frac{T_E - T_P}{r_E - r_P} - \right. \right. \\ \left. \left. r_w \epsilon_w^* \frac{T_P - T_W}{r_P - r_W} \right) (z_n - z_s) + \left( \epsilon_n^* \frac{T_N - T_P}{z_N - z_P} - \epsilon_s^* \frac{T_P - T_S}{z_P - z_S} \right) \left( \frac{r_e^2 - r_w^2}{2} \right) \right] - \end{aligned}$$

$$Bi_p \frac{\alpha_a}{\alpha_s} \left( \frac{8L}{D} + 2 \right) \frac{(1 - \epsilon_p^*)}{2} (T_i - T_p) \left( \frac{r_e^2 - r_w^2}{2} \right) (z_n - z_s). \quad (4.72)$$

This equation may be rewritten by letting

$$D_e = \frac{\alpha_a L^2 r_e \epsilon_e^* (z_n - z_s)}{\alpha_s R^2 (r_E - r_P)}, \quad (4.73)$$

$$D_w = \frac{\alpha_a L^2 r_w \epsilon_w^* (z_n - z_s)}{\alpha_s R^2 (r_P - r_W)}, \quad (4.74)$$

$$D_n = \frac{\alpha_a L^2 \epsilon_n^* (r_e^2 - r_w^2)}{\alpha_s 2H^2 (z_N - z_P)}, \quad (4.75)$$

$$D_s = \frac{\alpha_a L^2 \epsilon_s^* (r_e^2 - r_w^2)}{\alpha_s 2H^2 (z_P - z_S)}, \quad (4.76)$$

$$\alpha_p^0 = \epsilon_p^* \left( \frac{r_e^2 - r_w^2}{2} \right) \frac{(z_n - z_s)}{\Delta t}, \quad (4.77)$$

and,

$$S_T = -(Bi_p) \left( \frac{\alpha_a}{\alpha_s} \right) \left( \frac{8L}{D} + 2 \right) \frac{(1 - \epsilon_p^*)}{2} (T_i - T_p) \left( \frac{r_e^2 - r_w^2}{2} \right) (z_n - z_s). \quad (4.78)$$

Substitution of the above relations (equations 4.73 - 4.78), together with equations 4.49 - 4.52, into equation 4.72 yields

$$\begin{aligned} & \alpha_p^0 (T_p - T_p^0) + [F_e T_e - D_e (T_E - T_p)] - [F_w T_w - D_w (T_p - T_W)] \\ & + [F_n T_n - D_n (T_N - T_p)] - [F_s T_s - D_s (T_p - T_S)] = S_T. \end{aligned} \quad (4.79)$$

Now define

$$J_e = F_e T_e - D_e (T_E - T_p), \quad (4.80)$$

$$J_w = F_w T_w - D_w (T_p - T_W), \quad (4.81)$$

$$J_n = F_n T_n - D_n (T_N - T_p), \quad (4.82)$$

and,

$$J_s = F_s T_s - D_s (T_p - T_s). \quad (4.83)$$

This allows equation 4.79 to be rewritten as

$$\begin{aligned} \alpha_p^0 (T_p - T_p^0) + (J_e - F_e T_p) - (J_w - F_w T_p) + (J_n - F_n T_p) \\ - (J_s - F_s T_p) = S_T. \end{aligned} \quad (4.84)$$

Again following Patankar (1980), let

$$J_e - F_e T_p = \alpha_E (T_p - T_E), \quad (4.85)$$

$$J_w - F_w T_p = \alpha_W (T_W - T_p), \quad (4.86)$$

$$J_n - F_n T_p = \alpha_N (T_p - T_N), \quad (4.87)$$

and,

$$J_s - F_s T_p = \alpha_S (T_S - T_p) \quad (4.88)$$

where:

$$\alpha_E = D_e A \left( \left| \frac{F_e}{D_e} \right| \right) + |-F_e, 0|, \quad (4.89)$$

$$\alpha_W = D_w A \left( \left| \frac{F_w}{D_w} \right| \right) + |F_w, 0|, \quad (4.90)$$

$$\alpha_N = D_n A \left( \left| \frac{F_n}{D_n} \right| \right) + |-F_n, 0|, \quad (4.91)$$

$$\alpha_S = D_s A \left( \left| \frac{F_s}{D_s} \right| \right) + |F_s, 0|, \quad (4.92)$$

and,

$$A(P) = |0, (1 - 0.1P)^5|. \quad (4.93)$$

These derivations have employed expressions from the power-law scheme, which is recommended by Patankar for determining the interface variables.

The nondimensional source term may be written as

$$S_T = S_{Tc} + S_{Tp}T_p \quad (4.94)$$

where:

$$S_{Tc} = Bi_p \left( \frac{8L}{D} + 2 \right) (1 - \epsilon_p^*) T_i \left( \frac{r_o^2 - r_w^2}{2} \right) (z_n - z_s) \quad (4.95)$$

and,

$$S_{Tp} = \frac{-S_{Tc}}{T_i}. \quad (4.96)$$

The energy equation may now be expressed as

$$\begin{aligned} a_p^o(T_p - T_p^o) + a_E(T_p - T_E) + a_W(T_W - T_p) + a_N(T_p - T_N) \\ + a_S(T_S - T_p) = S_{Tc} + S_{Tp}T_p, \end{aligned} \quad (4.97)$$

or,

$$\begin{aligned} [a_p^o + a_E + a_W + a_N + a_S - S_{Tp}]T_p = [a_E T_E + a_W T_W \\ + a_N T_N + a_S T_S + a_p^o T_p^o + S_{Tc}]. \end{aligned} \quad (4.98)$$

Application of equations 4.71 and 4.98 over the entire grid results in a set of algebraic equations which may be solved iteratively to obtain the temperature and vapor density solution fields. Iteration is necessary since the equations are coupled to the inner domain equations. Since the inner and outer domain solutions must be obtained simultaneously, the equations for the inner domain will be derived before a discussion of the solution algorithm is presented.

#### 4.3.2. Governing Equations For The Inner Domain

The inner domain consists of a single element of the overall porous structure. Thus, it is a physically distinct



structure and another grid is required. The procedure previously discussed for establishing the grid was again used for the inner domain and so will not be discussed further.

The equations to be solved are the equation for conservation of mass,

$$\begin{aligned} \frac{\partial}{\partial z_i} \left[ \text{Lu}_L \left( \frac{\rho_s}{\Delta \rho_v} \right) K_L \frac{\partial u}{\partial z_i} + \text{Lu}_v \left( \epsilon - \frac{\rho_s}{\rho_L} u \right) K_v \frac{\partial \rho_{iv}}{\partial z_i} \right] = \\ \left( \frac{\rho_s}{\Delta \rho_v} \right) \left( 1 - \frac{\rho_{ve} + \Delta \rho_v \rho_{iv}}{\rho_L} \right) \frac{\partial u}{\partial t} + \left( \epsilon - \frac{\rho_s}{\rho_L} u \right) \frac{\partial \rho_{iv}}{\partial t}, \end{aligned} \quad (3.40)$$

the equation for conservation of energy,

$$\begin{aligned} \frac{\partial T_i}{\partial t} = \frac{\partial^2 T_i}{\partial z_i^2} - \text{Ko} \left( \frac{\Delta \rho_v}{\rho_s} \right) \left\{ \text{Lu}_v \frac{\partial}{\partial z_i} \left[ K_v \left( \epsilon - \frac{\rho_s}{\rho_L} u \right) \frac{\partial \rho_{iv}}{\partial z_i} \right] + \right. \\ \left. \frac{(\rho_{ve} + \Delta \rho_v \rho_{iv})}{\Delta \rho_v} \left( \frac{\rho_s}{\rho_L} \right) \frac{\partial u}{\partial t} - \left( \epsilon - \frac{\rho_s}{\rho_L} u \right) \frac{\partial \rho_{iv}}{\partial t} \right\} + \text{Bi} \left( \frac{4L}{D} \right) (T_a - T_i) - q_s \end{aligned} \quad (3.101)$$

and the equation of state,

$$\rho_{iv} = f(u, T) \quad u \leq u_{ms}, \quad (3.42a)$$

$$\rho_{iv} = \frac{1}{\Delta \rho_v R (T_e - \Delta T T_i)} e^{\left[ a + \frac{b}{(T_e - \Delta T T_i)} + c \ln(T_e - \Delta T T_i) \right]} \quad u > u_{ms}. \quad (3.42b)$$

For simplicity, equations (3.40) and (3.101) will be written in terms of "local" Luikov numbers. Thus, these equations become

$$\begin{aligned} \frac{\partial}{\partial z_i} \left[ \text{Lu}_{xL} \left( \frac{\rho_s}{\Delta \rho_v} \right) \frac{\partial u}{\partial z_i} + \text{Lu}_{xv} \left( \epsilon - \frac{\rho_s}{\rho_L} u \right) \frac{\partial \rho_{iv}}{\partial z_i} \right] = \left( \frac{\rho_s}{\Delta \rho_v} \right) \left( 1 - \frac{\rho_{ve} + \Delta \rho_v \rho_{iv}}{\rho_L} \right) \frac{\partial u}{\partial t} \\ + \left( \epsilon - \frac{\rho_s}{\rho_L} u \right) \frac{\partial \rho_{iv}}{\partial t} \end{aligned} \quad (4.99)$$

and,

$$\frac{\partial T_i}{\partial t} = \frac{\partial^2 T_i}{\partial z_i^2} - \text{Ko} \left( \frac{\Delta \rho_v}{\rho_s} \right) \left\{ \frac{\partial}{\partial z_i} \left[ Lu_{zv} \left( \epsilon - \frac{\rho_s}{\rho_L} u \right) \frac{\partial \rho_{iv}}{\partial z_i} \right] + \frac{(\rho_{ve} + \Delta \rho_v \rho_{iv})}{\Delta \rho_v} \left( \frac{\rho_s}{\rho_L} \right) \frac{\partial u}{\partial t} - \left( \epsilon - \frac{\rho_s}{\rho_L} u \right) \frac{\partial \rho_{iv}}{\partial t} \right\} + \text{Bi} \left( \frac{4L}{D} \right) (T_a - T_i) - q_s \quad (4.100)$$

where:

$$Lu_{zL} = \frac{D_L^*}{\alpha_s} \quad (4.101)$$

and,

$$Lu_{zv} = \frac{D_v^*}{\alpha_s} \quad (4.102)$$

Recall that the unknown quantities to be solved for are  $\rho_{iv}$ ,  $T_i$  and  $u$ . Equations 4.99 and 4.100 provide two equations which will be discretized and used in an iterative procedure to find the inner domain solution. The third equation is obtained from equation 3.42; however, the equation of state is normally provided in terms of an algebraic function and so does not need to be discretized. Since  $\rho_{iv}$ ,  $u$  and  $T_i$  all appear in the two equations to be discretized, any two of these variables may be picked as the "solution" variables. After some trial and error, it was decided to solve for the variables  $\rho_{iv}$  and  $T_i$  from the discretized equations. During the iterative procedure, values of these variables are used to obtain  $u$  from the equation of state (equation 3.42).

Numerical stability was enhanced by rewriting the temporal derivatives of  $u$  in terms of the two solution variables. This allowed more "current" values of the solution variables to be used in place of "older" (previous iteration) values of

u in the discretized equations, and resulted in a more accurate determination of the temporal derivative of u at each iteration. This procedure was necessary due to the shape of the sorption isotherm relation. A detailed discussion of the sorption isotherm is presented in Section 5.1. Substituting the relation,

$$\frac{\partial u}{\partial t} = \left. \frac{\partial u}{\partial \rho_{iv}} \right|_{T_i} \frac{\partial \rho_{iv}}{\partial t} + \left. \frac{\partial u}{\partial T_i} \right|_{\rho_{iv}} \frac{\partial T_i}{\partial t} \quad (4.103)$$

into (4.99) and (4.100) yields

$$\begin{aligned} \frac{\partial}{\partial z_i} \left[ \text{Lu}_{zL} \left( \frac{\rho_s}{\Delta \rho_v} \right) \frac{\partial u}{\partial z_i} + \text{Lu}_{zv} \left( \epsilon - \frac{\rho_s}{\rho_L} u \right) \frac{\partial \rho_{iv}}{\partial z_i} \right] = \\ \left( \frac{\rho_s}{\Delta \rho_v} \right) \left( 1 - \frac{\rho_{ve} + \Delta \rho_v \rho_{iv}}{\rho_L} \right) \left( \left. \frac{\partial u}{\partial \rho_{iv}} \right|_T \frac{\partial \rho_{iv}}{\partial t} + \left. \frac{\partial u}{\partial T_i} \right|_{\rho} \frac{\partial T_i}{\partial t} \right) + \\ \left( \epsilon - \frac{\rho_s}{\rho_L} u \right) \frac{\partial \rho_{iv}}{\partial t} \end{aligned} \quad (4.104)$$

and,

$$\begin{aligned} \frac{\partial T_i}{\partial t} = \frac{\partial^2 T_i}{\partial z_i^2} - \text{Ko} \left( \frac{\Delta \rho_v}{\rho_s} \right) \left\{ \frac{\partial}{\partial z_i} \left[ \text{Lu}_{zv} \left( \epsilon - \frac{\rho_s}{\rho_L} u \right) \frac{\partial \rho_{iv}}{\partial z_i} \right] \right. \\ \left. + \frac{(\rho_{ve} + \Delta \rho_v \rho_{iv})}{\Delta \rho_v} \left( \frac{\rho_s}{\rho_L} \right) \left( \left. \frac{\partial u}{\partial \rho_{iv}} \right|_T \frac{\partial \rho_{iv}}{\partial t} + \left. \frac{\partial u}{\partial T_i} \right|_{\rho} \frac{\partial T_i}{\partial t} \right) - \left( \epsilon - \frac{\rho_s}{\rho_L} u \right) \frac{\partial \rho_{iv}}{\partial t} \right\} \\ + \text{Bi} \left( \frac{4L}{D} \right) (T_a - T_i) - q_s. \end{aligned} \quad (4.105)$$

It will be assumed at this point that the derivatives of u with respect to density and temperature may both be determined exactly from analytical expressions for given values of the density and temperature. If this is not true, approximate expressions for these derivatives may be employed.

Integration of equation 4.104 over a single time interval and individual control volume yields

$$\begin{aligned}
& \left[ \left( \frac{\rho_s}{\Delta \rho_v} \right) (Lu_{zLn}) \frac{u_N - u_P}{z_N - z_P} - \left( \frac{\rho_s}{\Delta \rho_v} \right) (Lu_{zLs}) \frac{u_P - u_S}{z_P - z_S} \right] + \\
& \left[ Lu_{zvrn} \left( \epsilon - \frac{\rho_s}{\rho_L} u_n \right) \frac{\rho_{ivN} - \rho_{ivP}}{z_N - z_P} - Lu_{zvs} \left( \epsilon - \frac{\rho_s}{\rho_L} u_s \right) \frac{\rho_{ivP} - \rho_{ivS}}{z_P - z_S} \right] = \\
& \left( \frac{\rho_s}{\Delta \rho_v} \right) \left( 1 - \frac{\rho_{ve} + \Delta \rho_v \rho_{ivP}^o}{\rho_L} \right) \left[ \left( \frac{\partial u}{\partial \rho_{iv}} \right) \frac{\rho_{ivP} - \rho_{ivP}^o}{\Delta t} + \left( \frac{\partial u}{\partial T_i} \right) \frac{T_{iP} - T_{iP}^o}{\Delta t} \right] (z_n - z_s) \\
& + \left( \epsilon - \frac{\rho_s}{\rho_L} u_p^o \right) \frac{\rho_{ivP} - \rho_{ivP}^o}{\Delta t} (z_n - z_s). \tag{4.106}
\end{aligned}$$

Rearranging terms gives

$$\begin{aligned}
& \left\{ \left[ \left( \frac{\rho_s}{\rho_L} \right) \left( \frac{\rho_L - \rho_{ve}}{\Delta \rho_v} - \rho_{ivP}^o \right) \left( \frac{\partial u}{\partial \rho_{iv}} \right) \frac{(z_n - z_s)}{\Delta t} + \left( \epsilon - \frac{\rho_s}{\rho_L} u_p^o \right) \frac{(z_n - z_s)}{\Delta t} \right] + \right. \\
& \left. \left[ \left( \epsilon - \frac{\rho_s}{\rho_L} u_n \right) \frac{Lu_{zvrn}}{z_N - z_P} \right] + \left[ \left( \epsilon - \frac{\rho_s}{\rho_L} u_s \right) \frac{Lu_{zvs}}{z_P - z_S} \right] \right\} \rho_{ivP} = \left[ \left( \epsilon - \frac{\rho_s}{\rho_L} u_n \right) \frac{Lu_{zvrn}}{z_N - z_P} \right] \rho_{ivN} \\
& + \left[ \left( \epsilon - \frac{\rho_s}{\rho_L} u_s \right) \frac{Lu_{zvs}}{z_P - z_S} \right] \rho_{ivS} + \left[ \left( \frac{\rho_s}{\rho_L} \right) \left( \frac{\rho_L - \rho_{ve}}{\Delta \rho_v} - \rho_{ivP}^o \right) \left( \frac{\partial u}{\partial \rho_{iv}} \right) \frac{(z_n - z_s)}{\Delta t} + \right. \\
& \left. \left( \epsilon - \frac{\rho_s}{\rho_L} u_p^o \right) \frac{(z_n - z_s)}{\Delta t} \right] \rho_{ivP}^o + \left[ \frac{\rho_s Lu_{zLn} (u_N - u_P)}{\rho_L (z_N - z_P)} - \frac{\rho_s Lu_{zLs} (u_P - u_S)}{\rho_L (z_N - z_P)} \right. \\
& \left. + \left( \frac{\rho_s}{\rho_L} \right) \left( \frac{\rho_L - \rho_{ve}}{\Delta \rho_v} - \rho_{ivP}^o \right) \left( \frac{\partial u}{\partial T_i} \right) \frac{T_{iP} - T_{iP}^o}{\Delta t} (z_n - z_s) \right]. \tag{4.107}
\end{aligned}$$

Equation 4.107 may be rewritten as

$$[a_p^o + a_N + a_S] \rho_{ivP} = a_N \rho_{ivN} + a_S \rho_{ivS} + b \tag{4.108}$$

where:

$$a_N = \left( \epsilon - \frac{\rho_s}{\rho_L} u_n \right) \frac{Lu_{zvrn}}{z_N - z_P}, \tag{4.109}$$

$$a_s = \left( \epsilon - \frac{\rho_s}{\rho_L} u_s \right) \frac{Lu_{zvs}}{z_P - z_S}, \quad (4.110)$$

$$a_P^o = \left[ \left( \frac{\rho_s}{\rho_L} \right) \left( \frac{\rho_L - \rho_{ve}}{\Delta \rho_v} - \rho_{ivP}^o \right) \left( \frac{\partial u}{\partial \rho_{iv}} \right) + \left( \epsilon - \frac{\rho_s}{\rho_L} u_P^o \right) \right] \frac{(z_n - z_s)}{\Delta t}, \quad (4.111)$$

$$S = \left[ \frac{\rho_s Lu_{zLn}(u_N - u_P)}{\rho_L(z_N - z_P)} - \frac{\rho_s Lu_{zLs}(u_P - u_S)}{\rho_L(z_P - z_S)} + \left( \frac{\rho_s}{\rho_L} \right) \left( \frac{\rho_L - \rho_{ve}}{\Delta \rho_v} - \rho_{ivP}^o \right) \left( \frac{\partial u}{\partial T_i} \right) \frac{T_{iP} - T_{iP}^o}{\Delta t} (z_n - z_s) \right], \quad (4.112)$$

and,

$$b = a_P^o \rho_{vP}^o + S. \quad (4.113)$$

Integration of the inner domain energy equation over a single time interval and control volume gives

$$\begin{aligned} \frac{T_{iP} - T_{iP}^o}{\Delta t} (z_n - z_s) &= \frac{T_{iN} - T_{iP}}{z_N - z_P} - Ko \left( \frac{\Delta \rho_v}{\rho_s} \right) \left\{ Lu_{zvn} \left( \epsilon_n - \frac{\rho_s}{\rho_L} u_n \right) \frac{\rho_{vN} - \rho_{vP}}{z_N - z_P} \right. \\ &- Lu_{zvs} \left( \epsilon_s - \frac{\rho_s}{\rho_L} u_s \right) \frac{\rho_{ivP} - \rho_{ivS}}{z_P - z_S} + \left( \frac{\rho_s}{\rho_L} \right) \frac{(\rho_{ve} + \Delta \rho_v \rho_{ivP}^o)}{\Delta \rho_v} \left[ \left( \frac{\partial u}{\partial \rho_{iv}} \right) \frac{\rho_{ivP} - \rho_{ivP}^o}{\Delta t} \right. \\ &+ \left. \left. \left( \frac{\partial u}{\partial T_i} \right) \frac{T_{iP} - T_{iP}^o}{\Delta t} \right] (z_n - z_s) \right\} + Bi_P \left( \frac{4L}{D} \right) (T_a - T_{iP}) (z_n - z_s) \\ &- q_s (z_n - z_s). \end{aligned} \quad (4.114)$$

Letting

$$a_P^o = \left[ 1 + (Ko) \frac{\rho_{ve} + \Delta \rho_v \rho_{ivP}^o}{\rho_L} \left( \frac{\partial u}{\partial T_i} \right) \right] \frac{(z_n - z_s)}{\Delta t}, \quad (4.115)$$

$$a_N = \frac{1}{z_N - z_P}, \quad (4.116)$$

$$a_S = \frac{1}{z_P - z_S}, \quad (4.117)$$

$$\begin{aligned}
S_c = & \left\{ Ko \left( \frac{\Delta \rho_v}{\rho_s} \right) \left[ Lu_{xvs} \left( \epsilon_s - \frac{\rho_s}{\rho_L} u_s \right) \frac{\rho_{ivP} - \rho_{ivS}}{z_P - z_S} - Lu_{xvn} \left( \epsilon_n - \frac{\rho_s}{\rho_L} u_n \right) \frac{\rho_{ivN} - \rho_{ivP}}{z_N - z_P} \right. \right. \\
& \left. \left. \frac{\rho_s}{\rho_L} \left( \frac{\rho_{ve}}{\Delta \rho_v} + \rho_{ivP}^o \right) \left( \frac{\partial u}{\partial \rho_{iv}} \right) \frac{\rho_{ivP} - \rho_{ivP}^o}{\Delta t} (z_n - z_s) \right] + Bi_p \left( \frac{4L}{D} \right) (z_n - z_s) T_a \right. \\
& \left. - q_s (z_n - z_s) \right\}, \tag{4.118}
\end{aligned}$$

$$S_p = -Bi_p \left( \frac{4L}{D} \right) (z_n - z_s), \tag{4.119}$$

and,

$$b = S_c + a_p^o T_{ip}^o. \tag{4.120}$$

allows equation 4.114 to be rewritten as

$$[a_p^o + a_N + a_S - S_p] T_{ip} = a_N T_{in} + a_S T_{is} + b. \tag{4.121}$$

(Note: Treating the energy used for liquid vaporization as an energy "source" has some disadvantages associated with it. These disadvantages are discussed in Appendix B.)

### 4.3.3. Solution Algorithms For The Inner And Outer Domains

Application of equations (4.108) and (4.121) over the entire inner domain grid results in a second set of algebraic equations which must be solved in an iterative manner, as are the outer domain equations. Each outer domain control volume contains a (specified) number of inner domain elements. The vapor density and temperature of the air flowing through the outer domain directly influence the amount of mass and energy transferred from (to) the inner domain. Therefore, the inner

domain equations must be solved at each grid point in the outer domain. Since the correct vapor density and temperature of the air in the outer domain are not known in advance at the "current" time, the mass transfer predicted from the inner domain equations may not be correct. Thus, the solution proceeds in an iterative manner; the "correct" solution being obtained when the predicted mass and energy transferred from the inner domain result in no significant change in conditions (from the previous iteration) in the air in the outer domain. The full solution algorithm is shown schematically in Figures 4.3 and 4.4.

The solution algorithm proceeds as follows.

1. All variables are initialized so that the boundary and initial conditions (equations 3.44-3.51, 3.86, 3.87, 3.89-3.92, and 3.95-3.98 on pages 61 and 62) are satisfied.
2. The equations governing conservation of mass (equation 4.108) and conservation of energy (equation 4.121) for the inner domain elements are solved at each outer domain grid point. This determines the amount of mass and energy transferred from an inner domain element in each outer domain control volume. Thus, this determines the moisture content of each inner domain element.

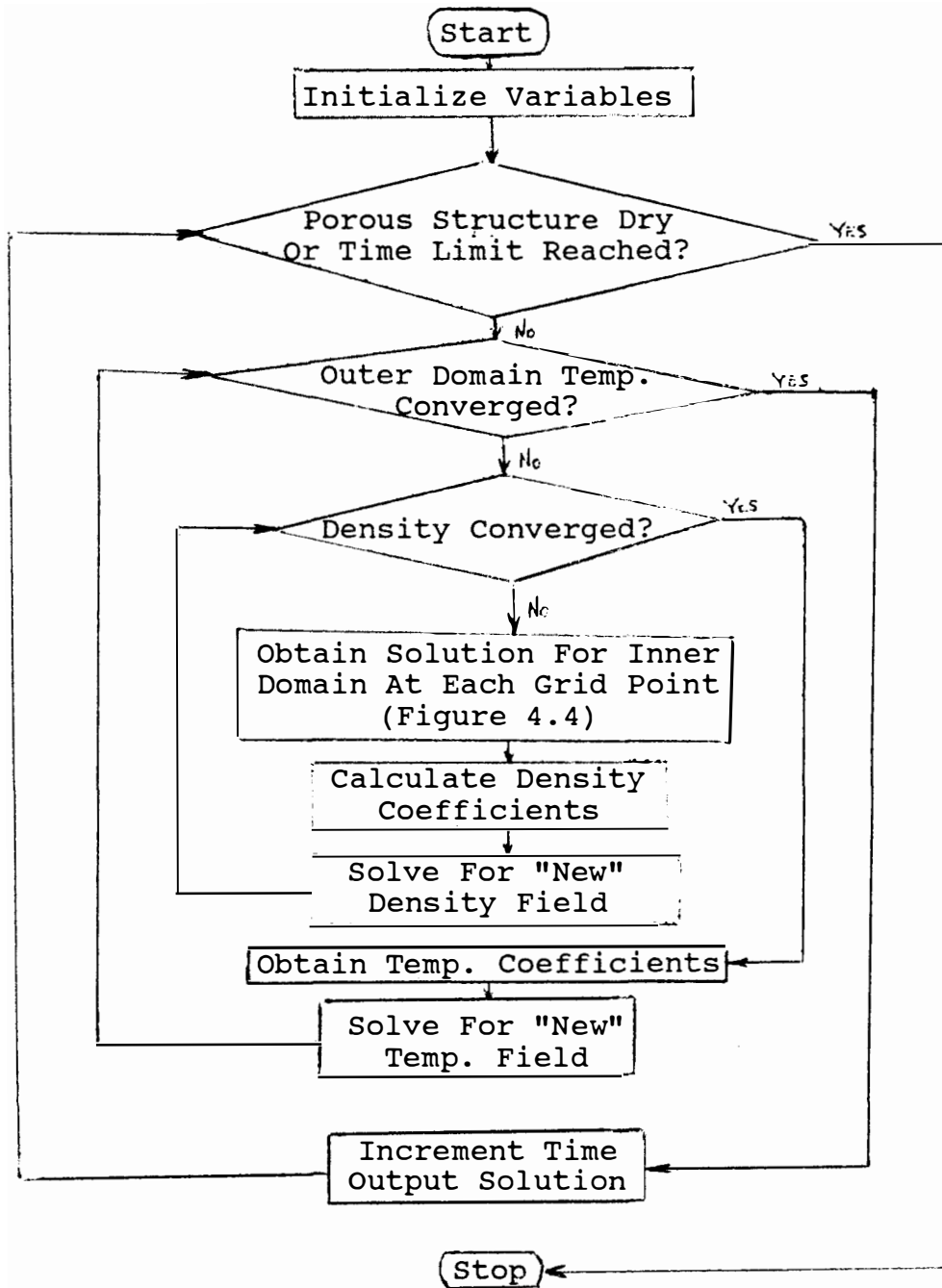


Figure 4.3. Outer Domain Solution Algorithm.



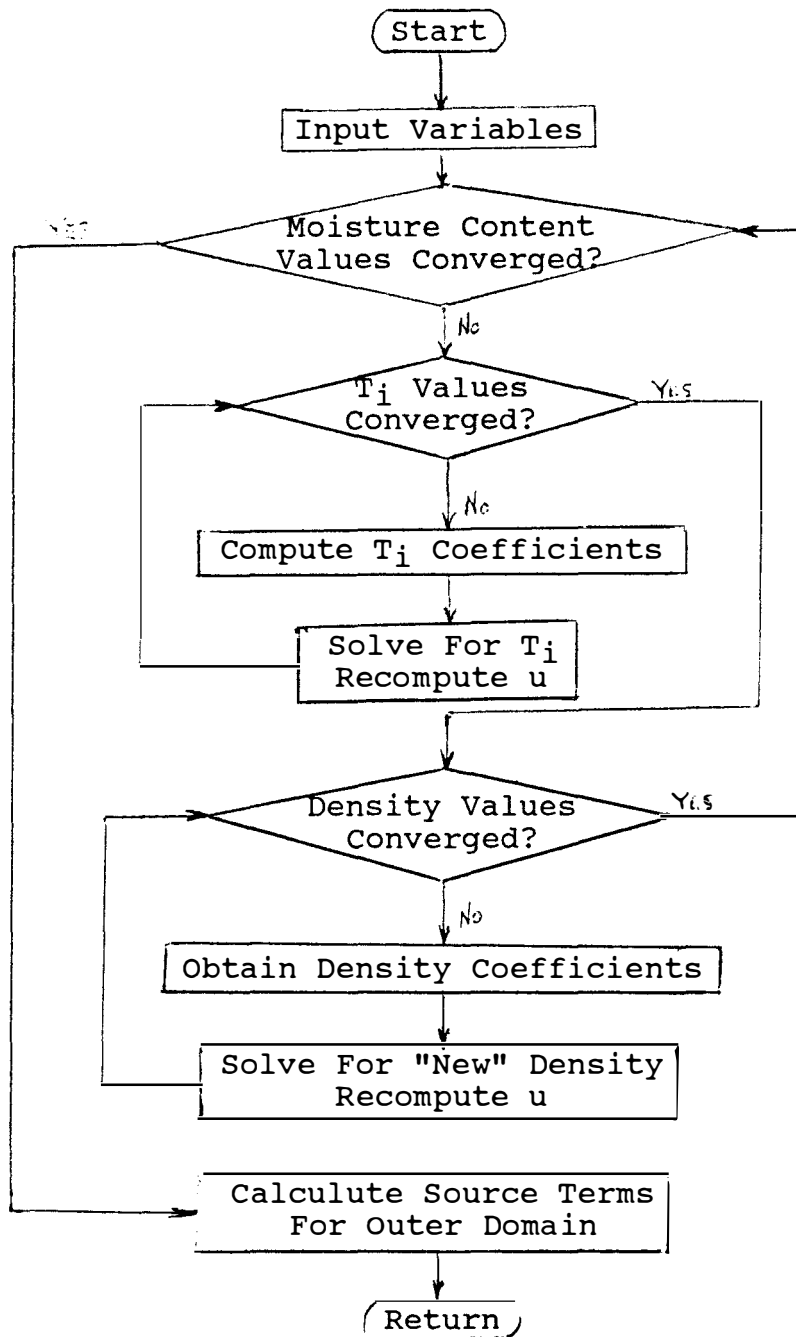


Figure 4.4. Inner Domain Solution Algorithm.

3. The equation governing conservation of mass for the water vapor in the outer domain (equation 4.71, page 84) is then solved to determine the "new" vapor density distribution.
4. If the difference between iterations at any point in the outer domain is "significant" (i.e. vapor density values have not converged), return to step 2.
5. A "new" temperature field is found by solving the equation for conservation of energy in the outer domain (equation 4.98, page 87).
6. If the difference between iterations at any point in the outer domain is "significant" (i.e. temperature values have not converged), return to step 2.
7. The time step is incremented and steps 2 - 6 are repeated until steady state conditions are obtained.

As discussed above, the equations governing the conservation of mass (4.108, page 91) and energy (4.121, page 93) in the inner domain are solved at each outer domain grid point. The solution algorithm for these equations is shown in Figure 4.4. The algorithm proceeds as follows.

1. Values of variables ( $\rho_v$ ,  $T$ ,  $\rho_{iv}^o$ ,  $T_i^o$ , and  $u^o$ ) are passed from the main program. "Current" values of the inner domain vapor density, temperature, and moisture content ( $\rho_{iv}$ ,  $T$ , and  $u$ ) are set equal to the values at the previous time step.
2. The equations governing the conservation of energy in the inner domain (4.121) is solved to obtain the "new" (current iteration)  $T_i$  values.
3. "New" moisture content ( $u$ ) values are calculated from the sorption isotherm relation (equation 3.42, page 60).
4. If the difference between iterations in the temperature ( $T_i$ ) at any location is "significant", return to step 2.
5. The equation governing conservation of mass (4.108, page 91) is solved for the "new" inner domain vapor density,  $\rho_{iv}$ .
6. "New" moisture content values are computed from the sorption isotherm relation (equation 3.42, page 60).
7. If the difference between iterations for the inner domain vapor density ( $\rho_{iv}$ ) at any grid point in the inner domain is "significant", return to step 4.

8. If any "significant" difference between the moisture content values obtained during the temperature field iterations and the vapor density field iterations is noted, return to step 2.
9. Return to the main program.

## 5. PARAMETRIC STUDY

In order to efficiently operate a drier, it is important to have an understanding of the affect of changing the pertinent dimensionless parameters in the problem. In this section, the important dimensionless parameters and a "base case", typical of the drying of hay bales, are identified. The drying process for the base case is examined somewhat in detail to provide an understanding of the drying process in hay bales. Then, the important dimensionless parameters are varied systematically to determine their impact on the drying process.

Once the effect of varying the important parameters is known, several conclusions are made relating to the drying process. A discussion of how these conclusions may influence drier operation is also presented.

### 5.1. Identification And Discussion Of Important Dimensionless Parameters In The Analytical Model

A review of the mathematical model reveals that there are 15 dimensionless parameters appearing in the problem. To determine the relative influence of these terms, a parametric study was performed. Not all the parameters, however, may be controlled in a practical situation. Typically, one may alter the drying process by varying one or more of the following physical variables: 1) the inlet air temperature, 2) the

relative humidity of the inlet air, 3) the inlet air velocity, 4) the dimensions of the overall porous structure, and 5) the dimensions of an inner domain element.

Examination of Table 3.1 (page 63) reveals that one, or more, of these factors may be changed by altering any of the following parameters

$$Ko, \frac{\rho_{ve}}{\Delta\rho_v}, \frac{\rho_s}{\Delta\rho_v}, Re_v, \frac{H}{R}, \frac{H}{L}, R_{IN}, \frac{\sqrt{\kappa_r}}{L}, \text{ and } \frac{L}{D}.$$

All of the parameters in this set, however, are not easily varied, or can only be varied over very narrow ranges. For example, the ratio of the equilibrium vapor density to the characteristic change in vapor density ( $\rho_{ve}/\Delta\rho_v$ ) is typically of order one. Physically, this ratio must always be greater than or equal to zero. Practically, however, it would be virtually impossible to lower the equilibrium vapor density to zero. In addition, the vapor density is also physically limited in value by the fact that the relative humidity of the air may not exceed 100%. The change in vapor density must also be large enough to allow the porous medium to dry the required amount (typically from 35% to 18% w.b.). A typical range of values for this parameter is from approximately 0.5 to 2.7. Thus, it is not practical to vary this parameter in order to control the drying process.

The porous structure itself is normally of fixed composition (i.e. the porous solid to be dried may not be replaced by another solid). Thus, the ratio of the solid

density to the characteristic change in vapor density,  $\rho_s/\Delta\rho_v$ , may also not be varied in a practical situation to control the drying process (a range of  $2.5 \times 10^4$  to  $12.4 \times 10^4$  is typical). In addition, neither the height of the porous structure nor the length of an inner domain element may be varied by a great amount (for the hay bale application being investigated) due to practical limitations of balers and the physical dimensions of typical hay stalks. The range of permeabilities for a hay bale is also constrained. The bale must be porous enough to blow air through, yet must be solid enough to withstand the rigors of handling. Thus, the values of  $H/L$  (ranging from approximately 225 to 540) and  $\sqrt{\kappa_r}/L$  (ranging from approximately 0.02 to 0.04) are also limited by practical considerations.

Based on the above discussion, it was decided to examine the effect of varying

$$K_0, Re_x, \frac{H}{R}, \frac{L}{D}, \text{ and } R_{IN}$$

on the velocity distribution and the drying process. It should be noted that the geometric parameters relating to the outer domain ( $H/R$  and  $R_{IN}$ ) appear in both the equations determining the velocity field and those governing the drying processes. Thus, even though these terms may not be varied over a large range of values (approximately 0.75 to 2.0 for  $H/R$  and 0.2 to 0.8 for  $R_{IN}$ ), they may have a significant

impact on the drying process due to their influence on the velocity field.

The inner domain aspect ratio ( $L/D$ ) also may not vary over a wide range for the present application (a range of effective  $L/D$  values of 0.7 - 2.1 is considered "practical"). However, since this is the only geometric parameter relating to the inner domain, it was desired to examine the effect of varying this parameter. A discussion relating to the values chosen for this parameter is presented in Appendix C.

In practice, the Kossovich number ( $Ko = L_v \Delta u / C_s \Delta T$ ) may be varied by either controlling  $\Delta u$  or  $\Delta T$ . This may be accomplished by varying the relative humidity and/or temperature of the inlet air stream.

The Reynolds number ( $Re = V_{IN} \sqrt{\kappa_r} / \nu$ ) may be varied by changing either the inlet air velocity or the permeability of the porous structure. For any given hay bale, the permeability is fixed. Thus, in practice the Reynolds number is varied by changing the inlet air velocity.

The terms  $H/R$ ,  $L/D$  and  $R_{IN}$  are geometric parameters. These terms may be varied by varying the appropriate geometric quantities.

The parameteric study was thus conducted by varying each of the five parameters ( $Ko$ ,  $Re_x$ ,  $H/R$ ,  $L/D$ , and  $R_{IN}$ ) separately while maintaining the rest of the parameters at



the constant values listed in Table 5.1. The ranges of values of the five variable parameters listed above are presented in Table 5.2.

The baling of large round hay bales typically occurs in a manner that produces regions of varying porosity within the bale. For this reason, it was also desired to examine a case where the porosity varies spatially throughout the hay bale. Thus, another case was run for a "typical" porosity distribution within the hay bale (Bledsoe, 1989).

## 5.2. Determination Of Physical Quantities Appearing In The Mathematical Model

As has been mentioned, the sorption isotherm relation is also very important in the drying of any hygroscopic porous solid. For this study, the sorption isotherm of alfalfa hay obtained from the data of Hill, Ross, and Barfield (1977) was employed. This data is reproduced in Figure 5.1. The resulting relations are given by a function of the form

$$u^* = c_1 \phi + c_2 T_i^* + c_3 \quad (5.1)$$

where  $c_1$ ,  $c_2$ , and  $c_3$  are constants determined from a least square fit of the experimental data for three different intervals of relative humidity (i.e. the experimental curve was divided into three approximately linear regions and a least square fit was performed for each region). The details of these relations are presented in Appendix D, however, some comments regarding the numerical solution are in order at this point.

Table 5.1. Values Of The Dimensionless Parameters Held Constant For The Entire Parametric Study.

| Dimensionless Parameter          | Value                 |
|----------------------------------|-----------------------|
| $\frac{K_a}{K_s}$                | 1.0                   |
| $\frac{\alpha_a}{\alpha_s}$      | 450                   |
| $\frac{H}{L}$                    | $3.59 \times 10^2$    |
| $\frac{\sqrt{\kappa_r}}{L}$      | $2.95 \times 10^{-2}$ |
| $\frac{\rho_{ve}}{\Delta\rho_v}$ | 1.65                  |
| $\frac{\rho_s}{\rho_l}$          | 0.535                 |
| $\frac{\rho_s}{\Delta\rho_v}$    | $9.59 \times 10^4$    |
| $Lu_l$                           | $5.46 \times 10^{-5}$ |
| $Lu_v$                           | $5.80 \times 10^2$    |
| $Pr$                             | 0.72                  |

Table 5.2. Ranges Of Values For The Dimensionless Parameters In the Parametric Study.

| Parameter     | Base Case Value | Range Of Values |
|---------------|-----------------|-----------------|
| $K_o$         | 110             | 10 - 400        |
| $Re_x$        | 9.4             | 4.7 - 18.8      |
| $\frac{H}{R}$ | 1.6             | 0.75 - 2.0      |
| $R_{IN}$      | 0.4             | 0.2 - 0.8       |
| $\frac{L}{D}$ | 1.4             | 0.7 - 2.1       |

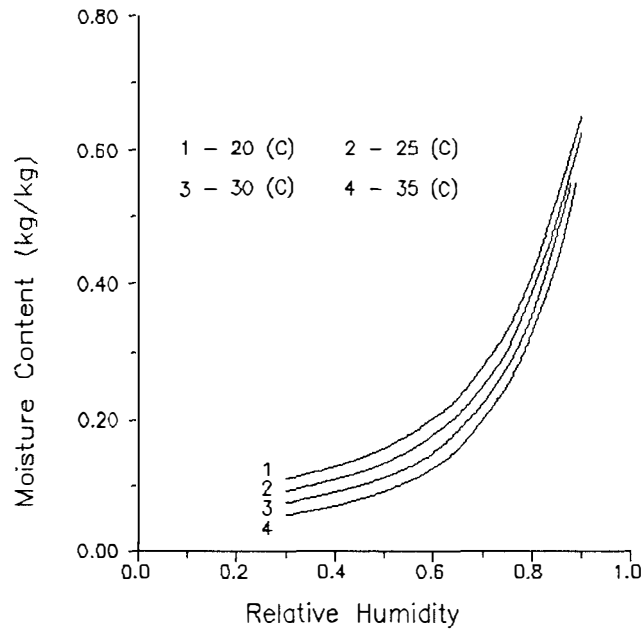


Figure 5.1. Sorption Isotherm For Alfalfa Hay (Reproduced From Hill, Ross and Barfield, 1977).

There was considerable difficulty in obtaining convergence of the numerical model during the preliminary stages of this project. Berger (1973), in modelling a single inner domain element, also had this difficulty. He was never able to obtain convergence for realistic values of the convection coefficients ( $h$  and  $h_m$ ). The difficulty apparently lies in the fact that the inner domain vapor density, temperature, and moisture content ( $\rho_{iv}$ ,  $T_i$ , and  $u$ ) all appear in the inner domain equations. Values for any two of the three variables (for the present study, the vapor density and temperature were chosen) are determined from the governing equations and the third (moisture content in the present study) is obtained by substitution of these two variables into the sorption isotherm relation. Thus, values of the third variable "lag" behind during the iterative solution process since previous iteration values of the other variables are used in the sorption isotherm relation. The sorption isotherm is typically very steep for conditions occurring at the start of most drying processes. The "lag" of information is thus critical and leads to convergence problems.

To provide more current information during the solution process, equation 4.103 (page 90) was used to express the temporal derivative of moisture content in terms of inner domain vapor density and temperature. The details of the

numerical formulation have already been presented and will not be discussed further except to say that this procedure averted the convergence problems described above.

Another aspect of the model that should be mentioned is the determination of the convection coefficients in the mathematical model. A correlation (Bird, Stewart, and Lightfoot, 1960) for heat transfer in packed beds was used to determine the convective heat transfer coefficient between the solid and the air. This correlation is presented in Appendix A and may be written as

$$j_H = C_1 (Re')^{\alpha_1} \psi \quad (A.1)$$

where:

$$j_H = \text{Chilton-Colburn Factor} = \frac{h}{\rho_a C_{pa} V^*} (Pr)^{2/3} ,$$

$\alpha_1, C_1 = \text{constants},$

$$Re' = \text{"Modified" Reynolds Number} = \frac{\rho_a V^*}{\alpha \mu_f \psi} ,$$

$\alpha = \frac{\text{Particle Surface Area}}{\text{Per Bed Volume}} ,$

$\psi = \text{Empirical Coefficient Which Depends On Particle Shape (.91 for cylinders)} ,$

and,

$$Pr = \text{Prandtl Number} = \frac{v}{\alpha_a} .$$

The Chilton-Colburn analogy for heat and mass transfer was then used to obtain a value for the mass transfer coefficient (Bird, Stewart, and Lightfoot, 1960). The details of these correlations are also provided in Appendix A.

Values of the porosity for both the inner and outer domains were also required. The measurements of Ohm, Vogtlander, and Kossen (1971) concerning the density of hay were used to determine the porosity of an inner domain element. Their measurements indicated that the solid density of alfalfa hay is 1500 (kg/m<sup>3</sup>), while the bulk density is approximately 535 (kg/m<sup>3</sup>). The porosity is therefore given by

$$\epsilon_i^* = 1 - \frac{\rho_b}{\rho_s} = 0.64. \quad (5.2)$$

The outer domain porosity was obtained using a representative dry matter density measurement (Bledsoe and Hitch, 1989) together with the bulk density of an inner domain element given above (note: the dry matter density represents the mass of solid hay matter in a given volume of the hay bale). The outer domain porosity is therefore given by

$$\epsilon^* = 1 - \frac{\rho_{dm}}{\rho_b}. \quad (5.3)$$

A dry matter density of approximately 112 (kg/m<sup>3</sup>) was ascertained to be representative of a "typical" hay bale. The porosity for the base case in the parametric study (and all other cases unless otherwise stated) is given by equation 5.2 as 0.79.

The permeability and the coefficient of the Forscheimer term were both calculated from a relation determined experimentally by Bledsoe and Hitch (1989). These relations are discussed in Appendix E. The permeability is given by

$$\kappa^* = 1.02 \times 10^{-2} \rho_{dm}^{-2.93} \quad (m^2) \quad (E.1)$$

With a uniform dry matter density of 112 (kg/m<sup>3</sup>), the permeability is 1.0 x 10<sup>-8</sup> (m<sup>2</sup>).

The relationship describing the coefficient of the Forscheimer term may be written in the form

$$b^* = 107.6 e^{0.0343 \rho_{dm}} \left( \frac{kg}{m^4} \right) \quad (E.2)$$

With a dry matter density of 112 (kg/m<sup>3</sup>), the coefficient of the Forscheimer term is given by the above relation as 46.6 (kg/m<sup>4</sup>).

Finally, values of the diffusion coefficients,  $D_v^*$  and  $D_l^*$  were also estimated. It was observed that the solution field was not sensitive to values of  $D_l^*$  for the range of parameters studied due both to the magnitude of the moisture content gradient and the magnitude of the liquid conductivity. Chen and Pei (1989) have shown that the bound liquid conductivity may be expressed as

$$D_l^* = D_{L_0} \left( \frac{u^* - u_e^*}{u_{ms}^* - u_e^*} \right)^3 \exp \left( \frac{-E_d}{RT_i^*} \right) \quad (5.4)$$

where:

$$D_{L_0} = \text{Constant.}$$

$u_e^*$  = Equilibrium moisture content,

$u_{ms}$  = Maximum sorptional moisture content,

and,

$E_a$  = Activation energy of liquid.

Representative values for the constant  $D_{lo}$  were presented by Chen and Pei (1989) for wool (0.062), brick (0.098), and corn (0.0001). An intermediate value of  $1.0 \times 10^{-3}$  (m<sup>2</sup>/s) was used in the present study as no data was available for alfalfa hay; however, as stated above, the solution field was not sensitive to this value. The activation energy,  $E_a$ , is the energy necessary to vaporize the bound water. The value of the heat of vaporization for pure water was used in the present study.

The vapor diffusion coefficient,  $D_v^*$ , was determined from the data of Fair and Lerner (1956) for the diffusion of water vapor through air. The difference between the initial and equilibrium temperatures was small (5 °C) for the cases examined. Thus, a constant value of  $2.8 \times 10^{-5}$  (m<sup>2</sup>/s) was used for  $D_v^*$  in all cases. Since a constant value of  $D_v^*$  was used,  $D_v$  was equal to one for all cases.

### 5.3. Discussion Of The "Base Case" For The Parametric Study

Before performing a comparison of the various cases in the parametric study, it is instructive to begin by examining



the drying process for the base case. The values used for all parameters for the base case are listed in Table 5.1, page 105, and Table 5.2, page 106. A grid refinement study was performed to determine an acceptable mesh size as well as a suitable time step. The results of this exercise resulted in using a 16 by 16 mesh size for the outer domain, a 10 by 1 mesh size for the inner domain, and a time step of approximately 7.5 (30 minutes). The solution of a "typical" case required approximately 3 hours of CPU time on the University of Tennessee VAX Cluster.

The total moisture content for the overall porous structure is defined as

$$U_b = \frac{1}{V_{OD}} \int_{V_{OD}} u \, dV \quad . \quad (5.5)$$

This moisture content represents the average moisture content for an entire bale based on the total amount of liquid present. The drying front is defined to be the region in which the moisture content varies between 0.05 and 0.95. Thus, the drying front is defined as the time-varying region in space where most of the drying occurs.

Figure 5.2 shows a plot of total moisture content as a function of time. This figure shows that the moisture content of a bale decreases very rapidly at the start of the drying process and then decreases more slowly as drying continues. At a nondimensional time of approximately 2320 (6.5 days), the drying process is completed and equilibrium is reached.

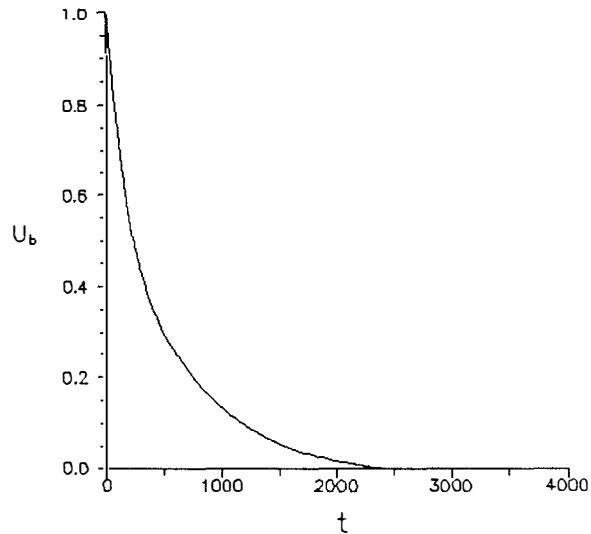


Figure 5.2. Variation Of Total Moisture Content In A Bale With Time For The Base Case.

Some insight into the shape of this drying curve may be obtained by examining Figure 5.3. This figure shows a combined plot of the streamlines for the flow through a bale and the velocity profile along the boundary of the bale. As expected, the velocity profile shows that most of the inlet air stream exits through the bottom portion of the outer surface of the bale. Thus, the lower region of the bale is exposed to a relatively large flow rate of hot dry air and tends to dry quickly. The upper portion of the structure, however, is exposed to a smaller volume of air per unit time and therefore dries at a slower rate. The result is that the bale dries "quickly" at the start of the drying process when the bottom portion of the bale is being dried. However, as the drying proceeds, the moisture content in the lower region of the

bale approaches zero and the processes occurring in the upper portion of the bale begin to dominate. Thus, the overall drying rate for the bale decreases with increasing time.

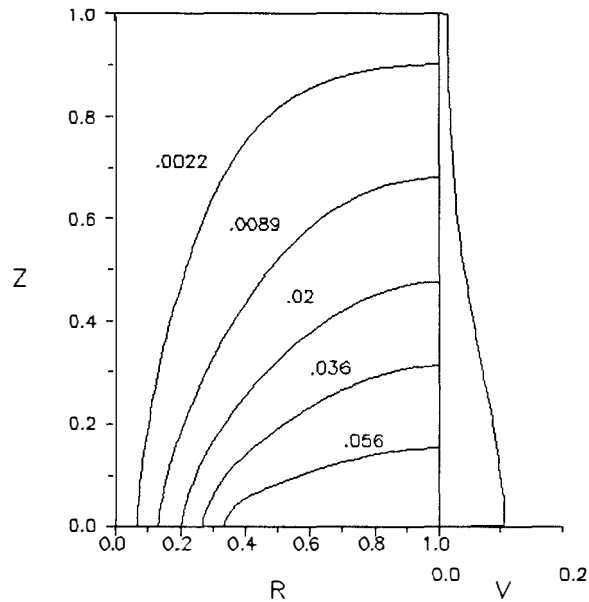
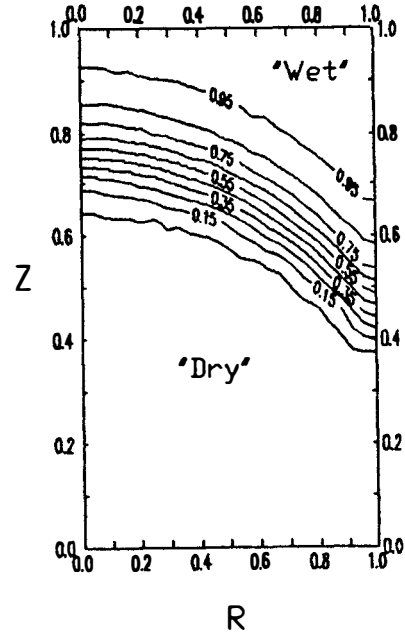
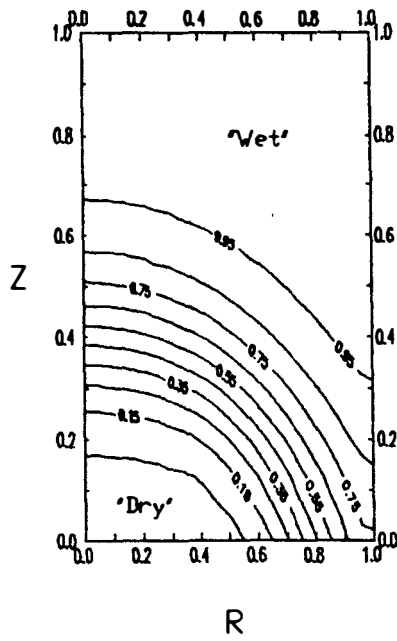
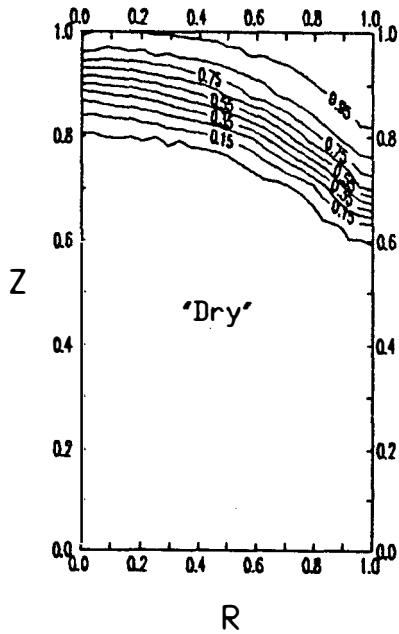


Figure 5.3. Air Flow Distribution In The Bale For The Base Case.

This trend is also evident in Figures 5.4 and 5.5. Figure 5.4 shows the progression of the "drying front" through the bale with time. At the start of the drying process, the front is very thick, as shown in Figure 5.4a. Again, this is due to the fact that a relatively large quantity of hot dry air is flowing past the inner domain elements in this region of the bale. Thus, both the potential for mass transfer and the

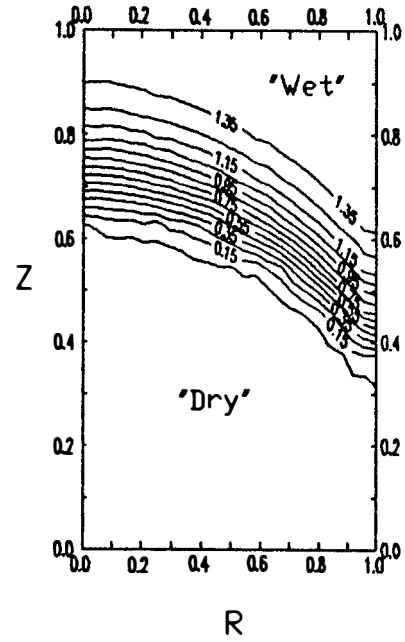
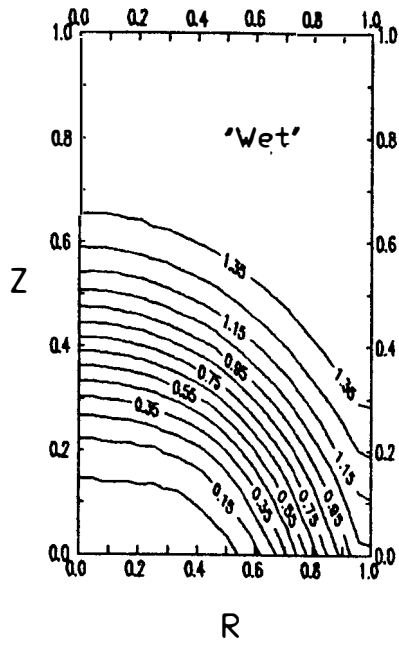


(a) Dimensionless Time = 75      (b) Dimensionless Time = 375

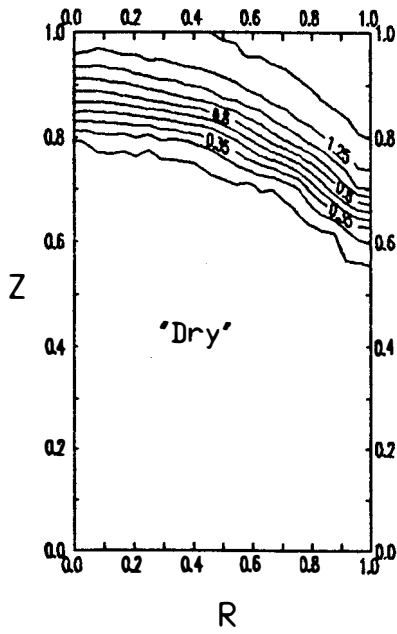


(c) Dimensionless Time = 750

Figure 5.4. Drying Front Location Shown With Lines Of Constant Moisture Content For The Base Case At Different Times.



(a) Dimensionless Time = 75      (b) Dimensionless Time = 375



(c) Dimensionless Time = 750

Figure 5.5. Isotherms Shown Within The Bale For The Base Case At Different Times.

velocity (which enhances convection) are greater in this area than they are in the uppermost regions of the bale. As drying proceeds, the "dry" side of the front moves rapidly (due to the high potential for mass transfer and the high air velocity). The "wet" side moves more slowly, however, since it is moving into a region in the bale where the air velocity is lower. The result is that the drying front tends to become thinner with time, and the drying process proceeds more slowly as shown in Figure 5.4.

Another aspect of the drying process is illustrated in Figure 5.5. As the air flows through the bale, it transfers thermal energy to the inner domain elements, which causes mass transfer to occur. Thus, the air stream becomes cooler (recall that as the dimensional temperature decreases the nondimensional temperature increases) and picks up more and more moisture as it flows through the outer domain. If the air stream picks up enough moisture (and cools sufficiently), the vapor density in the air stream approaches that of the inner domain elements (or approaches the saturation density). Thus, less and less mass transfer occurs, such that the air stream loses less energy to the inner domain. The result is that the temperature decreases through the drying front and then stays essentially constant in the wet region of the bale.

Further insight into the drying process may be gained from examination of Figure 5.6. This figure shows the time-varying moisture content,  $u$ , at axial locations of 0,

0.54, and 1.0 at a radial location of 0.74. The moisture content at the bottom of the bale ( $z=0$ ) decreases very quickly at the start of the drying process and reaches equilibrium at a dimensionless time of approximately 194 (1.1 days). At a point approximately half way up the length of the bale (at  $z = 0.54$ ), the drying process is displaced in time and equilibrium conditions are reached at a dimensionless time of approximately 540 (1.5 days).

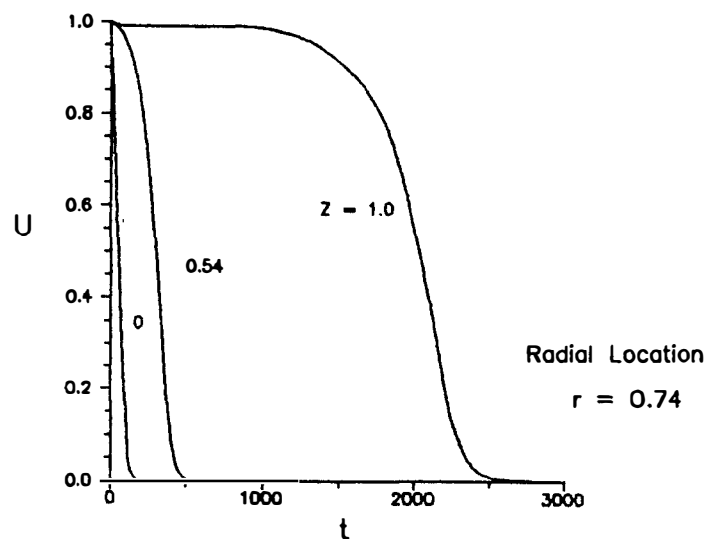


Figure 5.6. Variation Of The Moisture Content At Three Different Axial Locations And A Radial Location Of  $r=0.74$  For The Base Case.

This delay is explained by once again considering the streamline and velocity distributions in the bale. As shown in Figure 5.3, the drying inlet air travels a shorter distance at a greater velocity near the bottom of the bale. Thus, the tendency is to dry faster in this lower region. At an axial

location of 0.54, the flow path followed by the air is longer and the velocity of the air is lower. Thus, the air picks up a greater amount of moisture, which results in a higher vapor density and less potential for mass transfer. Hence, the drying is somewhat delayed in the upper regions of the bale. At the top of the bale ( $z=1$ ), the flow path is longer still, and the air picks up so much moisture that the local mass transfer rates in this region of the bale is quite low for dimensionless times less than 1160 (3.2 days). As the moisture content approaches zero in the lower regions of the bale, the air does not pick up as much moisture. The drying process then begins in the top region of the bale, and equilibrium is reached at a time of approximately 2610 (7.3 days).

#### 5.4. The Effects Of Varying The Reynolds Number On The Drying Process

A comparison of the drying processes at different Reynolds numbers is presented in Figure 5.7. As expected, an increase in the Reynolds number results in a decrease in the overall drying time for the global structure.

For the base case ( $Re = 9.4$ ), equilibrium is reached at a nondimensional time of approximately 2320 (6.5 days). Doubling the Reynolds number to 18.8 results in a drying time of approximately 970 (2.7 days). This represents a reduction in drying time of approximately 58%. Halving the Reynolds number to a value of 4.7, however, results in a marked increase



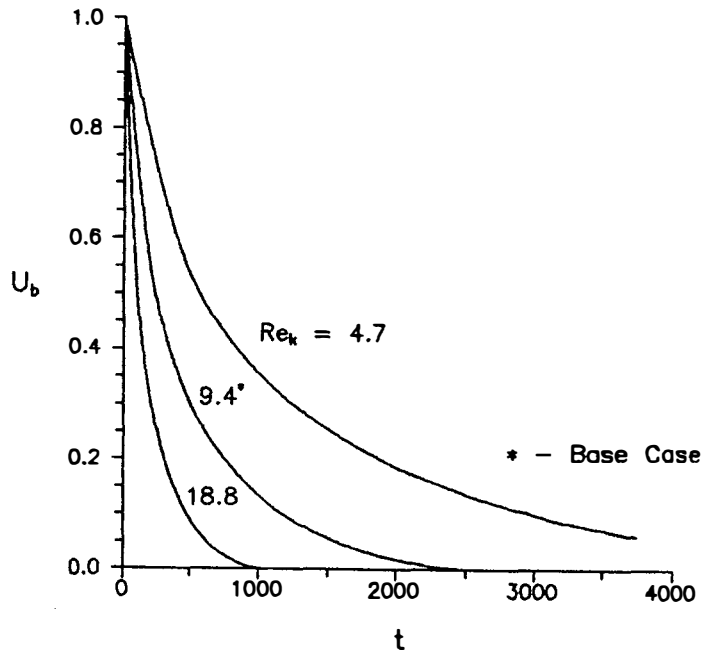
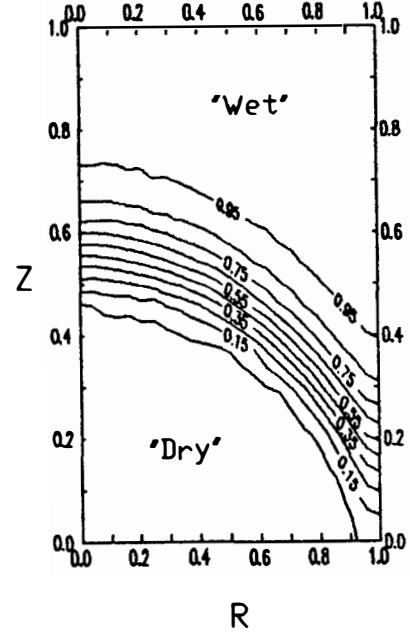
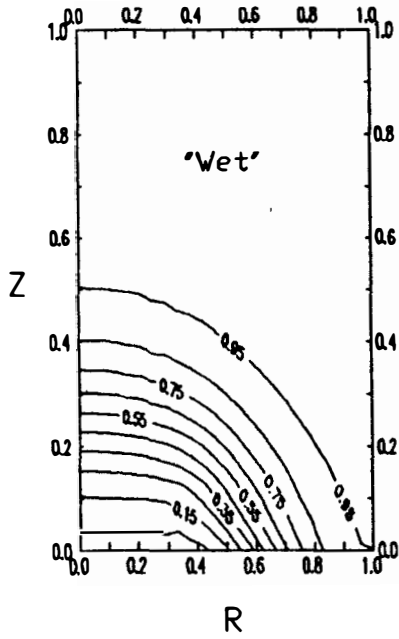


Figure 5.7. Variation Of The Total Moisture Content Of A Bale With Time For Different Reynolds Numbers.

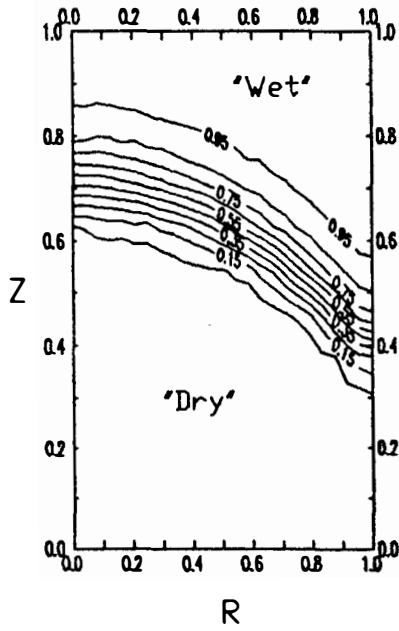
in the drying time. The numerical solution was stopped at a time of approximately 3680 (10.2 days); at which time the bale still has a moisture content of approximately 0.06. By contrast, the base case reaches this same moisture content at a time of approximately 1450 (4.0 days) and the higher Reynolds number case at approximately 580 (1.6 days). Thus, the drying time is a strong function of the Reynolds number.

The nondimensional velocity distributions for these two cases are the same as that of the base case since no parameters affecting the nondimensional velocity were changed. The streamlines and the velocity profile along the vertical side

of the bale are thus identical to that shown in Figure 5.3 (p.114). The convection coefficients,  $h$  and  $h_m$ , however, are both functions of the Reynolds number. As the Reynolds number increases, both of the convection coefficients also increase. Thus, at a higher Reynolds number, heat is convected to and mass is convected away from the inner domain elements more readily. This results in a faster moving drying front and lower drying times. This trend is illustrated in Figures 5.8 and 5.9. As shown in these figures, the drying processes for Reynolds numbers of 4.7 and 18.5 proceed in the same manner as that of the base case; that is, the front is initially rather thick and then becomes thinner with increasing time. As has been noted, the difference between these two cases lies in the speed with which the "front" moves through the bale. Figures 5.8c and 5.9c show the drying front locations at a time of 750 (approximately 2 days) for Reynolds numbers of 4.7 and 18.8, respectively. For a Reynolds number of 4.7, approximately half the bale is "dry", while the front almost passes completely through the structure for the case with a Reynolds number of 18.8. From Figures 5.8 and 5.9, one notices that at earlier times the drying occurs over a greater volume at higher Reynolds numbers. Again, this is due to the larger convective coefficients and volumetric flowrate of air in the outer domain at higher Reynolds numbers.

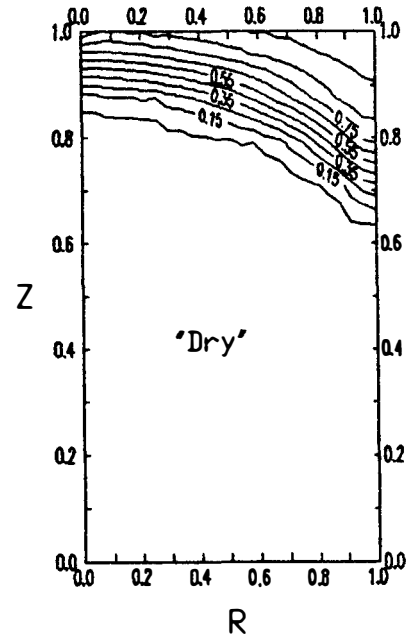
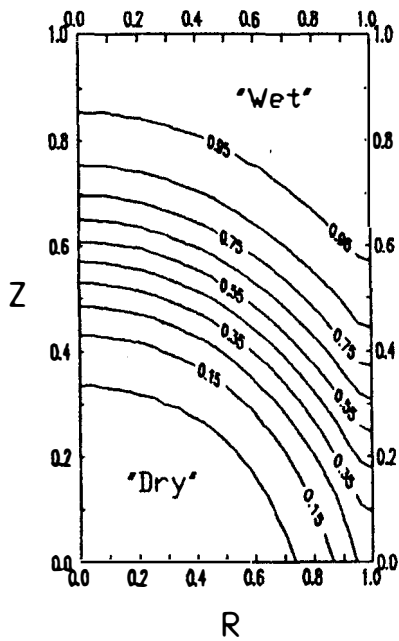


(a) Dimensionless Time = 75      (b) Dimensionless Time = 375

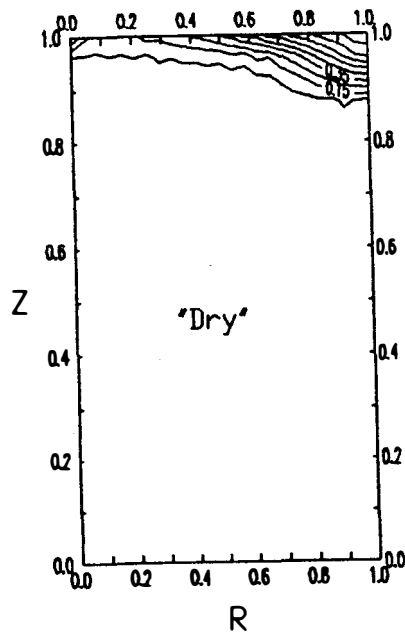


(c) Dimensionless Time = 750

Figure 5.8. Drying Front Location Shown With Lines Of Constant Moisture Content For A Reynolds Number Of 4.7 At Different Dimensionless Times.



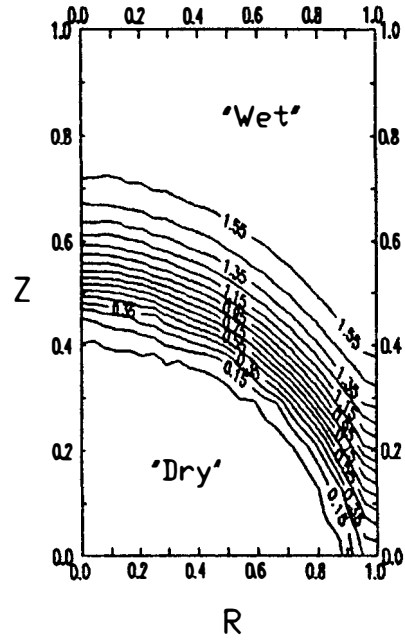
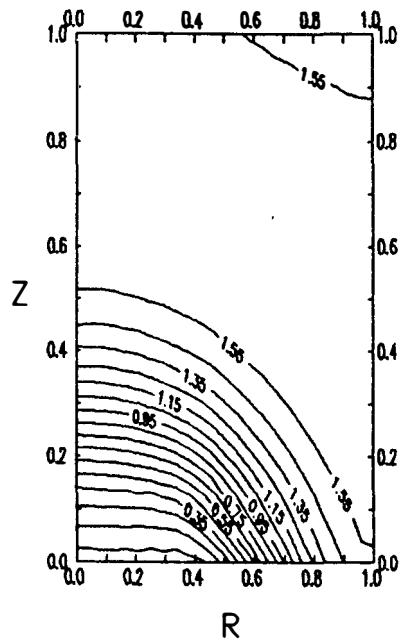
(a) Dimensionless Time = 75      (b) Dimensionless Time = 375



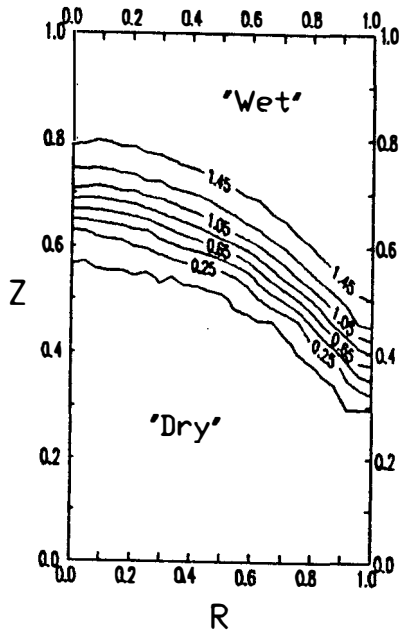
(c) Dimensionless Time = 750

Figure 5.9. Drying Front Location Shown With Lines Of Constant Moisture Content For A Reynolds Number Of 18.8 At Different Dimensionless Times.

One interesting difference between the drying processes at different Reynolds numbers may be seen by examining the temperature profiles for these cases, which are shown in Figures 5.10 and 5.11. For the lowest Reynolds number case of 4.7, the temperature decreases through the drying front and then increases again in the wet region. This may be explained by noting that the air is cooled in the drying front below the initial temperature of the solid structure. Once the air stream passes through the drying front, it no longer experiences this cooling. In fact, just the opposite occurs. The solid structure which is then warmer than the air stream, gives up energy to the flowing air. This results in a warming of the air stream. As the flow path of the air stream beyond the region where drying occurs increases, this effect becomes more pronounced. Since the front does not progress as far into the porous structure at lower Reynolds numbers, the path length taken from the wet side of the drying front to the structure boundary is longer. Thus, a warming trend is exhibited at a Reynolds number of 4.7. The drying front extends almost all the way through the global structure for the higher Reynolds number of 18.8. Thus, no region exists in which the air stream is reheated at this higher Reynolds number.

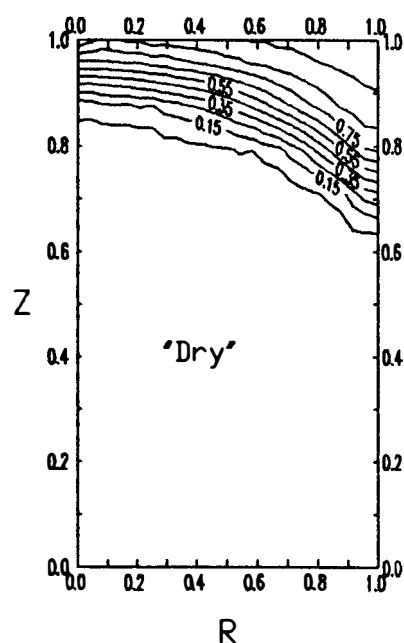
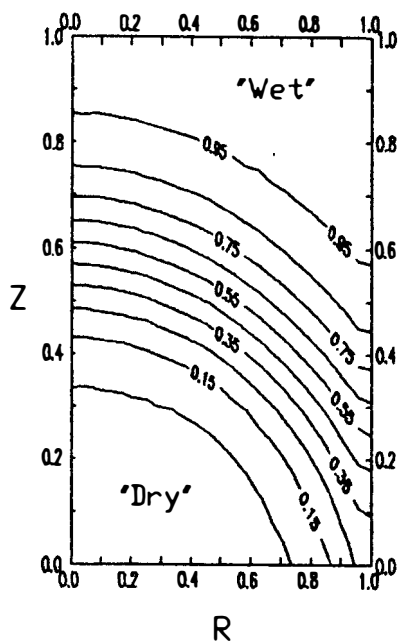


(a) Dimensionless Time = 75      (b) Dimensionless Time = 375

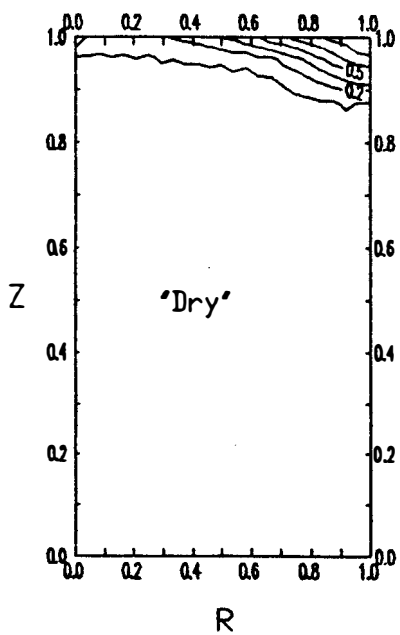


(c) Dimensionless Time = 750

Figure 5.10. Isotherm Distribution For A Reynolds Number Of 4.7 At Different Dimensionless Times.



(a) Dimensionless Time = 75      (b) Dimensionless Time = 375



(c) Dimensionless Time = 750

Figure 5.11. Isotherm Distribution For A Reynolds Number Of 18.8 At Different Dimensionless Times.

### 5.5. The Effects Of Varying The Overall Aspect Ratio Of The Bale On The Drying Process

The next parameter to be investigated was the aspect ratio,  $H/R$ , of the bale. A change in this ratio has a direct influence on the velocity distribution in the outer domain. This effect is shown in Figures 5.12 and 5.13 for aspect ratios of 2.0 and 0.75, respectively.

For an aspect ratio of 2.0, the resistance to flow in the axial direction is large compared to that in the radial direction. The result is that most of the incoming flow of air exits from the bottom half of the bale. A dramatic difference is seen for  $H/R$  equal to 0.75. Here the axial resistance to flow is smaller than the radial resistance to flow. The result is a virtually uniform radial velocity profile over the entire height of the outside surface of the bale. Hence, inner domain elements throughout the bale are exposed to higher air flow velocities which results in increased heat and mass transfer. Thus, enhancement of the drying process by decreasing the aspect ratio,  $H/R$ , of the bale is to be expected.

This trend is seen Figure 5.14, which shows the total moisture content of a bale versus time for the range of aspect ratios examined in this study. Decreasing the aspect ratio from 1.6 (base case) to 0.75 results in an approximate decrease of 66% in the drying time. Increasing the aspect ratio to



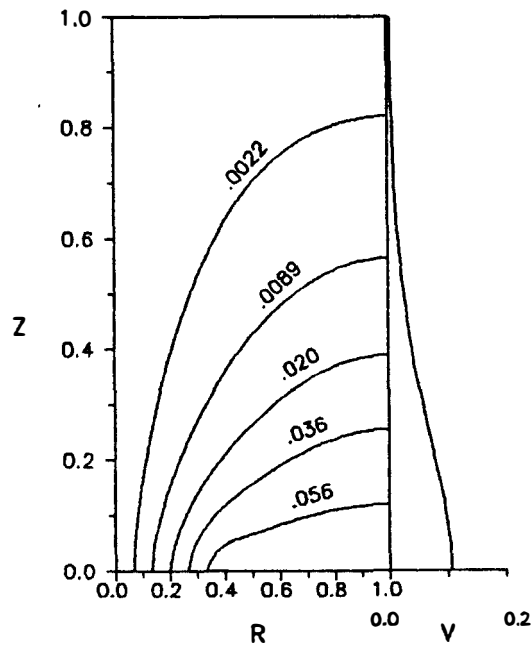


Figure 5.12. Streamlines And The Velocity Distribution On The Outer Surface For The Air Flow Through A Bale With An Aspect Ratio Of 2.0.

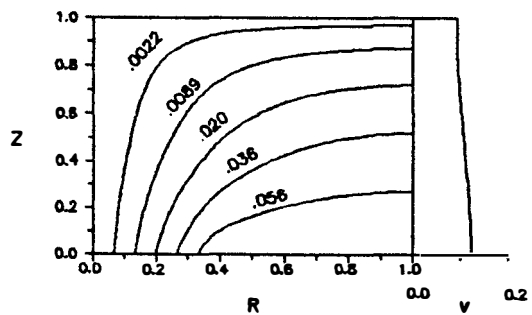


Figure 5.13. Streamlines And The Velocity Distribution On The Outer Surface For The Air Flow Through A Bale With An Aspect Ratio Of 0.75.

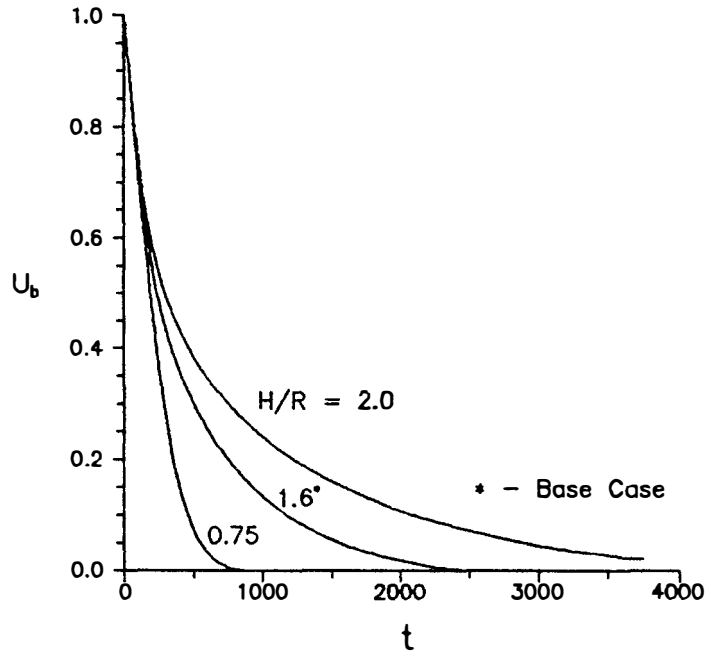
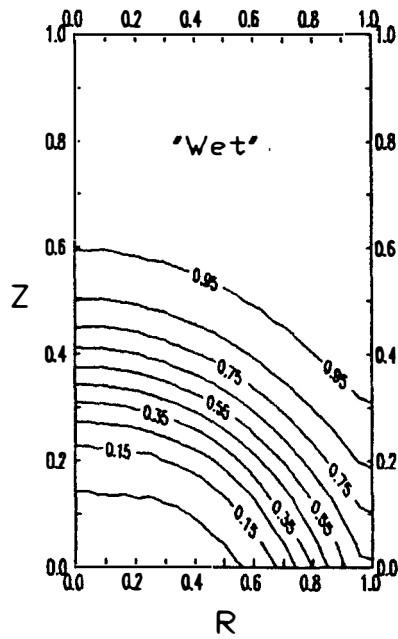


Figure 5.14. Variation Of The Total Moisture Content Of A Bale With Time For Different Bale Aspect Ratios.

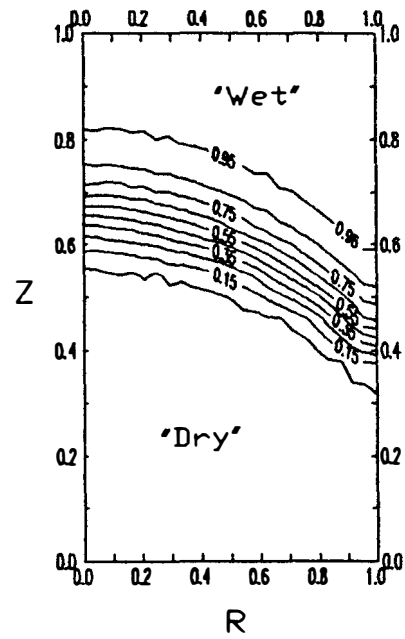
a value of 2.0 results in a significant increase in the drying time. Again, the numerical solution was stopped before equilibrium conditions were obtained. At a time of 3680 (approximately 10.2 days), the moisture content was about 0.02. This same moisture content is obtained at a time of approximately 1940 (5.4 days) for the base case ( $H/R = 1.6$ ) and a time of approximately 620 (1.7 days) for an aspect ratio of 0.75.

Figures 5.15 and 5.16 show the effects of varying the aspect ratio on the moisture content distribution within the bale structure. For an aspect ratio of 0.75, the drying front occupies approximately one-half of the volume of the bale at a time of 75 (5 hours). At this same time, the drying fronts in bales with aspect ratios of 1.6 and 2.0 occupy much smaller portions of the total volumes of these bales. At a time of 750 (2.1 days), drying is almost completed for an aspect ratio of 0.75, while a significant portion of a bale is still drying at this time for an aspect ratio of 2.0.

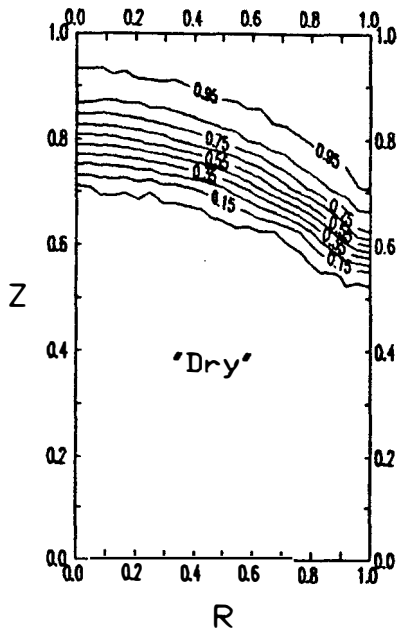
The temperature profiles are shown in Figures 5.17 and 5.18. One sees that for the fastest drying case ( $H/R = 0.75$ ), the temperature decreases along the flow path throughout the entire bale. As was the case for the drying processes at different Reynolds numbers, however, the slowest drying case



(a) Dimensionless Time = 75

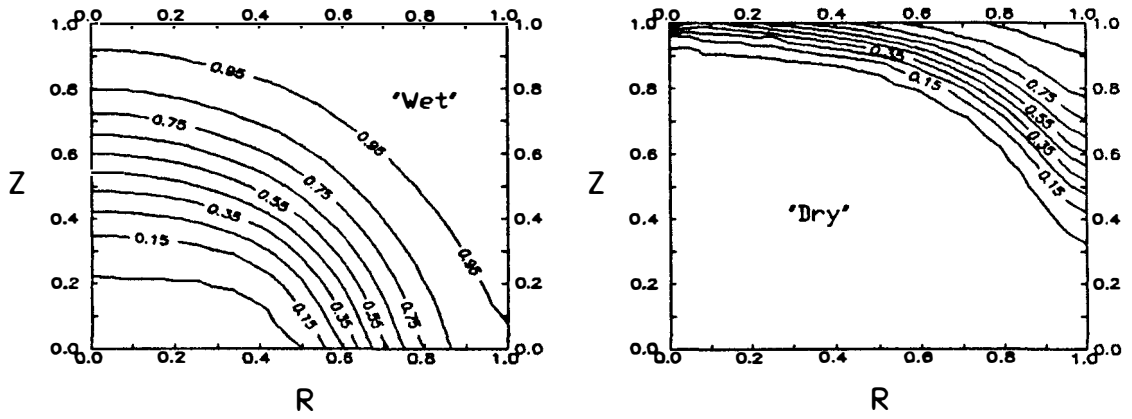


(b) Dimensionless Time = 375

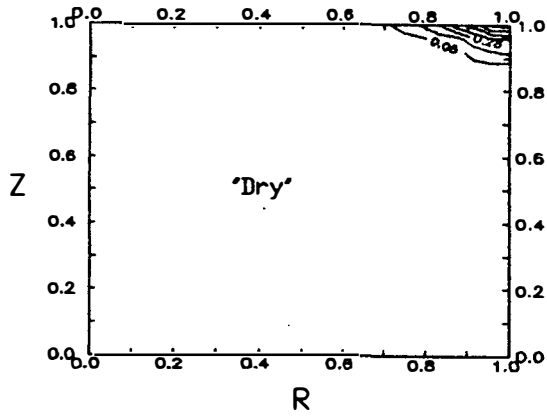


(c) Dimensionless Time = 750

Figure 5.15. Drying Front Locations Shown With Lines Of Constant Moisture Content For An Aspect Ratio Of 2.0 At Different Dimensionless Times.

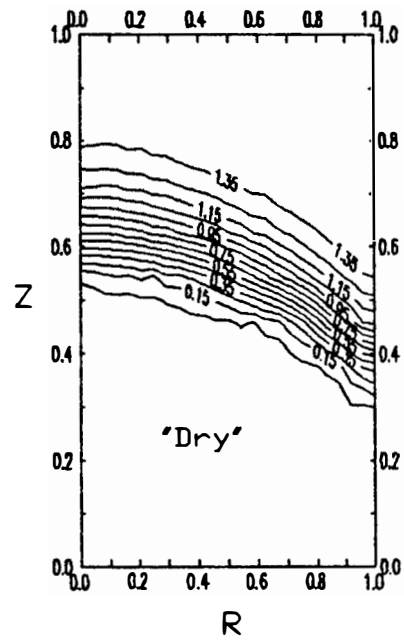
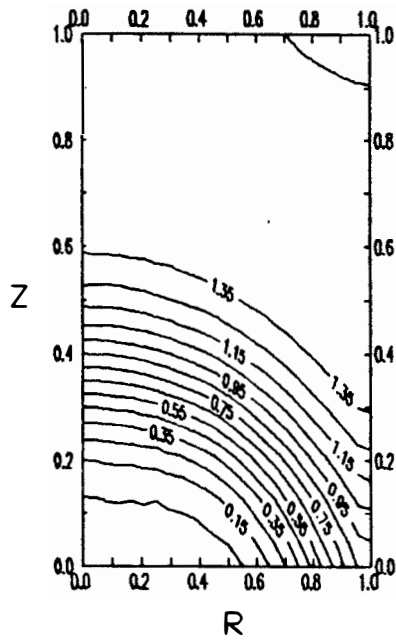


(a) Dimensionless Time = 75      (b) Dimensionless Time = 375

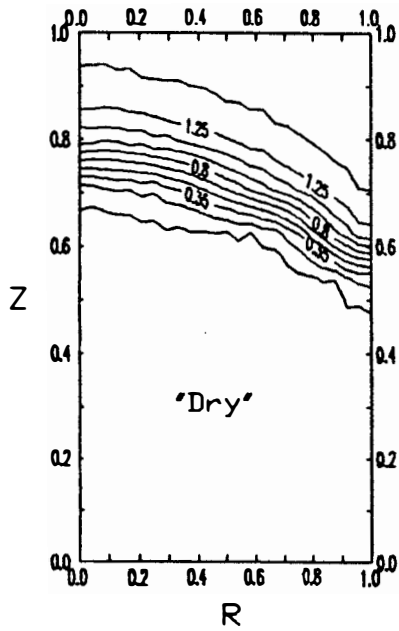


(c) Dimensionless Time = 750

Figure 5.16. Drying Front Locations Shown With Lines Of Constant Moisture Content For An Aspect Ratio Of 0.75 At Different Dimensionless Times.

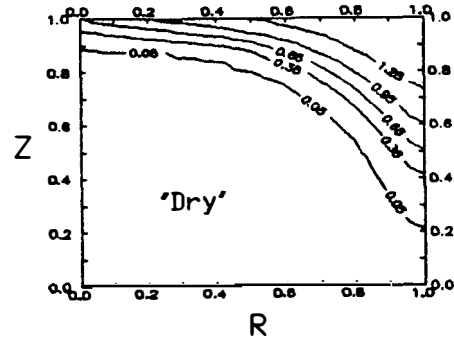
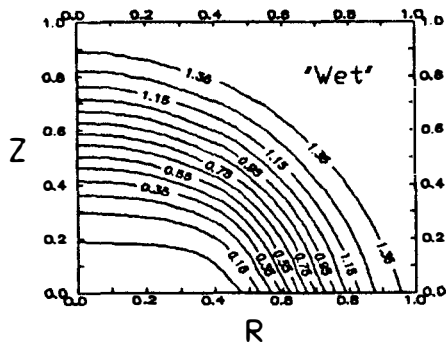


(a) Dimensionless Time = 75      (b) Dimensionless Time = 375

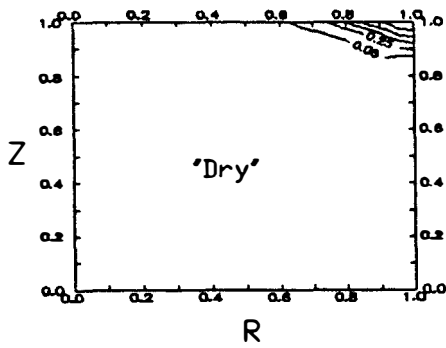


(c) Dimensionless Time = 750

Figure 5.17. Isotherm Distributions In A Bale For An Aspect Ratio Of 2.0 At Different Dimensionless Times.



(a) Dimensionless Time = 75      (b) Dimensionless Time = 375



(c) Dimensionless Time = 750

Figure 5.18. Isotherm Distributions In A Bale For An Aspect Ratio Of 0.75 At Different Dimensionless Times.

( $H/R = 2.0$ ) exhibits a region of increasing temperature. The temperature reaches a minimum value, which is slightly greater than 1.4, and then the air warms again to approximately 1.3.

#### 5.6. The Effects Of Varying The Inlet Radius Width On The Drying Process

The third parameter to be varied was the dimensionless air inlet radius ( $R_{IN}$ ). Since the Reynolds number is kept constant, increasing the nondimensional inlet radius results in an increased volume of air flowing through the bale, while decreasing the inlet radius decreases the volumetric flow rate of air. Thus, a decrease in drying time is expected as the air inlet radius is increased. Figure 5.19 reveals that this is indeed the case. Doubling the inlet radius,  $R_{IN}$ , from 0.4 to 0.8 results in a decrease of approximately 65% in the drying time from the base case. A case with an inlet radius of 0.2 was also examined. This case required considerable computational time and was terminated at a nondimensional time of 2710 (7.6 days). At this time, the total moisture content of the bale is approximately 0.213. The same moisture content is reached at a nondimensional time of approximately 715 (2.0 days) for the base case and 252 (0.7 days) for an inlet radius of 0.8. Thus, a considerable increase in the drying time is observed when the air inlet radius is decreased.



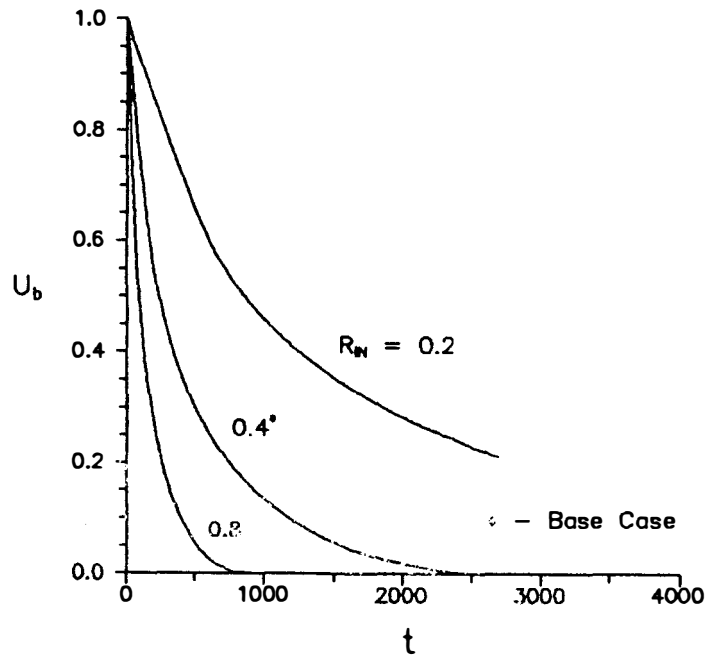


Figure 5.19. Variation Of The Total Moisture Content Of A Bale With Time For Different Air Inlet Radii.

Some physical insight into these results may be gained from examination of Figures 5.20 and 5.21. (Note that there is a difference in the velocity scales between these two figures.) These figures show the streamlines for the air flow through the bale and the radial velocity profile along the outer boundary of the bale. It may be seen that the velocities are much greater throughout the outer domain in the bale for the larger air inlet radius. In addition, it is easily seen that the air travels a shorter path to reach

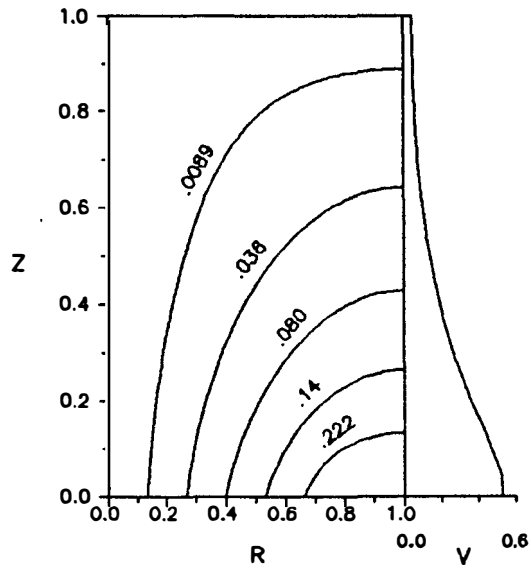


Figure 5.20. Streamlines And The Velocity Distribution On The Outer Surface For The Air Flow Through A Bale With An Inlet Radius Of 0.8.

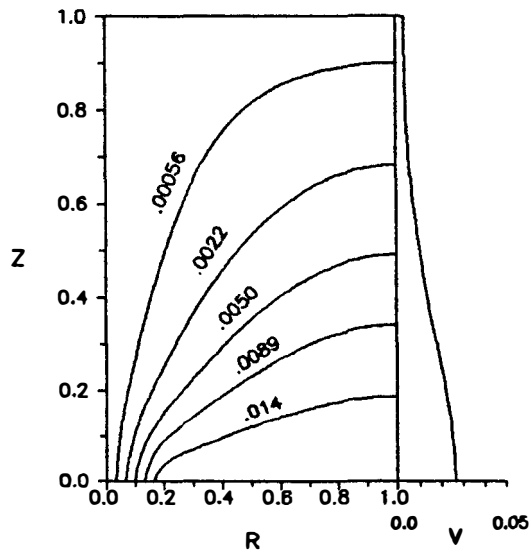
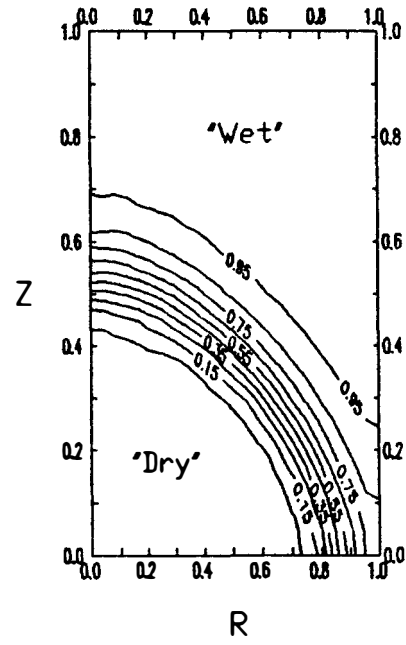
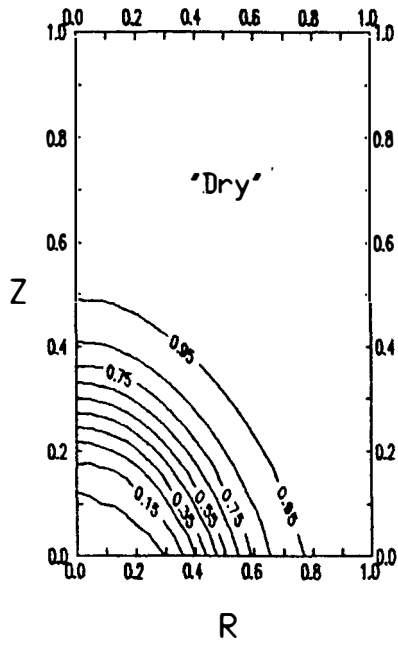


Figure 5.21. Streamlines And The Velocity Distribution On The Outer Surface For The Air Flow Through A Bale With An Inlet Radius Of 0.2.

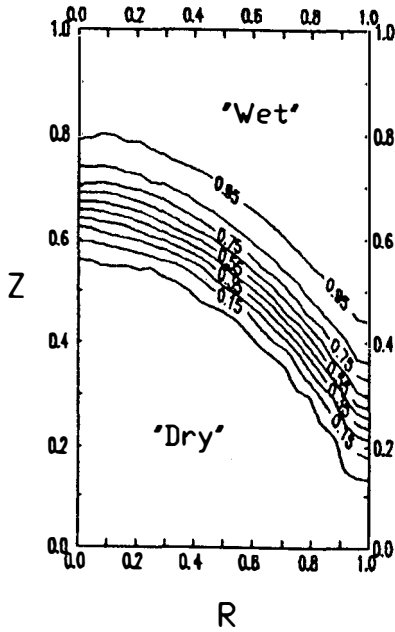
the exit through much of the bale. Thus, increasing the inlet size (at constant  $Re$ ) not only increases the amount of air flow (and, hence, the local air velocities), but also shortens the length of the flow path through the lower regions of the bale. Both of these factors enhance the drying of the bale and result in decreased drying times.

This effect is also evident in Figures 5.22 and 5.23, which show the moisture content profiles at different times for the flows with dimensionless air inlet radii of 0.8 and 0.2, respectively. Comparison of the moisture content distributions at a dimensionless time of 75 (5 hours) reveals that the drying front for  $R_{IN}$  equal to 0.8 is very thick compared to that for 0.2. This indicates that drying occurs throughout a much larger volume in the former case. Again, this is due to the increased amount of air flowing through the outer domain for an air inlet radius of 0.8.

In both cases mentioned above, the drying front becomes thinner as it passes through the solid. This narrowing of the drying zone, however, is much less pronounced, however, for an air inlet radius of 0.2. This is due to the fact that drying occurs over a relatively small volume at the start of the drying process because of the lower velocities and convective coefficients for this case. Thus, the front is initially much thinner and the decrease in the thickness of the drying zone is therefore less pronounced.

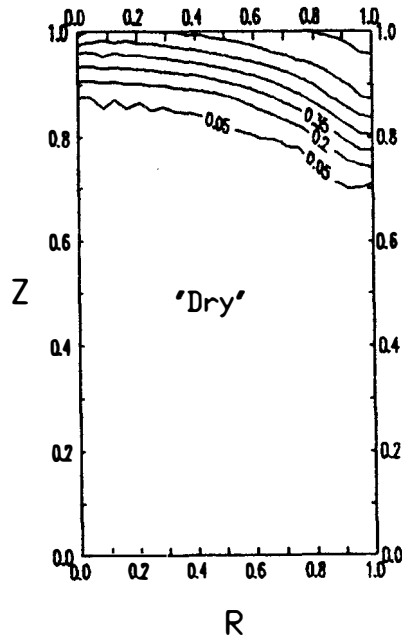
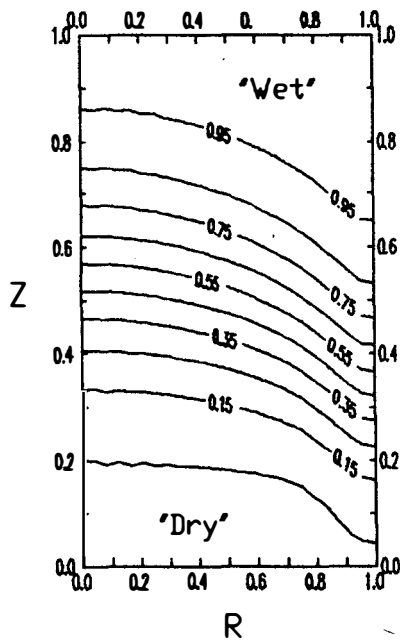


(a) Dimensionless Time = 75      (b) Dimensionless Time = 375

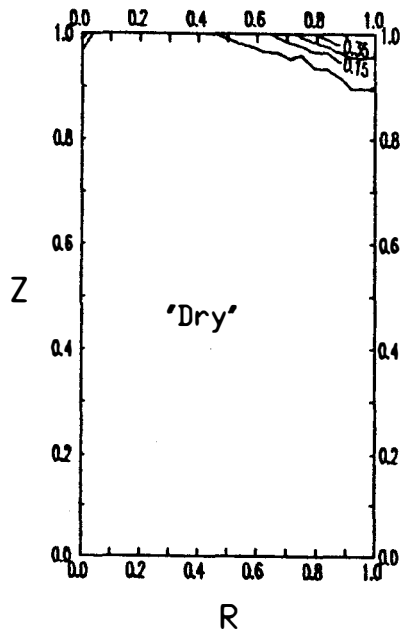


(c) Dimensionless Time = 750

Figure 5.22. Drying Front Locations Shown With Lines Of Constant Moisture Content For An Air Inlet Radius Of 0.8 At Different Dimensionless Times.



(a) Dimensionless Time = 75      (b) Dimensionless Time = 375



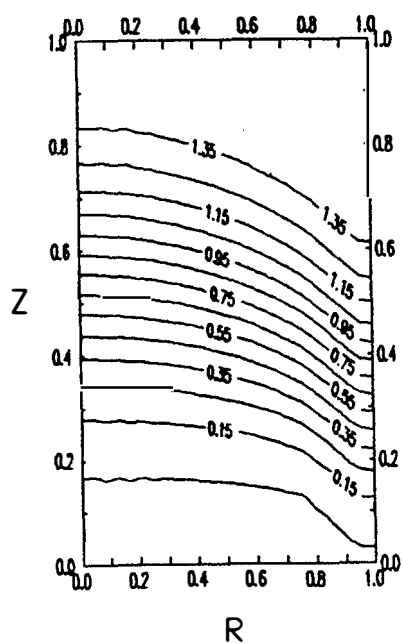
(c) Dimensionless Time = 750

Figure 5.23. Drying Front Locations Shown With Lines Of Constant Moisture Content For An Air Inlet Radius Of 0.2 At Different Dimensionless Times.

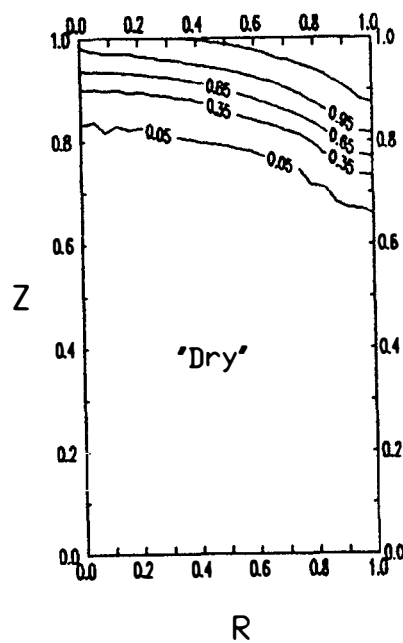
Marked differences between the isotherm distributions for the flows with dimensionless air inlet radii of 0.8 and 0.2 may also be observed. Figures 5.24 and 5.25 show the isotherm distributions for these cases at three dimensionless times. Figure 5.24 reveals that the air temperature decreases as the air flows through the bale for an inlet radius of 0.8. This occurs in some, but not all, regions of the bale for an air inlet radius of 0.2. As shown in Figure 5.25a, for an air inlet radius of 0.2 there is a region in the bale where the air stream temperature increases. This effect is greater for this case than for any other examined; therefore, these results will be discussed in greater detail below. Figure 5.26 shows the axial temperature at a fixed radial location ( $r = 0.96$ ) and time ( $t = 75$ ). Two regions may be identified in this figure.

In region 1, the air stream temperature is approximately constant. In region 2, the air stream is heated (i.e. the nondimensional temperature decreases). The change in moisture content across this region is very small. The moisture content is approximately 0.99 at the bottom of the bale ( $z=0$ ) and approximately 1.0 at the top of the bale ( $z=1$ ). The occurrence of two physically-distinct regions in this flow may be explained by considering the latent heat effects.

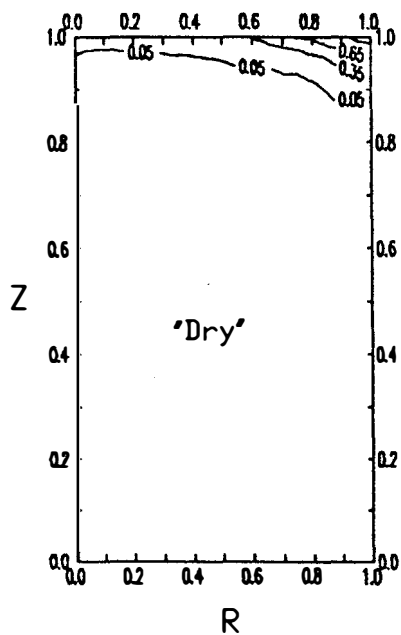
As stated previously, the latent heating of liquid in the inner domain acts to cool the air stream. When the air stream



(a) Dimensionless Time = 75

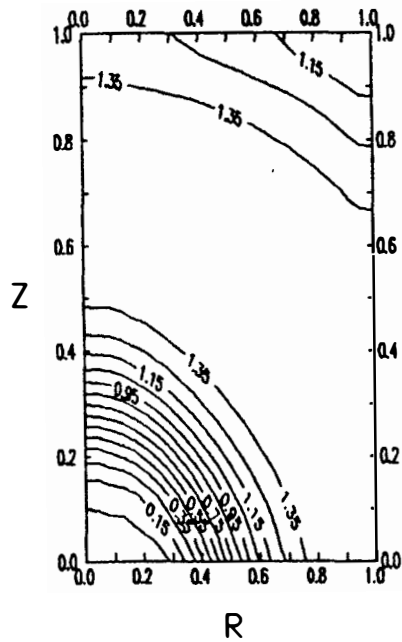


(b) Dimensionless Time = 375

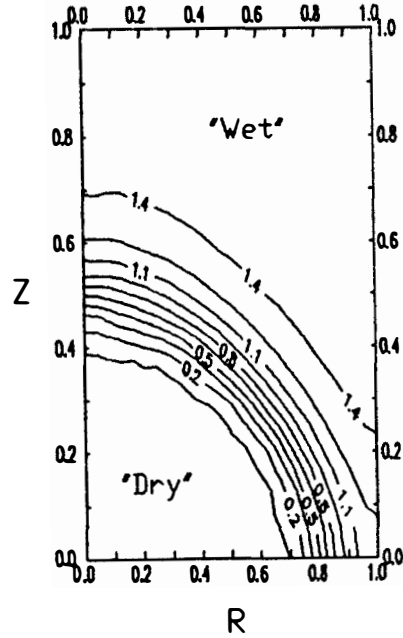


(c) Dimensionless Time = 750

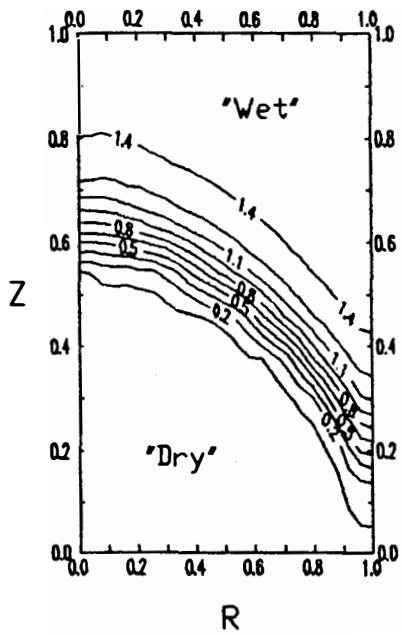
Figure 5.24. Isotherms In The Bale For A Dimensionless Air Inlet Radius Of 0.8 At Different Times.



(a) Dimensionless Time = 75



(b) Dimensionless Time = 375



(c) Dimensionless Time = 750

Figure 5.25. Isotherms In The Bale For A Dimensionless Air Inlet Radius Of 0.2 At Different Times.



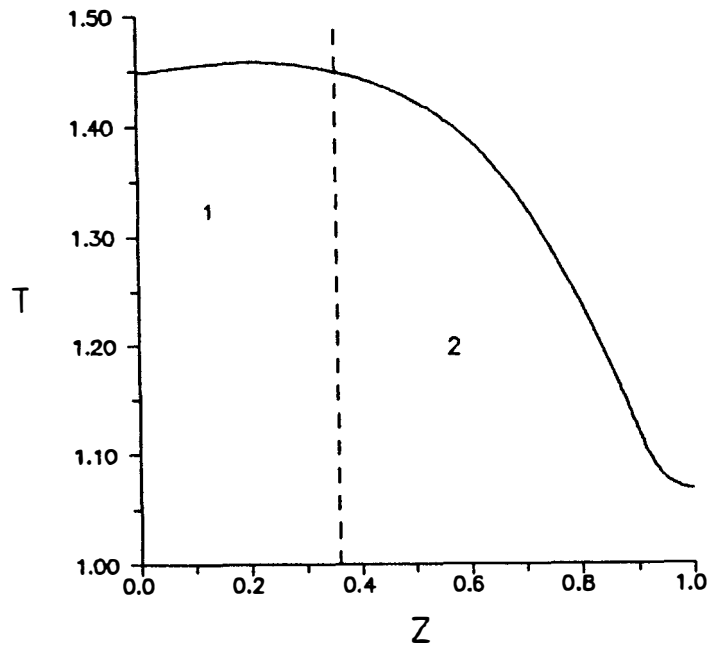


Figure 5.26 Axial Temperature Distribution For A Dimensionless Air Inlet Radius Of 0.2.

cools, there is also some sensible heating which tends to increase the (dimensional) air temperature since the solid is initially at a higher temperature than the air stream. Thus, there are two competing effects which act to change the air temperature: 1) the latent heating of the liquid which tends to decrease the (dimensional) air temperature and 2) the sensible heating which tends to increase this temperature. In region 1, the latent heating dominates the sensible heating and the air temperature remains approximately constant. As the moisture content approaches unity, however, the amount

of latent heating decreases and the sensible heating begins to dominate. Thus, in region 2, the air stream is warmed slightly.

#### 5.7. The Effects Of Varying The Kossovich Number On The Drying Process

Another parameter varied was the Kossovich number. This term represents the ratio of the latent heat necessary for vaporizing the liquid to the sensible heat required to warm the solid structure. Figure 5.27 shows the variation of the total moisture content of the bale with time for the range of Kossovich numbers examined. This figure shows that decreasing the Kossovich number decreases the total drying time. For a Kossovich number of 10, the drying time is approximately 1100 (3.1 days); which is a 53% decrease from the base case time of 2320 (6.5 days). Equilibrium conditions were not obtained for a Kossovich number of 400; however, a significant increase in drying time may be observed for this case in Figure 5.27. At a time of approximately 3740 (10.4 days), the moisture content for a Kossovich number of 400 is approximately 0.06. This same moisture content is reached at times of approximately 1500 (4.2 days) for a Kossovich number of 110 (base case) and 690 (1.9 days) for a Kossovich number of 10.

This trend may be explained from energy considerations. The Kossovich number appears in the inner domain energy equation (3.101, p. 59) as a coefficient of the latent energy

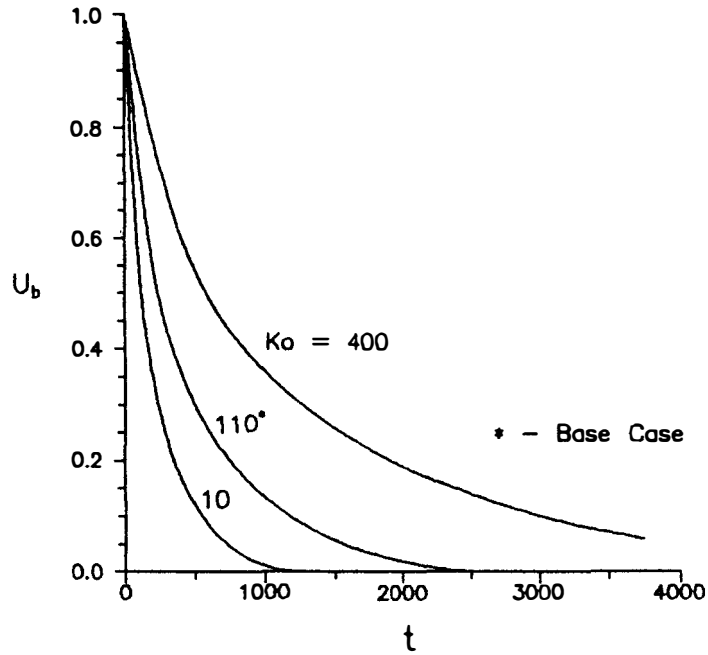
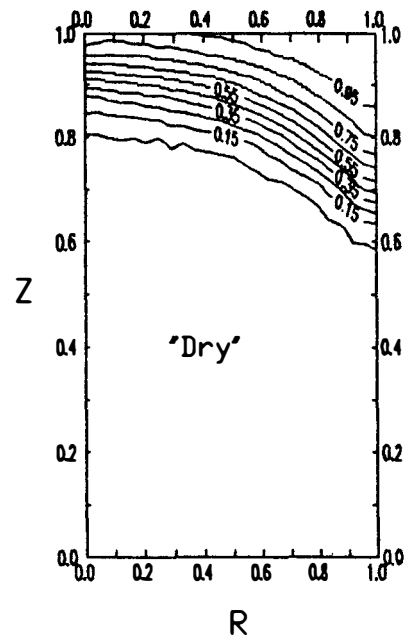
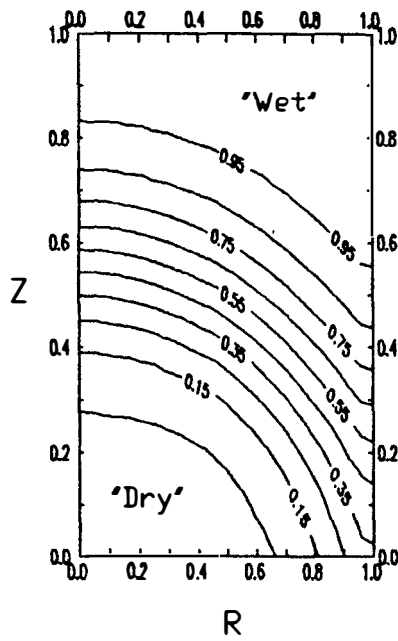


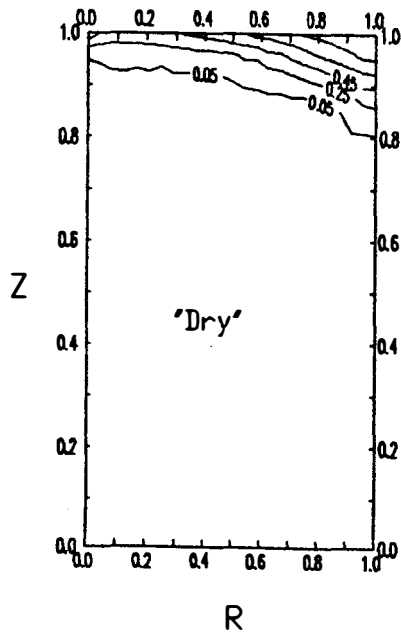
Figure 5.27. Variation Of The Total Moisture Content Of A Bale With Time For Different Kossovich Numbers.

term. Thus, lower values of the Kossovich number result in a smaller decrease of the inner domain temperature. The higher inner domain temperatures result in higher temperatures for the air stream flowing through the outer domain. Thus, the air may hold more moisture before it becomes saturated and drying may take place over a larger region in the bale. This is shown in Figures 5.28, 5.29, 5.30, and 5.31 which depict the drying front and isotherm distributions throughout the bale for Kossovich numbers of 10 and 400.

Early in the drying process (at about 5 hours), the drying front extends most of the way through the bale for the lowest Kossovich number case of 10. For a Kossovich number of 400,

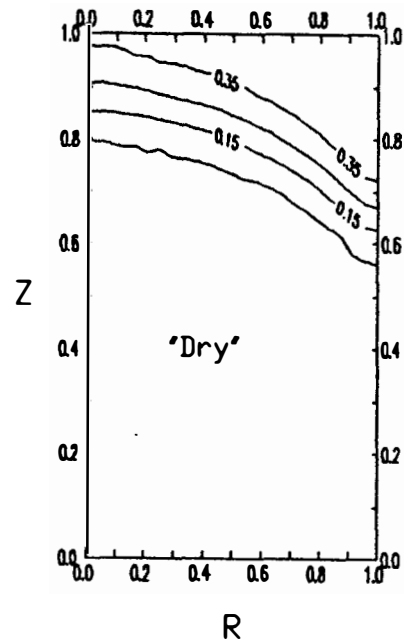
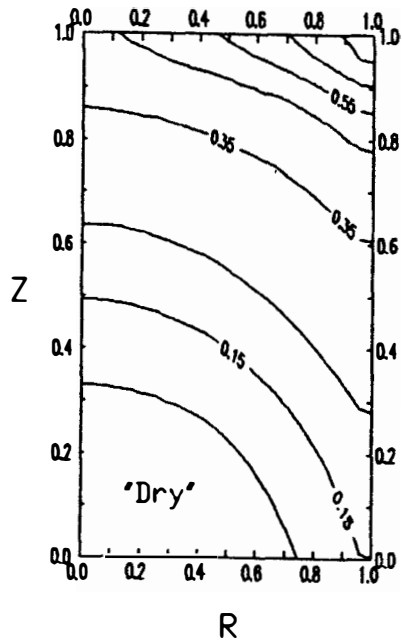


(a) Dimensionless Time = 75    (b) Dimensionless Time = 375

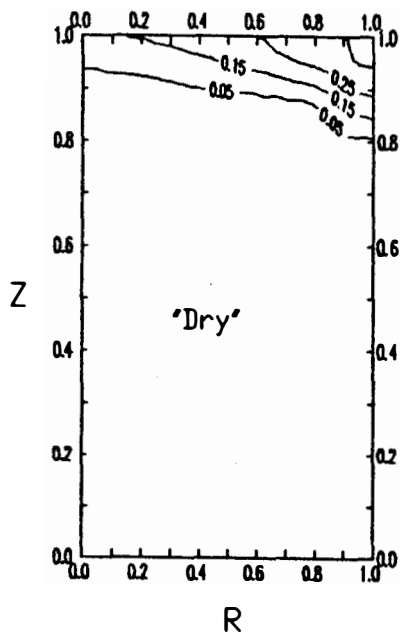


(c) Dimensionless Time = 750

Figure 5.28. Drying Front Locations Shown With Lines Of Constant Moisture Content For A Kossovich Number Of 10 At Different Dimensionless Times.

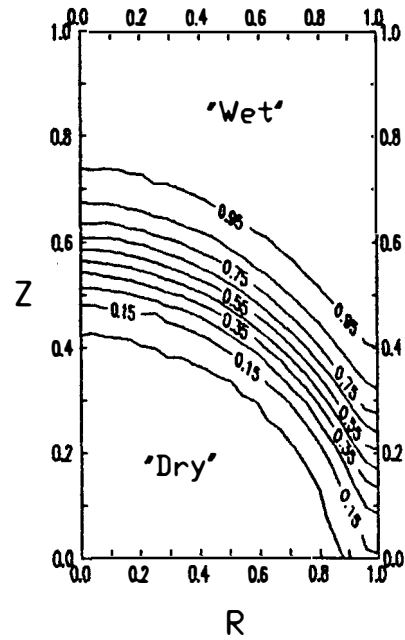
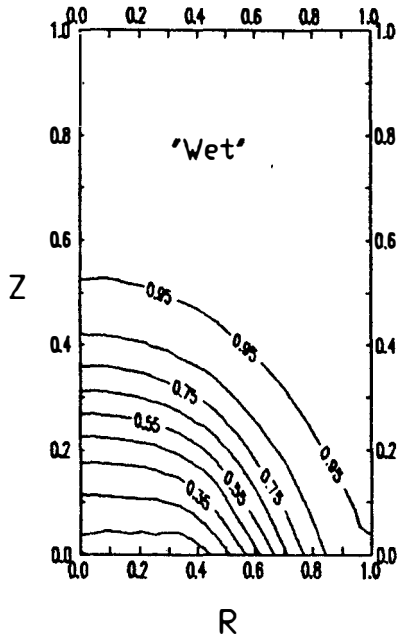


(a) Dimensionless Time = 75      (b) Dimensionless Time = 375

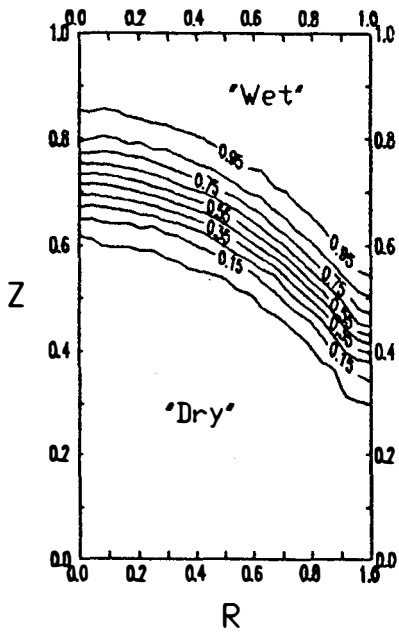


(c) Dimensionless Time = 750

Figure 5.29. Isotherm Distributions In A Bale For A Kossovich Number Of 10 At Different Dimensionless Times.

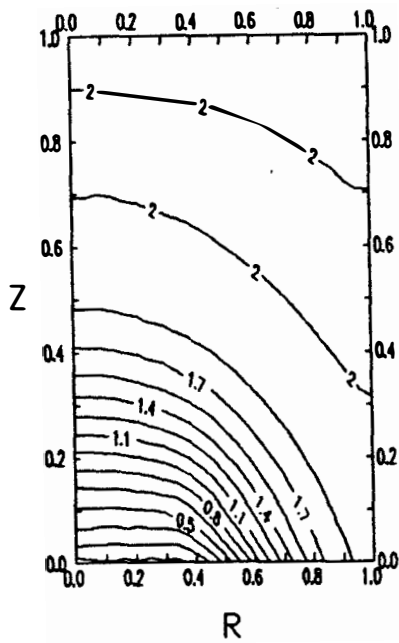


(a) Dimensionless Time = 75      (b) Dimensionless Time = 375

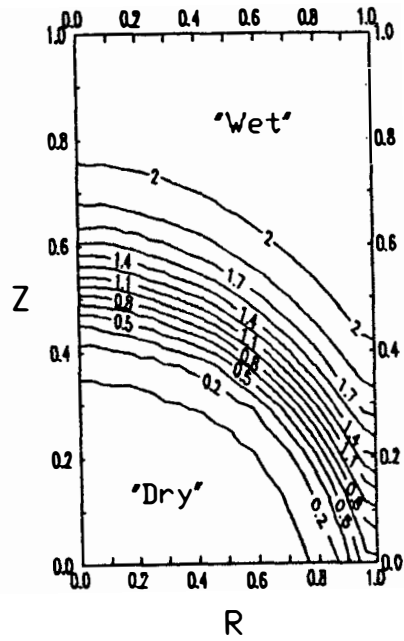


(c) Dimensionless Time = 750

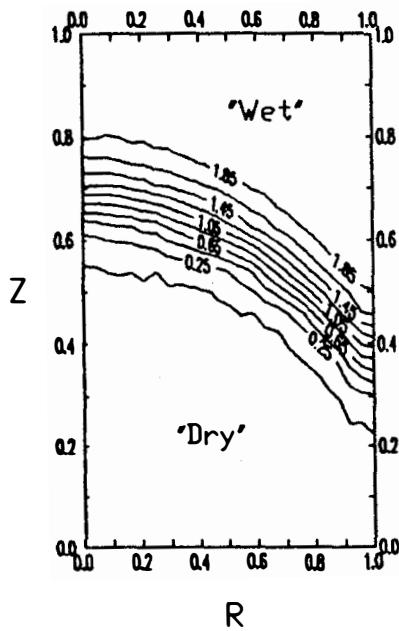
Figure 5.30. Drying Front Locations Shown With Lines Of Constant Moisture Content For A Kossovich Number Of 400 At Different Dimensionless Times.



(a) Dimensionless Time = 75



(b) Dimensionless Time = 375



(c) Dimensionless Time = 750

Figure 5.31. Isotherm Distributions In A Bale For A Kossovich Number Of 400 At Different Dimensionless Times.

the drying front does not penetrate as far into the bale at a given time. The isotherm distributions are also quite different for Kossovich numbers of 10 and 400. For a Kossovich number of 10, the nondimensional temperature does not rise above one. This indicates that the air does not cool below the initial temperature in this flow. Again, this is due to the fact that the inner domain temperatures are greater resulting in higher air temperatures in the outer domain. For higher Kossovich numbers, the inner domain becomes cooler which results in a greater cooling of the air stream in the outer domain. At a dimensionless time of 75 (5 hours), the nondimensional temperature of the air stream rises to a maximum value of approximately 2.0 (hence the dimensional temperature reaches a minimum of approximately 15 °C) for a Kossovich number of 400.

It may also be noticed that for a Kossovich number of 400, a region of increasing temperature exists. This occurs because as the air cools and picks up moisture, the relative humidity increases. Thus, the potential for mass transfer is lowered and mass transfer may even cease to occur. This effect is more pronounced at higher Kossovich numbers where the cooling of the air stream is greater.

#### 5.8. The Effect Of A Nonuniform Porosity Distribution In The Outer Domain On The Drying Process

The last case examined is one in which the structure of the bale in the outer domain has a nonuniform distribution



of solid matter which results in a nonuniform porosity. A "typical" variation of dry matter density in a hay bale is shown in Figure 5.32 (Bledsoe, 1989). There is a "low" density core (region 1) surrounded by a "high" density region (region 3) sandwiched between two "intermediate" density regions (regions 2 and 4). Each region is assumed to have a constant dry matter density and, hence, a constant porosity. This type of distribution results from the way the hay is baled.

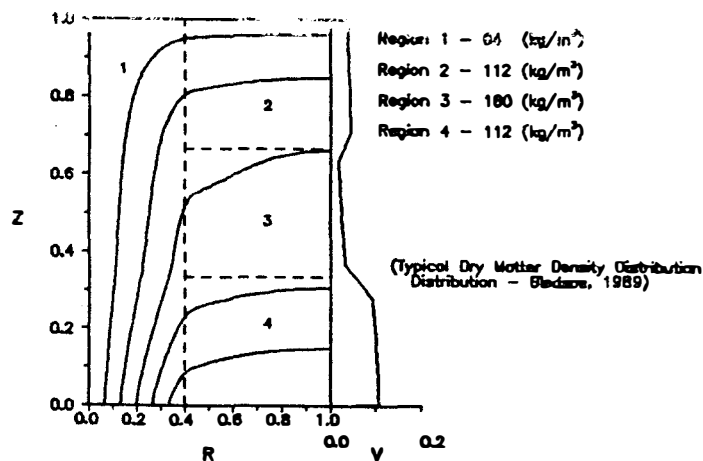
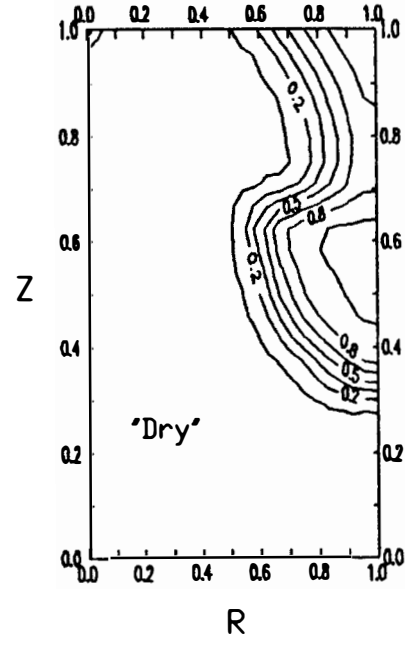
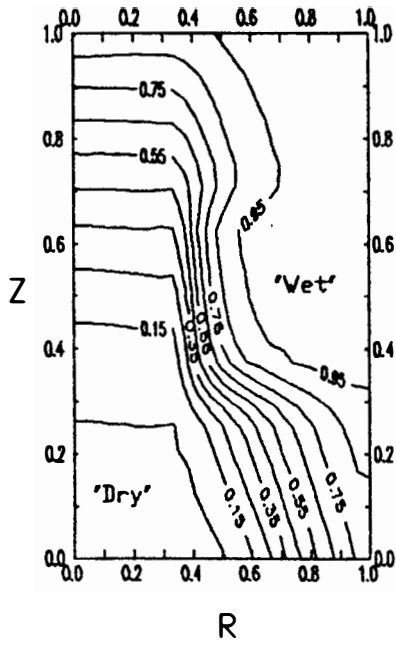


Figure 5.32. Streamlines And The Velocity Distribution On The Outer Surface For The Air Flow Through A Bale With A Typical Dry Matter Density Distribution.

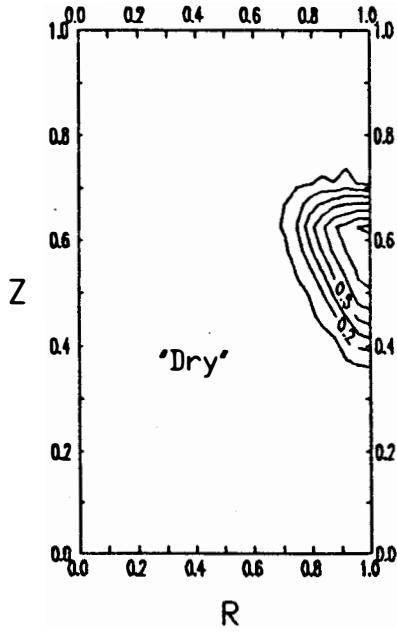
Figure 5.32 also shows the streamlines for the flow through the bale and the radial velocity profile along the outer boundary of the bale. This figure reveals that the lower resistance to flow in the core allows much of the air to flow around the high density material in region 3 and exit through

the uppermost portion of the outer surface of the bale. Thus, the velocity distribution along the outer boundary shows a decrease in the exit velocity in region 3 compared to that in regions 2 and 4. Thus, there is less air flowing, but more liquid to be removed in region 3 than in the other regions of the bale. Consequently, it is anticipated that this region will be the slowest region to dry.

Examination of Figures 5.33 and 5.34 reveals that this is indeed the case. Early in the drying process (at  $t=75$ , which corresponds to 5 hours), the front is relatively thick. However, the location and shape of the drying front are dramatically influenced by the nonuniform distribution of dry matter in the bale. Instead of extending across the entire radius of the bale as it did for the uniform porosity distribution, the front tends to curve around the high density material in region 3. Significant amounts of air, however, flow through regions 1 and 4 which causes the drying front to migrate through these regions. As the air flows through the high porosity material in region 1, it picks up a considerable amount of moisture. This results in a reduced rate of mass transfer in region 2. Thus, the front does not penetrate far into region 2 early in the drying process. The amount of air flowing through region 3 is lower than that flowing through regions 1,2, and 4 which results in the tendency of the drying front to curve around this region.

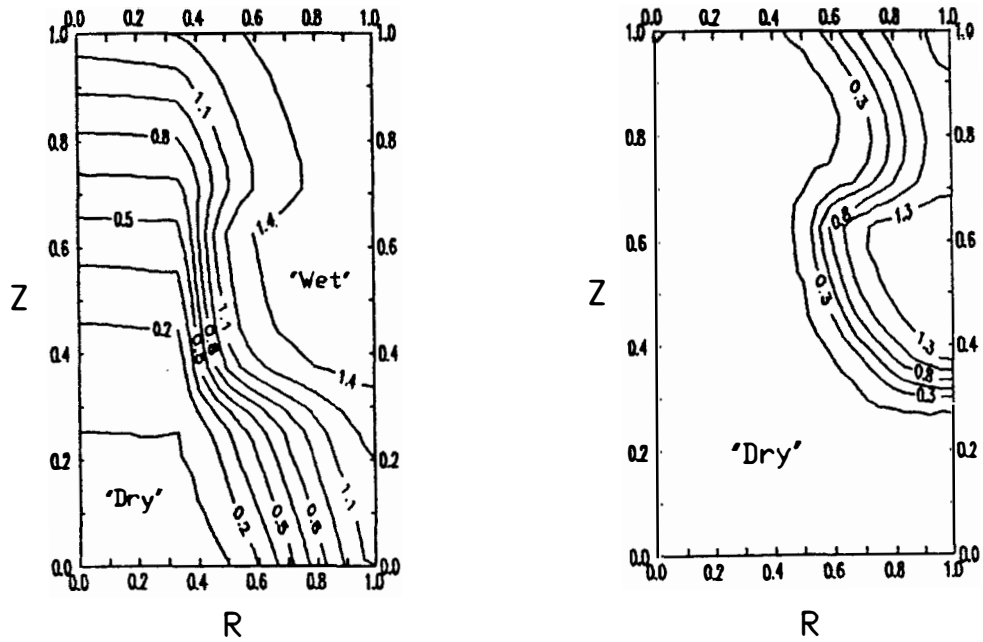


(a) Dimensionless Time = 75      (b) Dimensionless Time = 375

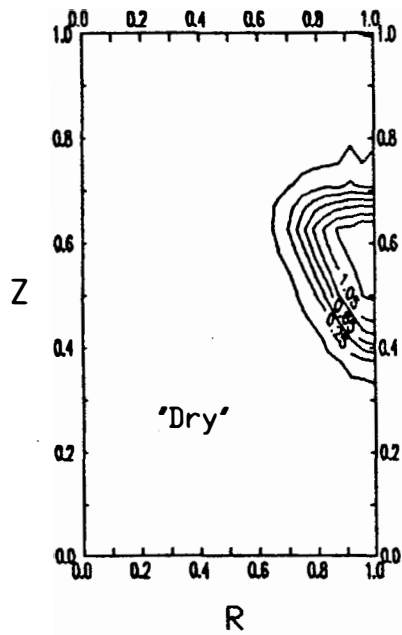


(c) Dimensionless Time = 750

Figure 5.33. Drying Front Locations Shown With Lines Of Constant Moisture Content For A Nonuniform Porosity Distribution At Different Dimensionless Times.



(a) Dimensionless Time = 75    (b) Dimensionless Time = 375



(c) Dimensionless Time = 750

Figure 5.34. Isotherm Distributions In A Bale With A Nonuniform Porosity Distribution.

As shown in Figures 5.33b, 5.33c, 5.34b, and 5.34c, when the drying process progresses, the front passes completely through regions 1 and 4, and less moisture is picked up by the air flowing through these regions. This results in increased drying in both regions 2 and 3. However, the drying process progresses faster in region 2 than in region 3 due to the greater amount of air flowing in this region. Thus, region 2 dries faster than region 3. At a dimensionless time of approximately 750 (2.1 days), the drying front is located entirely in region 3, and all other regions have reached equilibrium conditions.

The drying process for this case is also portrayed in Figure 5.35. This shows the variation of the total moisture content of the bale with time. As in the uniform porosity cases, drying occurs at a higher rate at the start of the drying process and then decreases with increasing time. The bale is "dry" at a time of approximately 1360 (3.8 days). Again, the decreasing rate of the drying process is due to the fact that the drying front progresses into regions with lower air velocities as time increases.

#### 5.9. The Effects Of Varying The Characteristic Aspect Ratio Of An Inner Domain Element On The Drying Process

The next parameter to be varied was the inner domain aspect ratio ( $L/D$ ). This ratio was approximately 1.4 for the base case and was varied between 0.7 and 2.1 (A discussion of the

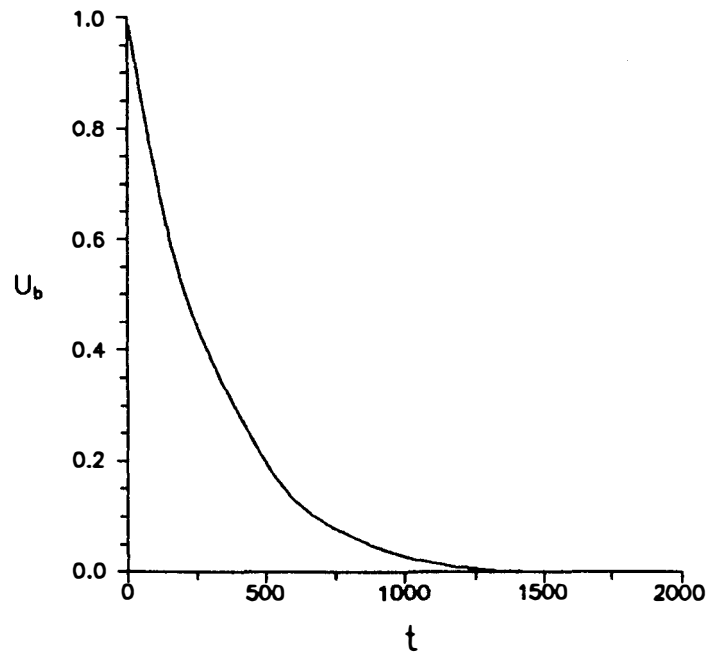


Figure 5.35. Variation Of The Total Moisture Content Of A Bale With Time For A Nonuniform Porosity Distribution.

range of values chosen for this parameter is presented in Appendix C). For this range of values, however, no significant change in the solution field is observed; that is, a change of less than 1% over the range of values examined is observed.

#### 5.10. Summary Of Conclusions

Several general conclusions may be drawn from the results of the parametric study. These are:

1. An increase in the Reynolds number results in a decrease in the overall drying time of the bale.

2. An increase in the dimensionless inlet radius results in a decrease in drying time of the bale.
3. An increase in the aspect ratio of the bale ( $H/R$ ) results in an increase in drying time.
4. An increase in the Kossovich number ( $Ko$ ) results in an increase in the drying time of the bale.
5. Variation of the inner domain aspect ratio ( $L/D$ ) over a "practical" range of 0.7 - 2.1 has a negligible effect on the drying process in the bale.
6. The specific velocity distribution of the air flowing through the outer domain plays a significant role in determining the drying behavior of the bale.
7. The physics of the drying process are such that the drying rate is initially "high", but decreases with time.

#### 5.11. Implications Of The Results For The Practical Operation Of Driers

Each of the above conclusions has a direct impact on the efficient utilization of a drier. Thus, the relationship of the results to drier operation will be discussed.

Assuming the drier is employed to dry a medium of fixed composition (material, porosity, permeability, etc.), a Reynolds number variation is obtained in practice by varying the air inlet velocity. To obtain such increases in inlet air velocity, fans of different size are needed. Obviously,

economic considerations must be taken into account when choosing a fan; however, the parametric study suggests using the largest capacity fan that the designer can afford.

It was also noted above that increasing the air inlet radius results in lower drying times. However, an increased air inlet size results in decreased air inlet velocity and, hence, a decrease in the Reynolds number for a fixed volumetric flowrate of air. Thus, there is a tradeoff between these two effects; and, it is expected that the selection of an "optimal" combination of Reynolds number and air inlet size should minimize the necessary drying time for a given application.

Possibly the greatest potential for achieving reduced drying times lies in a variation of the global aspect ratio ( $H/R$ ) of the bale. Decreasing this ratio may result in a significant reduction in drying time. A reduction of this ratio has other benefits as well. As was seen, reducing this ratio also results in a more uniform flow of air through the bale. This results in reduced "overdrying" of material near the air inlet, which can be beneficial.

A decrease in the Kossovich number ( $K_o$ ) for a fixed material may be obtained by either of two methods. First, the difference between the initial and equilibrium moisture contents may be decreased. The Kossovich number may also be decreased by increasing the difference between the initial and equilibrium air temperatures. It was noted above that the initial moisture content of a hay bale is usually not below 35% (w.b.). In



addition, the final moisture content of the "dried" hay must be below 18% (w.b.). Thus, the difference in moisture content is constrained; and, perhaps the easiest way to vary the Kossovich number is to vary the inlet temperature of the air. Thus, the inlet air stream should be heated as much as possible above the initial temperature of the hay bale. Of course, this is also constrained in the present application due to the "binding" of proteins that occurs in hay at high temperatures.

The importance of the velocity distribution was demonstrated in the nonuniform porosity case. The drying front tends to migrate around the high density region of the hay bale, where the air velocity is relatively low. To improve the drying for this case, it would be necessary to increase the air flow through any high density regions of the bale. Again, decreasing the overall aspect ratio ( $H/R$ ) of the bale is probably the most "practical" approach to improving the air flow through the high density regions.

One further point regarding drier operation should be noted. In the drying of hay, the temperature and humidity of the inlet air are typically such that the equilibrium moisture content of the bale is below that needed for safe storage (18% w.b.). Thus, the drying process is terminated before equilibrium conditions are reached; that is, when the safe storage conditions are reached. Therefore, the characteristics of the drying curve are important. It is

desireable to have all of the drying take place during the "high drying rate" period that occurs early in the drying process. The drying rate generally decreases as equilibrium is approached. Thus, the equilibrium condition of the air should be such that the equilibrium moisture content is as low as possible. This may be accomplished by increasing the air inlet temperature and/or decreasing the relative humidity of the inlet air. Increasing the air temperature has the benefit of lowering the Kossovich number ( $K_o$ ), although the resulting change in moisture content tends to counteract this tendency. Dehumidification of the inlet air is a technically attractive option in regions where ambient air is typically at a "high" relative humidity, but this may not be economically viable.

## BIBLIOGRAPHY

## BIBLIOGRAPHY

- Bachmat, Y., (1965), "Basic Transport Coefficients As Aquifer Characteristics," IASH Symposium, Hydrology Of Fractured Rocks, Dubrovnik, Vol. 1, pp. 63-75.
- Bagnall, L.O., Millier, W.F., and Scott, N.R., (1970), "Drying The Alfalfa Stem," Trans. ASAE, pp. 232-245.
- Baker, A.J., (1983), Finite Element Computational Fluid Mechanics, Hemisphere Publishing Corporation, New York.
- Bakker-Arkema, F.W., (1984), "Selected Aspects Of Crop Processing And Storage," J. Ag. Eng. Res., Vol. 30, pp. 1-22.
- Bear, J., (1972), Dynamics Of Fluids In Porous Media, American Elsevier, New York.
- Beavers, G.S. and Sparrow, E.M., (1969), "Non-Darcy Flow Through Fibrous Porous Media," Transactions Of The ASME, December, pp. 711-714.
- Berger, D., (1973), "Dry Behaviour Of Hygroscopic Capillary Porous Solids Under Non-Isothermal Drying Conditions," Ph.D. Thesis, University Of Waterloo, Canada.
- Berger, D. and Pei, D.C.T., (1973), "Drying Of Hygroscopic Capillary Porous Bodies Solids - A Theoretical Approach," IJHMT, Vol. 16, pp. 293-302.
- Bird, R.B., Stewart, W.E., and Lightfoot, E.N., (1960), Transport Phenomena, John Wiley & Sons.
- Bledsoe, B.L., (1988-1989), Personal Interview, University Of Tennessee, Knoxville, Tennessee, USA.
- Bledsoe, B.L. and Hitch, W., (1989), University Of Tennessee Agricultural Engineering Report.
- Bledsoe, B.L., Shoulders, S., Hitch, J.W., and Maples, J.E., (1985), "Rapid Solar-Heated Forced Air Drying Of Large Round Hay Bales: Design And Operating Considerations," Paper No. 85-4538, ASAE, Presented in Chicago, Illinois, December 17-20.
- Bruin, S. and Luyben, K.Ch.A.M., (1980), "Drying Of Food Materials: A Review Of Recent Developments," Advances In Drying, Vol. 1, pp. 155-216.
- Buckingham, E.A., (1907), "Studies On The Movement Of Soil Moisture," U.S. Dept. Agr. Bull., 38.

- Ceaglske, N.H. and Hougen, O.A., (1937), "Drying Granular Solids," Industrial And Engineering Chemistry, Vol. 29, No. 7, pp. 805-813.
- Chen, C.S. and Johnson, W.H., (1969), "Kinetics Of Moisture Movement In Hygroscopic Materials (I. Theoretical Considerations Of Drying Phenomena)," Trans. ASAE, pp. 109-113.
- Chen, P., (1987), "Mathematical Modeling Of Drying And Freezing Processes In The Food Industry," Ph.D. Thesis, University Of Waterloo, Canada.
- Chen, P. and Pei, D.C.T., (1989), "A Mathematical Model Of Drying Processes," IJHMT, Vol. 32, No.2, pp. 297-310.
- DeVries, D.A., (1958), "Simultaneous Transfer Of Heat And Moisture In Porous Media," Trans. Am. Geophys. Union, Vol. 39, No. 5, pp. 909-916.
- Dyer, D.F. and Suderland, J.E., (1968), "The Role Of Convection In Drying," Chem. Eng. Sci., Vol. 23, pp. 965-970.
- Fair, J.R. and Lerner, B.J., (1956), AIChE Journal, Vol. 2, p.13.
- Filkova, I., (1984), "Drying Research And Development In Czechoslovakia," Drying 1984, pp. 11-18.
- Fortes, M. and Okos, M.R., (1980), "Drying Theories: Their Bases And Limitations As Applied To Foods And Grains," Advances In Drying, Vol. 1, pp. 119-154.
- Fulford, G.D., (1969), "A Survey Of Recent Soviet Research On The Drying Of Solids," The Canadian Journal Of Chemical Engineering, Vol. 47, pp. 378-391, August.
- Gebhart, B., Jaluria, Y., Mahajan, R.L., and Sammakia, B., (1988), Buoyancy-Induced Flows And Transport, Hemisphere Publishing Corporation, New York.
- Harmathy, T.Z., (1969), "Simultaneous Moisture And Heat Transfer In Porous Systems With Particular Reference To Drying," I&EC Fund., Vol. 8, No. 1, 92-103.
- Hill, J.D., Ross, I.J., and Barfield, B.J., (1977), "The Use Of Vapor Pressure Deficit To Predict Drying Time For Alfalfa Hay," Trans. ASAE, pp. 372-374.
- Hougen, McCauley, and Marshal, (1940), "Limitations Of Diffusion Equations In Drying," Trans. Am. Inst. Chem. Eng., Vol. 36, pp. 183-209.

Hussain, A., Chen, C.S., and Clayton, J.T., (1970), "Coupled Heat And Moisture Diffusion In Porous Food Product (An Application To Rough Rice Drying)," ASAE, Paper No. 70-833, Winter Meeting Of ASAE, Chicago.

Hussain, A., Chen, C.S., Clayton, J.T., and Whitney, L.F., (1972), "Mathematical Simulation Of Mass And Heat Transfer In High Moisture Foods," Trans. ASAE, Vol. 15(4), pp. 732-736.

Hussain, A., Nelson, G.L., and Clay, B.L., (1970), "Evaluating Thermodynamic Parameters Of Moisture Transfer For Food Products (Rice, Corn, Potato)," ASAE, Paper No. 70-385, Summer Meeting Of ASAE, Minneapolis.

Irmay, S., (1958), "On The Theoretical Derivation Of Darcy And Forchheimer Formulas," Transactions, American Geophysical Union, Vol. 39, August, pp. 702-707.

Jaluria, Y. and Torrance, K.E., (1986), Computational Heat Transfer, Hemisphere Publishing Corporation, New York.

Joseph, D.D., Nield, D.A., and Papanicolaou, G., (1982), "Nonlinear Equation Governing Flow In A Saturated Porous Medium," Water Resources Research, Vol. 18, No. 4, pp. 1049-1052.

Key, R.B., (1980), "Theoretical Foundations Of Drying Technology," Advances In Drying, Vol. 1, pp. 1-22.

King, C.J., (1968), "Rates Of Sorption And Desorption In Porous Dried Foodstuffs," Food Technology, Vol. 22, pp. 165-171, April.

Krischer, O., (1963), Die Wissenschaftlichen Grundlagen Der Trocknungstechnik, Chapter IX, Springer, Berlin.

Lebedev, P.D. and Ginzburg, A.S., (1971), "General Problems Of Drying Theory and Technique," Progress In Heat And Mass Transfer, Vol. 5, pp. 55-76.

Lewis, W.K., (1921), "The Rate Of Drying Of Solid Materials," Industrial And Engineering Chemistry, Vol. 13, pp. 427-432.

Luikov, A.V., (1964), "Heat And Mass Transfer In Capillary - Porous Bodies," Advances In Heat Transfer, Vol. 1, pp. 123-184, Academic Press, New York.

Luikov, A.V. and Mikhailov, Yu., A., (1965), Theory Of Energy And Mass Transfer, Pergamon Press, Oxford.

McCready, D.W. and McCabe, W.L., (1933), "The Adiabatic Air Drying Of Hygroscopic Solids," Trans. AIChE, Vol. 29, pp. 131-160.

Miller, E. and Miller, R., (1955), "Theory Of Capillary Flow I. Practical Implications," Proc. Soil Sci. Soc. Am., Vol. 19, pp. 267-271.

Miller, H., (1947), "Dry Matter Loss In Haymaking Due To Bacterial Action," Ag. Eng., June, pp.243-244.

Mujumdar, A.S. and Raghavan, G.S.V., (1984), "Canadian Research And Development In Drying - A Survey," Drying 1984, pp. 1-10.

Nield, D.A. and Joseph, D.D., (1985), "Effects Of Drag On Convection In A Saturated Porous Medium," Phys. Fluids, Vol. 28, March, pp. 995-997.

Ohm, A., Vogtlander, J.G., and Kossen, N.W.F., (1971), "Heat And Mass Transfer In Barn Hay-Drying Systems," J. Ag. Eng. Res., Vol. 16, pp. 254-268.

Parry, J.L., (1985), "Mathematical Modeling And Computer Simulation Of Heat And Mass Transfer In Agricultural Grain Drying: A Review," J. Ag. Eng. Res., Vol. 32, pp. 1-29.

Patankar, S.V., (1980), Numerical Heat Transfer And Fluid Flow, Hemisphere Publishing Corporation, New York.

Philip, J.R. and DeVries, D.A., (1957), "Moisture Movement In Porous Materials Under Temperature Gradients," Trans. Am. Geophys. Union, Vol. 38, No. 2, pp. 222-232.

Richards, L.A., (1931), "Capillary Conduction Of Liquids Through Porous Mediums," Journal Of Applied Physics, Vol. 1, pp. 318-333.

Rotz, A.C. and Chen, Yi, (1985), "Alfalfa Drying Model For The Field Environment," Trans. ASAE, Vol. 28, pp. 1686-1691.

Scheidegger, A.E., (1960), The Physics Of Flow Through Porous Media, MacMillan, New York.

Sharp, J.R., (1982), "A Review Of Low Temperature Drying Simulation Models," J. Ag. Eng. Res., Vol. 27, pp. 169-190.

Sherwood, T.K., (1929), "The Drying Of Solids. I," Industrial And Engineering Chemistry, Vol. 21, pp. 12-16.

Sherwood, T.K., (1929), "The Drying Of Solids. II," Industrial And Engineering Chemistry, Vol. 21, pp. 976-980.

Sherwood, T.K., (1930), "The Drying Of Solids. III," Industrial And Engineering Chemistry, Vol. 22, pp. 132-136.

Sherwood, T.K., (1931), "Application Of The Theoretical Diffusion Equations To The Drying Of Solids," Transactions Of The American Institute Of Chemical Engineering, Vol. 27, pp. 190-202.

Suzuki, M. and Maeda, S. "On The Mechanism Of Drying Of Granular Beds, Mass Transfer From Discontinuous Source, J. Chem. Eng. Japan, Vol. 1, pp. 26-31.

Van Arsdel, W.B., (1947), "Approximate Diffusion Calculations For The Falling-Rate Phase Of Drying," Trans. Am. Inst. Chem. Eng., Vol. 43, No. 1, pp. 13-24.

Van Brakel, J. and Heertjes, P.M., (1978), "On The Period Of Constant Drying Rate, Proc. 1<sup>st</sup> Symp. On Drying, pp. 70-75, Science Press, Princeton, New Jersey.

Whitaker, S., (1966), "The Equations Of Motion In Porous Media," Chemical Engineering Science, Vol. 21, pp. 291-300.

Whitaker, S., (1967), "Diffusion And Dispersion In Porous Media," AICHE Journal, Vol. 13, No. 3, pp. 420-427.

Whitaker, S., (1969), "Advances Of Theory Of Fluid Motion In Porous Media," Ind. Eng. Chem., Vol. 61, No. 12, pp. 14-28.

Whitaker, S., (1971), "On The Functional Dependence Of The Dispersion Vector For Scalar Transport In Porous Media," Chem. Eng. Sci., Vol. 26, pp. 1893-1899.

Whitaker, S., (1973), "The Transport Equations For Multiphase Systems," Chem. Eng. Sci., Vol. 28, pp. 139-147.

Whitaker, S., (1977), "Simultaneous Heat, Mass, And Momentum Transfer In Porous Media," Advances In Heat Transfer, Vol. 13, pp. 119-202.

Whitaker, S., (1977), "Toward A Diffusion Theory Of Drying," Ind. Eng. Chem., Fundam., Vol. 16, No. 4, pp. 408-414.

Whitaker, S., (1986), "Flow In Porous Media I: A Theoretical Derivation Of Darcy's Law," Transport In Porous Media, Vol. 1, pp. 3-25.

Whitaker, S., (1986), "Flow In Porous Media II: The Governing Equations For Immiscible Two Phase Flow," Transport In Porous Media, Vol. 1, pp. 105-125.

Whitaker, S., (1986), "Flow In Porous Media III: Deformable Media," Transport In Porous Media, Vol. 1, pp. 127-154.



## APPENDIXES

## APPENDIX A

### DETERMINATION OF THE FUNCTIONAL DEPENDENCIES OF THE BIOT NUMBERS ON THE OTHER NONDIMENSIONAL PARAMETERS

In the development of the mathematical model (Section 3, page 30), the nondimensional parameters  $Bi$  and  $Bi_m$ , which are the heat and mass transfer Biot numbers, appear in the governing equations. As will be shown, these parameters may be rewritten in terms of the other dimensionless parameters that appear in the model formulation. Therefore, they are not independent parameters.

The heat transfer coefficient may be obtained from an empirical correlation presented by Bird, Stewart, and Lightfoot (1960) describing heat transfer in packed beds. This correlation may be written as

$$j_H = C_1 (Re')^{\alpha_1} \psi \quad (A.1)$$

where:

$$j_H = \text{Chilton-Colburn Factor} = \frac{h}{\rho_a C_{pa} |\vec{V}^*|} (Pr)^{2/3},$$

$\alpha_1, C_1 = \text{constants.}$

$$Re' = \begin{array}{l} \text{"Modified" Reynolds Number} \\ \text{For The Flow Through} \\ \text{Packed Beds} \end{array} = \frac{\rho_a |\vec{V}^*|}{\alpha \mu_f \psi},$$

$\alpha = \begin{array}{l} \text{Particle Surface Area Per Unit Volume} \\ \text{Of The Packed Bed} \end{array},$

$\psi = \begin{array}{l} \text{Empirical Coefficient Which Depends} \\ \text{On Particle Shape (= .91 for cylinders)} \end{array},$

$V^*$  = Air Velocity Through The  
Packed Bed ,

$\rho_a$  = Density Of The Air ,

$\mu_f$  = Dynamic Viscosity Of The Air ,

and ,

$$Pr = \text{Prandtl Number} = \frac{\nu}{\alpha_a}$$

Substituting the definitions of  $j_H$  and  $Re'$  presented above into equation A.1 yields

$$\frac{h}{\rho_a C_{p_a} |\vec{V}^*|} (Pr)^{2/3} = C_1 \left( \frac{\rho_a |\vec{V}^*|}{\alpha \mu_f \psi} \right)^{\alpha_1} \psi \quad (A.2)$$

Noting that ,

$$Re_\kappa = \frac{V_{IN} \sqrt{\kappa_r}}{\nu} \quad , \quad (A.3)$$

and ,

$$\alpha = \frac{N_{ID} A_s}{V_{OD}} = \left( \frac{A_s}{A} \right) \left( \frac{1 - \epsilon^*}{2L} \right) \quad , \quad (A.4)$$

where ,

$N_{ID}$  = Number Of Stalks In The  
Outer Domain ,

$A_s$  = Surface Area Of A Stalk ,

$V_{OD}$  = Outer Domain Volume ,

$A$  = Cross Sectional Area Of A Stalk ,

$L$  = Half-Length Of Stalk ,

and ,

$\epsilon^*$  = Porosity Of The Outer Domain

allows equation A.2 to be rewritten as

$$\frac{h}{\rho_a C_{pa} V_{IN} |\vec{V}|} (Pr)^{2/3} = C_1 \left( \frac{V_{IN} \sqrt{\kappa_r}}{v} \right)^{\alpha_1} \left( \frac{A}{A_s} \right)^{\alpha_1} \left( \frac{L}{\sqrt{\kappa_r}} \right)^{\alpha_1} \left( \frac{2}{1-\epsilon^*} \right)^{\alpha_1} \left( \frac{|\vec{V}|}{\psi} \right)^{\alpha_1} \psi. \quad (A.5)$$

The Biot number may be obtained from equation A.5 by writing

$$\frac{hL}{K_s} = (C_1) \left\{ \left[ (\rho_a C_{pa} V_{IN}) \left( \frac{L}{K_s} \right) \right] \left[ \left( \frac{A}{A_s} \right) \left( \frac{L}{\sqrt{\kappa_r}} \right) \left( \frac{2}{1-\epsilon^*} \right) Re_\kappa \right]^{\alpha_1} \psi^{1-\alpha_1} (|\vec{V}|)^{1+\alpha_1} Pr^{-2/3} \right\} \quad (A.6)$$

or,

$$Bi = (C_1) \left\{ \left[ \left( \frac{V_{IN} \sqrt{\kappa_r}}{v} \right) \left( \frac{v}{\alpha_a} \right) \left( \frac{K_a}{K_s} \right) \left( \frac{L}{\sqrt{\kappa_r}} \right) \right] \left[ \left( \frac{A}{A_s} \right) \left( \frac{L}{\sqrt{\kappa_r}} \right) \left( \frac{2}{1-\epsilon^*} \right) (Re_\kappa) \right]^{\alpha_1} \psi^{1-\alpha_1} (|\vec{V}|)^{1+\alpha_1} Pr^{-2/3} \right\}. \quad (A.7)$$

This may be simplified to obtain

$$Bi = C_1 \left\{ \left( \frac{A}{A_s} \right)^{\alpha_1} \left( \frac{L}{\sqrt{\kappa_r}} \right)^{(1+\alpha_1)} \left( \frac{K_a}{K_s} \right) (Re_\kappa)^{(1+\alpha_1)} (Pr)^{1/3} (\psi)^{(1-\alpha_1)} \left( \frac{2}{1-\epsilon^*} \right)^{\alpha_1} (|\vec{V}|)^{1+\alpha_1} \right\}. \quad (A.8)$$

Thus, the functional dependence of the Biot number is given by

$$Bi = f_1 \left( \frac{A}{A_s}, \frac{L}{\sqrt{\kappa_r}}, \frac{K_a}{K_s}, \epsilon^*, Re_\kappa, Pr, |\vec{V}| \right). \quad (A.9)$$

All of the dimensionless parameters appearing in the function above are independent parameters in the present mathematical formulation of the problem. The convective mass transfer coefficient may be obtained by Chilton-Colburn analogy (Bird, Stewart, and Lightfoot, 1960) with the heat transfer coefficient. This gives

$$j_H = j_M \quad (A.10)$$

where:

$$j_M = \begin{array}{l} \text{Chilton-Colburn Factor For} \\ \text{Mass Transfer} \end{array} = \frac{h_m M_a}{|\vec{V}|^* M_v} (Sc)^{2/3}$$

$$M_a = \text{Molecular Weight Of Air,}$$

and,

$$M_v = \text{Molecular Weight Of Water Vapor.}$$

Substituting the definitions of  $j_H$  and  $j_M$  presented above into equation A.10 yields

$$\frac{h}{\rho_a C_{pa} |\vec{V}|^*} Pr^{2/3} = \frac{M_a h_m}{M_v V^*} Sc^{2/3}, \quad (A.11)$$

or,

$$(Bi) \left( \frac{K_s}{\rho_a C_{pa}} \right) Pr^{2/3} = \left( \frac{h_m L}{\alpha_s} \right) \frac{\alpha_s M_a Sc^{2/3}}{M_v}. \quad (A.12)$$

Equation A.12 may be rewritten in the form

$$Bi_m = \left( \frac{M_v}{M_a} \right) \left( \frac{K_s}{\rho_a C_{pa} \alpha_s} \right) \left( \frac{Pr}{Sc} \right)^{2/3} Bi. \quad (A.13)$$

Assuming that the coefficient of diffusion for water vapor through air is the same in both the inner domain and outer domain, the Schmidt number may be expressed as

$$Sc = \frac{D_v}{\alpha_a} = \left( \frac{D_v}{\alpha_s} \right) \left( \frac{\alpha_s}{\alpha_a} \right) = \left( \frac{\alpha_s}{\alpha_a} \right) (Lu_v). \quad (A.14)$$

Substituting equation A.14 into equation A.13 and simplifying yields

$$Bi_m = \left( \frac{M_v}{M_a} \right) \left( \frac{K_s}{K_a} \right) \left( \frac{\alpha_a}{\alpha_s} \right)^{5/3} (Lu_v)^{-2/3} (Pr)^{2/3} Bi. \quad (A.15)$$

Thus, the functional dependence of the mass transfer Biot number is given by

$$Bi_m = f_2 \left( \frac{\alpha_a}{\alpha_s}, \frac{A}{A_s}, \frac{K_a}{K_s}, \frac{L}{\sqrt{\kappa_r}}, \epsilon^*, Lu_v, Re_x, Pr, |\vec{V}| \right). \quad (A.16)$$

The dimensionless parameters appearing in the function  $f_2$  above are all independent parameters appearing in the mathematical model.

The functional dependencies derived above depend on the validity of the correlation given by equation A.1. Several authors (Chen and Pei, 1989, Van Brakel and Heertjes, 1978, and Suzuki and Maeda, 1968) have noted that for moisture contents high enough to produce a partially wetted surface of the porous solid, there is not good agreement for convection coefficients obtained from experiment and values obtained from relations such as that given by equation A.1. For the present application, the drying process starts in the so-called sorption region. Thus, the surface moisture content is low and the functional dependencies displayed in equations A.9 and A.16 should be valid. In applications involving higher surface moisture contents, the functional dependencies

would have to be altered to take the influence of surface moisture content into account. For the purposes of the present work, however, the relationships given by equations A.9 and A.16 should suffice.

## APPENDIX B

### COMMENTS ON THE NUMERICAL TREATMENT OF THE LATENT HEAT TERM IN THE ENERGY EQUATION FOR THE INNER DOMAIN

In Section 4 (page 70), the numerical solution algorithm is discussed in some detail. The finite volume procedure is formulated by starting with a "general" conservation equation of the form given by equation 4.5 (page 74). Any terms not fitting this "standard" conservation form are treated by lumping them into the source term. This approach has some important consequences that should be discussed.

A source (or, sink) term in the energy equation may cause the temperature to increase (or, decrease) such that the temporal derivative of temperature derivative of temperature does not approach zero after "long" times. That is, there may not be a steady-state solution when a source (sink) is present. In the formulation of the inner domain numerical algorithm, the energy required for evaporation of the liquid is included in the source term.

As drying progresses, this energy source (or, sink) term should decrease in strength and approach zero when drying reaches completion since the moisture content approaches zero (or equilibrium conditions). However, the value of the moisture content is determined from the values of temperature and vapor density using the sorption isotherm relation. The values of these variables may be such that during the iterative process the moisture content obtained is less than zero (i.e.



drier than equilibrium conditions). Since the moisture content decreases, the temporal derivative of the moisture content is negative (as it is throughout the drying process), and hence, the latent energy term is nonzero. This results in a nonzero source term which continues to drive a change in temperature. Thus, the solution does not converge to the equilibrium state which results in a physically unrealistic solution.

A remedy for this problem is obtained by noting that once the moisture content has reached zero, the latent heat term should be zero; that is, once the solid is "dry", no further energy is used for evaporation. Thus, if a negative value of the moisture content is obtained during the iterative process, it is set to zero and the iteration is continued. The overall energy balance remains correct because the latent energy term can only be large enough to account for the evaporation of the liquid present (since the moisture content is not allowed to take on negative values). Thus, the source term includes only that energy necessary to dry the solid and a physically realistic solution is assured.

## APPENDIX C

### RATIONALE FOR SELECTING A CHARACTERISTIC VALUE AND RANGE OF VARIATION OF THE INNER DOMAIN ASPECT RATIO

The inner domain aspect ratio ( $L/D$ ) appears as a parameter in the inner domain equations governing the drying processes (equations 3.101, 3.102, and 3.103 on page 59). A typical criticism of a mathematical model of a complex physical process such as drying is that the values of all of the parameters in the model, such as the aspect ratio, are not well known. A hay bale is made up of many hay stalks which vary in length and diameter. In addition, many of the stalks are split down their length or are crushed so that there is not a single  $L/D$  ratio for all of the stalks.

Thus, for the purposes of the present model, a characteristic value of the  $L/D$  ratio must be chosen so that the drying time for a given volume of material matches experimental data.

To accomplish this task, an experiment was performed in which hay was placed in a 6 inch diameter tube and dried by blowing air through the tube (Bledsoe and Hitch, 1989). A dynamic measurement of the mass of the hay and water was obtained by hanging the tube from a load cell. Figure C.1 shows a comparison of the moisture content versus time for the experimental case and an  $L/D$  ratio of 1.4 (the base case values presented in Table 5.1 and Table 5.2 on pages 105 and 106 were used for all of the other parameters). It is seen

that the drying time predicted by the numerical solution matches very closely with experiment for this L/D ratio.

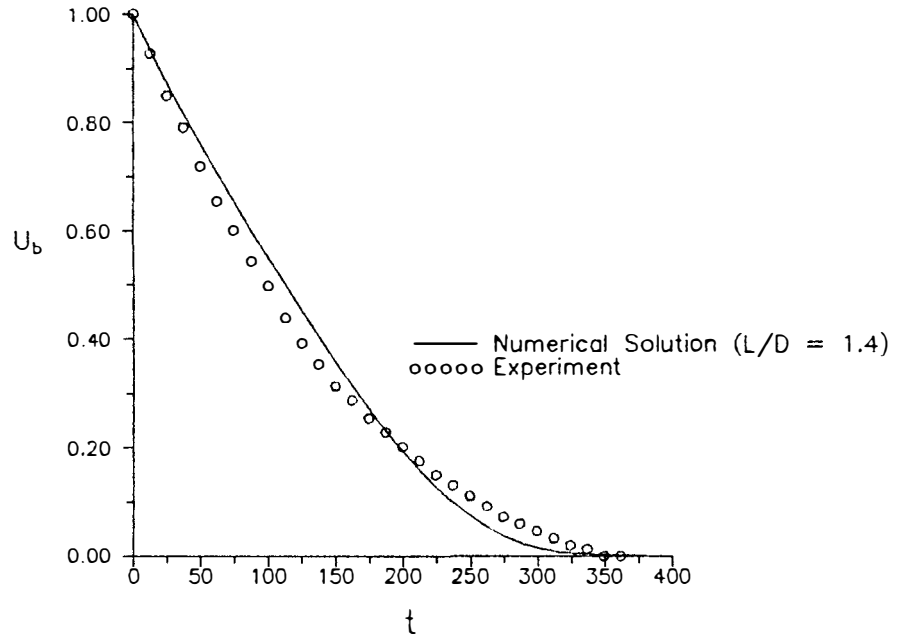


Figure C.1. Comparison Of the Experimental Drying Curve To The Numerical Solution For A One Dimensional Case (Hay Dried In A Tube).

A comparison of this L/D value to values obtained from actual hay stalk samples was also obtained. Approximately 200 samples of hay stalks (unbroken lengths) were obtained and their aspect ratios measured. The aspect ratios ranged from approximately 1.7 to 67.5 with an average value of 18.8. Thus, the value of 1.4 used in the model is lower than the measured values of actual stalks. The agreement obtained with this low value may be explained by considering several factors.

First, and probably most important, examination of many hay stalks revealed that the splits in the stalks were typically rather severe; that is, the stalks were split over significant portions of their overall lengths (roughly estimated as approximately 20% of the unbroken lengths). Since the liquid water in these split regions is exposed directly to the air flowing through the outer domain (i.e. the water vapor does not have to diffuse through a length  $L$ ), these split lengths would have a significantly lower resistance to mass transfer (which is precisely why they are broken in this manner during the conditioning process) and would thus tend to considerably lower the value obtained for an effective length used in the numerical model.

Second, there is also leafy matter present in the bales, which also has a considerably lower resistance to mass transfer than the stalks. This lower resistance results from the fact that the leaves have considerably greater surface area per unit volume than do the stalks. This would also tend to lower the effective value of  $L/D$  that yields good agreement between the numerical model and experiment.

Finally, it should be noted that no data is available for the thermal properties of hay. Thus, the thermal diffusivity and thermal conductivity of alfalfa hay are both unknown. Changing the values of the dimensionless parameters which

contain these properties may influence the value of the inner domain aspect ratio which results in the best match with experimental data.

One additional point should be made regarding the comparison between experimental and numerical values which is presented here. This comparison does not represent a validation of the mathematical model since the L/D ratio was varied to achieve a match with the experimental data. Additional experiments should be performed to check the validity of the present numerical model.

The range of values of L/D (0.7 - 2.1) used in the parametric study was obtained by considering a 50% change in L/D from the base case value (1.4) to be a practical limit (Bledsoe, 1989). However, it should be noted that this figure is merely an estimate of the actual length to diameter ratios that can be obtained in practice. As was discussed above, the length to diameter ratio, L/D, which appears in the present model represents an effective length to diameter ratio. Several factors such as the severity of splitting and crushing of the hay stalks during handling influence the effective value of L/D obtained from the numerical model. If the factors which influence the value of the effective ratio have the same relative importance at different values of the actual L/D ratios, a 50% change in the effective ratio will correspond to a 50% change in the actual ratio. However, it is more probable that factors such as splitting, crushing, etc. may

vary with L/D. For example, as the hay stalks are cut shorter and shorter to decrease L/D, a greater percentage of stalks may be split or crushed during handling. Thus, a decrease of, say, 50% of the actual L/D may result in a greater than 50% change in the effective L/D. Since the influence of these effects is not known, no attempt to compensate for such effects was made in this study.

## APPENDIX D

### NUMERICAL TREATMENT OF THE SORPTION ISOTHERM RELATION

The sorption isotherm is an empirically determined relation between relative humidity and moisture content at a specified temperature. Hill, Ross, and Barfield present graphical data for the sorption isotherm for alfalfa hay in the temperature range from 20 - 35 °C . An expression of the form

$$1 - \phi = e^{-cT_i^* u'^n}, \quad (D.1)$$

was used to correlate the data. There are large differences, however, between the values predicted by their correlation and the experimental data.

To minimize this type of error in the present work, a least squares fit was performed on the data presented by Hill et al. For simplicity, it was decided to approximate each isotherm by a series of linear segments. Thus, a least squares fit was performed on the experimental data for each linear segment, which is represented by a function of the form

$$u^* = c_1 \phi + c_2 T_i^* + c_3 \quad (D.2)$$

where  $c_1$ ,  $c_2$ , and  $c_3$  are "constants" which depend on the relative humidity interval in which a point lies. A minimum of 10 data points for each isotherm was obtained from the experimental curves. The curves were broken into three intervals corresponding to

$$0.3 \leq \phi \leq 0.6 \quad (\text{Region 1}),$$

$$0.6 < \phi \leq 0.75 \quad (\text{Region 2}),$$

and,

$$0.75 < \phi \leq 1.0 \quad (\text{Region 3}).$$

(Note: This range of relative humidity should cover the range of relative humidity encountered in "practical" drying situations.) The results of this procedure are presented in Table D.1 and a comparison between the experimental points and the fit used is presented in Figure D.1.

Table D.1. Least Squares Fit Coefficients For The Sorption Isotherm Of Alfalfa Hay.

| Region                            | $C_1$ | $C_2 \left( \frac{1}{C} \right)$ | $C_3$  |
|-----------------------------------|-------|----------------------------------|--------|
| 1<br>( $0.3 \leq \phi \leq 0.6$ ) | 0.269 | -0.00432                         | 0.116  |
| 2<br>( $0.6 < \phi \leq 0.75$ )   | 0.839 | -0.00432                         | -0.227 |
| 3<br>( $0.75 < \phi \leq 1.0$ )   | 2.08  | -0.00432                         | -1.16  |



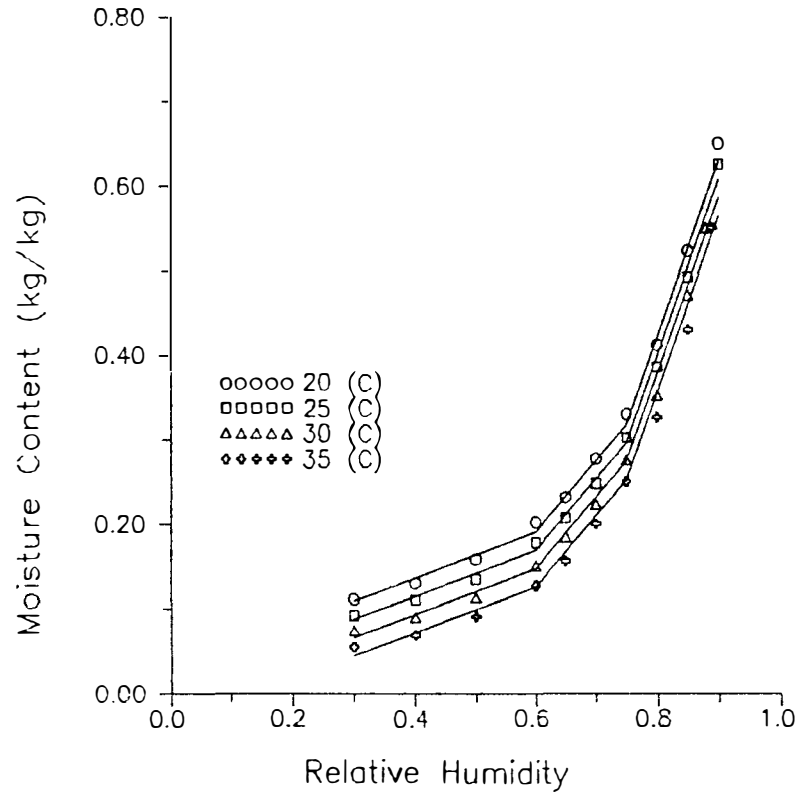


Figure D.1. Comparison Of Fit For The Sorption Isotherm Of Alfalfa Hay With The Experimental Data Of Hill, Ross, And Barfield (1977).

## APPENDIX E

### DETERMINATION OF PERMEABILITY OF A HAY BALE AND THE COEFFICIENT OF THE FORSCHEIMER TERM IN DARCY'S LAW

Values of the permeability,  $\kappa^*$ , and the coefficient of the Forcheimer term,  $b^*$ , were determined from experimental correlations obtained by Bledsoe and Hitch (1989). Both terms above were correlated as functions of dry matter density within the hay bale, and were assumed to be independent of moisture content.

The permeability was found to be represented by

$$\kappa^* = 1.02 \times 10^{-2} \rho_{dm}^{-2.93} \quad (m^2) \quad (E.1)$$

where the dry matter density has units of  $(kg/m^3)$ .

The coefficient of the Forcheimer term was found to be represented by

$$b^* = 107.6 e^{.0343 \rho_{dm}} \left( \frac{kg}{m^4} \right). \quad (E.2)$$

Both these expressions were found to be valid for a range of dry matter densities of approximately 32.0 to 160.2  $(kg/m^3)$ . The functional forms of these variables were obtained by simple curve fits to experimental data and thus the functions shown above are not necessarily indicative of theoretically expected functional forms.

## VITA

Thomas J. Phillips was born in Frankfurt, Germany on October 8, 1958. He obtained his elementary and secondary education at many different schools across the country. He graduated from Ooltewah High School in Ooltewah, Tennessee in June of 1976.

In September of 1976, he entered the Georgia Institute of Technology in Atlanta, Georgia. He attended this institution for two years in the cooperative education program, working off-quarters at Combustion Engineering, Incorporated in Chattanooga, Tennessee.

In January of 1979, he was admitted to the University of Tennessee in Knoxville and received his Bachelor of Science Degree in Mechanical Engineering in June of 1982. He accepted a research assistantship in the summer of 1982 at the University of Tennessee and began a research project concerned with natural convection heat transfer. He was awarded the Master of Science Degree in Mechanical Engineering in June of 1985.

In June of 1985, he accepted a teaching assistantship with the University of Tennessee and taught an undergraduate course in engineering mathematics. He subsequently accepted a research assistantship and began his doctoral studies in Mechanical Engineering. While working toward his doctorate, he accepted an adjunct faculty position in the Mathematics

Department at Pellissippi State Technical Community College and taught courses in basic physics and mathematics. He completed his doctoral work in September of 1989 and accepted a position with General Electric in Cincinnati, Ohio in October of 1989.